

TABLE OF CONTENTS

NASA CR 72034

	<u>Page</u>
ABSTRACT.	xi
SUMMARY	xiii
Forecast	xiv
INTRODUCTION.	xv
I. TEST PREPARATION SUB-TASKS.	1
Shaft Displacement Gauge Evaluation.	2
Loader Bearing Friction Torque Determination	17
Force-Gauge Dynamic Evaluation	19
II. MECHANICAL DESIGN	23
Critical Speed Analysis.	23
Parts Procurement and Fabrication.	26
Unbalance Disks.	28
Self-Aligning Pivoted Pad Bearing.	28
REFERENCES.	33
TABLES.	35
FIGURES	43

LIST OF ILLUSTRATIONS

<u>Figure No.</u>	<u>Title</u>	<u>Page No.</u>
1.	Program Schedule	43
2.	Bently Sensing Heads - Characteristics and Physical Data .	44
3.	Shaft Displacement Probe Holder Assembly - Photograph. . .	45
4.	Schematic Diagram Opposed Bently Gauge Distance Detectors.	46
5.	True and Apparent Shaft Runout. Type 420 S.S. Shaft 1.25" Dia.	47
6.	True and Apparent Shaft Runout. Type 420 S.S. Shaft 1.25" Dia. With Silver Plate 0.010" Thick.	48
7.	Maximum Variation in Bently Probe Calibration Over the Circumference of a 420 S.S. Shaft because of Non- homogeneities in the Shaft Material.	49
8.	Maximum Variation in Bently Probe Calibration Over the Circumference of a 420 S.S. Shaft Overlaid with 0.005 Inch Silver Plate because of Non-homogeneities in the Plating.	50
9.	Typical Calibration Curves - Bently Distance Detector. . .	51
10.	Proximity Gage Static Calibration Curve for Various Media.	52
11.	Proximity Probe Static Calibration Curve, Probe Tip is Shielded With a Teflon Cap.	53
12.	Bently Detection System Calibration No. 1 Probe, Detector D152	54
13.	Bently Detection System Calibration, No. 1 Probe Detector D252R	55
14.	Bently Detection System Calibration, No. 1 Probe Pair, Combined Probes.	56
15.	Calibration Test Device.	57
16.	Demonstration of Temperature Growth Compensation Using Opposed Gauges No. 4 and 4R.	58

17.	Comparison of Shaft Runout Measurements Bently and Capacitance Probes at Various Speeds.	59
18.	Comparison of Shaft Runout Measurements using Bently and Capacitance Probes	60
19.	Gauge Zero Shift With Speed	61
20.	Dynamic Displacement Gauge Checkout Test Rig.	62
21.	Measurements on Shaft for Dynamic Gauge Evaluation Test	63
22.	Location of Probes for Dynamic Gauge Tests of 10/22/65	64
23.	View Showing Opposed Gauge Installation for Dynamic Gauge Evaluation.	65
24.	Oscilloscope Photographs - Orbiting of Ball Bearing Mounted Shaft Data of 10/22/65.	66
25.	Oscilloscope Photographs - Orbiting of Ball Bearing Mounted Shaft Data of 11/11/65.	67
26.	Calibration Curve - No. 2 Bently Displacement Gauge Probe Pair Data of 11/22 and 12/30/65	68
27.	Oscilloscope Photographs - Orbiting of Ball Bearing Mounted Shaft Data of 12/1 and 12/2/65.	69
28.	Oscilloscope Photographs - Orbiting of Ball Bearing Mounted Shaft Data of 12/2/65	70
29.	Oscilloscope Traces - Probe Signal vs Time at 9000 rpm Data of 12/6/65.	71
30.	Oscilloscope Traces - Probe Signal vs Time at 15,000 rpm Data of 12/7/65.	72
31.	Oscilloscope Traces - Probe Signal vs Time at 26,100 rpm Data of 12/10/65	73
32.	Apparent Gauge Zero Shift With Time at 9000 rpm Data of 12/16/65.	74
33.	Apparent Gauge Zero Shift With Time at 15,000 rpm Data of 12/7/65	75

34.	Apparent Gauge Zero Shift With Time at 21,000 rpm Data of 12/7/65	76
35.	Apparent Gauge Zero Shift With Time at 26,100 rpm Data of 12/10/65	77
36.	Apparent Gauge Zero Shift With Time at 15,000 rpm Data of 12/11/65	78
37.	Disassembled View - New Displacement Probe Holders	79
38.	Bently Individual Probe Calibration - Gauge 8 and 8R	80
39.	Bently Combined Probe Calibration - Gauge 8 and 8R	81
40.	Partial Arc Loader Bearing Details	82
41.	View of Partial Arc Loader Bearing	83
42.	Test Rig for Measuring Loader Bearing Friction Torque	84
43.	Overall View of Loader Bearing Friction Torque Test Rig	85
44.	Closeup View of Loader Bearing Friction Torque Test Rig	86
45.	Loader Bearing Shaft Moment Coefficient vs. Sommerfeld No.	87
46.	Principle of Radial Force Measuring Technique	88
47.	Test Device for Evaluating Radial Force Measuring Technique	89
48.	View of Assembled Force-Gauge Checkout Device	90
49.	View of Partially Assembled Force Gauge Checkout Device	91
50.	Oscilloscope Photographs - Unbalance Force vs. Time	92
51.	Schematic Diagram and Arrangement of Load Cells for Radial Force Measurement.	93
52.	Typical Static Calibration - Four Force Gauges Assembled in Checkout Device.	94
53.	Load Cell Calibration Curves at Various Plate Thicknesses	95
54.	Force Gauge Evaluation - Dynamic Load Amplitude vs. Rotor Speed	96

	<u>Page No.</u>
55. Test Rig Assembly Drawing.	97
56. Analytical Model Established by Representing The Two Test Bearings And the Loader Bearings by Springs.	99
57. Analytical Model of Shaft System.	99
58. Plot of Mode Shapes at Critical Speeds of System	100
59. System Evaluation.	101
60. Exploded View of Test Housings	102
61. Inner Bearing Housing (Upper).	103
62. Outer Bearing Housing (Upper).	104
63. Bearing Housing Support Section.	105
64. Outer Bearing Housing (Lower).	106
65a. Bently Probe Mounted in Gauge Holder	107
65b. Bently Probe and Gauge Holder Disassembled	108
66. Test Shaft Inspection Traces	109
67a. Test Shaft	110
67b. Test Shaft	111
68. Support Structure.	112
69. Exploded View of Modified Shaft and New Unbalance Disk	113
70. Loss of Bearing Clearance as Result of Misalignment.	114
71. Self-Aligning Pivoted Pad Bearing Flooded Design	115

LIST OF TABLES

<u>Table No.</u>		<u>Page No.</u>
1.	Displacement Gauge Calibration Data 10/15-22/65	35
2.	Displacement Gauge Calibration Data 11/20-22/65	36
3.	Displacement Gauge Calibration Data 1/10-14/66	37
4.	Loader Bearing Friction Torque Data Summary	38
5.	Calibration Data for Load Cells	39
6.	Assumed Spring Constants Versus Cases Run	40
7.	Results of Cases Considering Shaft Model	41

ABSTRACT

The results of the dynamic evaluation testing of the Bently Proximity Probes (when provided with a teflon cap to shield against water) are presented. Also, the results of the dynamic loader bearing friction torque calibration are included. In addition, the force gauges which support the test bearings have been calibrated on a special test rig operated to 7000 rpm.

Manufacture of the main test rig for this program has been completed and all parts received. Design of a self-aligning pivoted pad bearing is in progress. A critical speed analysis of the test rig for test-planning purposes has been completed.

SUMMARY

During this quarter, static and dynamic evaluation of displacement gages was completed. Static evaluation consisted of comparing the readings of the Bently gages with contact probes on an accurate bench center-test shaft setup, wherein the Bently gages were positioned adjacent to dimensionally accurate silver plated shaft surfaces. Dynamic gage check-out involved mounting the test shaft in the high speed ball bearing test rig, and observing dynamic characteristics of the gages at speeds up to 30,000 rpm. In running, it was found that gage zero drift was minimized by using opposed gages (minimizing thermal expansion effects), and by covering the ends of the gages with Teflon caps to eliminate the wetting of gages.

The loader bearing friction torque testing was also completed on a special test rig which drove a simulated shaft to speeds from 1000 to 30,000 rpm. Bearing loads were varied between 17 and 122 lbs., and the results of torque vs. speed are presented herein.

The force gage dynamic check-out was completed on a special test rig to allow calibration of gages at speeds up to 7000 rpm. A bearing housing was mounted in the gages in the same manner as will be employed in the bearing test rig, and the response of the force buttons due to a known unbalance load in the shaft was determined.

Also during this quarter, fabrication of the high speed test rig components was completed. Design effort was initiated on a self-aligning

pivoted pad journal bearing which will be tested instead of the single degree-of-freedom pad bearing tested on the previous program (contract NAS 3-2111). In addition, the shaft unbalance disks which were previously used, have been redesigned and new ones have been fabricated.

A critical speed analysis of the test rig was performed assuming the bearings as springs with single-valued spring constants and no damping, for the purpose of identifying general critical speed regions.

The program schedule is shown in Figure 1.

Forecast

During the next quarter, preparations for testing in the new test rig will continue. Disassembly of the gage check-out test rig and other test apparatus discussed above will be completed, and installation of the newly purchased test equipment will be done.

INTRODUCTION

The Space Power and Propulsion Section, in cooperation with the Research and Development Center of the General Electric Company, has been under contract since April 29, 1965 to the National Aeronautics and Space Administration for the design, fabrication, and testing of journal bearings which possess characteristics, e.g. stability under zero radial load, required for use in space power systems. Requirements include long term unattended operation under zero "g" conditions using low viscosity lubricants such as potassium at temperatures from 600°F to 1200°F.

The program represents a continuation of work carried out under contract NAS 3-2111 (Reported in report NASA-CR-54039), and involves the testing and evaluation of two bearings, the four pivoted-pad and the three-lobe bearings, under conditions of angular and transverse linear misalignment, and non-rigid bearing supports. Bearing test shall begin after the test assembly, including instrumentation, has demonstrated the ability to obtain the required data with acceptable accuracy.

The program is primarily experimental and is paralleled by analytical studies. These analytical investigations will compare the physical testing of bearing parameters with results based on theoretical assumptions. The goal of such experiments is to generalize the various bearing parameters thereby extending the usefulness of the results as design tools. The experimental tool of this program is a high speed test assembly comprised of a rotor and two test bearings which permits

interchangeability of bearings and rotor. The lubricant will be distilled water, temperature-controlled to simulate the kinematic viscosity of potassium. The stability behavior of the rotating shaft will be measured with non-contacting Bently inductance gages.

The specific requirements of the system are:

- | | |
|------------------------------------|--------------------------------|
| 1. Shaft speed | 3600 to 30,000 rpm |
| 2. Inlet lubricant temperature | 70 to 150 ⁰ F |
| 3. Inlet lubricant supply pressure | 0 to 150 psia |
| 4. Bearing linear misalignment | 0 to 0.004 <u>+</u> 0.0005 in. |
| 5. Bearing angular misalignment | 0 to 400 <u>+</u> 12 sec. |
| 6. Nominal bearing diameter | 1.25 in. |
| 7. Bearing L/D ratio | 1 |
| 8. Diametral clearance | 0.005 in. |

The program will be performed in two tasks, the first of which will be the modification of the existing bearing test assembly and instrumentation and a demonstration of the ability to obtain accurate data. Task II will involve testing and analysis of the 4 pad pivot-pad and 3-lobed bearings. Data shall be presented in a way to permit application to bearings of similar design but of different dimensions.

The present report covers progress during the quarter ending January 29, 1966.

I. TEST PREPARATION SUB-TASKS

In this report, the results of three separate experimental studies are described which were carried out in preparation for the first test using the newly-modified test rig. These studies are: the evaluation of improved non-contacting shaft displacement measuring systems under static and dynamic conditions; the determination of friction torque produced by the partial arc loader bearings used to apply steady loads to the test shaft; and an evaluation of the technique proposed for measuring the dynamic radial loads transmitted through the test bearings.

In the previous bearing program conducted for the NASA (1), an erratic zero-shift was experienced with the shaft displacement gauges. Therefore, the absolute bearing film thickness measurements (eccentricity ratios) were not reliable, even though the measurement of frequency of shaft motion was not hampered. This allowed the six test bearing configurations to be compared according to their ability to resist fractional frequency whirl instability, which was the major contract objective.

Several potential improvements to the displacement measuring system were proposed for evaluation, including: shaft plating to reduce the effects of material inhomogeneities; opposed gauges to eliminate symmetrical temperature expansion of the gauge holders; and Teflon plastic caps on the sensing head elements to reduce wetting and, thereby, eliminate errors due to water droplets or varying humidity in the gap between probe and shaft. These modifications have now been demonstrated to improve substantially the reliability of film thickness measurements. It is estimated that dynamic measurements of shaft eccentricity ratio can be made within ± 150 microinches, and shaft vibrational amplitude within ± 50 microinches. Further improvements in eccentricity ratio measurements will depend primarily upon minimizing the effects of non-uniform thermal changes of the test device itself, which must serve as the reference surface.

The purpose of evaluating loader bearing friction torques is to permit test bearing torque to be separated from the total input torque, which includes both loader and test bearings. A special test device was built to make friction measurements on the loader bearings. Tests were carried out over a speed range from 1,000 to 30,000 rpm and are summarized later in this report.

An important part of the test program to be conducted is the determination of spring and damping coefficients for aligned and misaligned bearings. Direct determination of these quantities requires the measurement of dynamic radial forces. A special test device was built to evaluate the technique proposed for measuring dynamic radial forces transmitted through the test bearing fluid film. These tests have verified the feasibility of the force-measurement technique.

Shaft Displacement Gauge Evaluation

1. Selection of Gauge Type

Two types of non-contacting probes were initially considered to measure shaft position, i.e., capacitance and inductance probes. Both types are sufficiently compact and sensitive to meet the test device requirements. The capacitance gauge is insensitive to the shaft material, provided it is an electrical conductor, but is directly affected by the dielectric medium between probe and shaft. The eddy-current probe, on the other hand, depends primarily upon the material being sensed, and to a lesser extent upon the medium between probe and shaft, provided the medium is a poor electrical conductor in comparison with the shaft material.

In the water-lubricated bearing test rig, a high humidity environment exists. The dielectric constant may vary by a factor of 81 when water completely fills the gap to 1 when dry air fills the gap between probe and shaft. The Capacitance gauge therefore is extremely sensitive to water vapor and must be provided with a constant environment.

The inductance gauge is affected by the magnetic permeability and the electrical resistivity of the medium between probe and shaft; however, the permeability differs by minute amounts between a medium of air and water; also the electrical resistivity of water is much smaller than that of a metallic shaft. Water can therefore be expected to influence an inductance gauge to a much smaller extent than a capacitance gauge.

In order to evaluate whether one probe offered a substantial advantage over the other in practice, a comparative evaluation test had been conducted under the previous program, NAS 3-2111 (2). Both probes were evaluated in a high humidity atmosphere, with a protecting air curtain blown around the probe tip to maintain a constant environment. It was found that the capacitance gauge was indeed sensitive to water. When the probe tip was once wet, the signal could be restored only by removing the probe from the device and drying it thoroughly. The inductance gauge was likewise found to be affected by water. However, a stable signal could be achieved by the protecting air curtain without requiring probe removal. Consequently, the inductance gauge was selected as the shaft displacement sensing element for the previous program. In the interim, no suitable alternative displacement sensing system has emerged. The eddy-current inductance gauge therefore remains as the choice for the newly modified test rig.

2. Static Gauge Evaluation

In the previous program, the shaft position in each of two orthogonal directions was measured by a single inductance probe. In the newly modified test device, however, opposed probes are provided in each of the two (x,y) coordinate directions. Opposed probes can eliminate the effect of a uniform thermal expansion of the probe holder. Each probe of a pair consists of:

1. A sensing head (Figure 2), Model H-1-084-3 manufactured by Bently-Nevada Corp., Minden, Nevada, and recommended for small area resolution and high scale factor. Figure 3 shows the sensing head in the gauge holder.
2. A distance detector, Model D152 or D252R of Bently-Nevada Corp. The distance detector contains the detection circuitry and provides an output for connection to an external device. The D252R detector provides a reversed output for use in push-pull or opposed gauge arrangements. This distance detector is recommended by the manufacturer for high sensitivity, accuracy, response and long term stability.
3. An energy source. A diode regulated, battery power supply is being used to supply the distance detector with the necessary d.c. power.

A schematic wiring diagram showing the power supply, distance detector and signal amplification system is shown in Figure 4. The summing amplifier performs two functions:

1. It permits adjustment of the sensitivity of each probe to approximately the same value of volts per unit displacement.
2. It permits the signals to be combined algebraically without affecting the individual probe calibrations.

The summing amplifiers are contained in a Donner Scientific Co. Model 3400 analog computer. The amplifiers are chopper-stabilized, Donner Model 3101. The voltage read-out instrument for calibration is a differential D.C. digital voltmeter manufactured by the John Fluke Co., with an accuracy of $\pm 0.05\%$ of input voltage from 0.1 volt to 500 volts.

The calibration sensitivity of the Bently detection system depends upon several basic factors:

1. the setting of the supply voltage resistance potentiometer, which is adjustable for each distance detector unit.
2. the "sensed" material, e.g. the electrical resistivity of the material whose displacement is being measured. Other factors being equal, an increased electrical conductivity increases sensitivity. Homogeneity of the material also affects calibration. (The eddy-current gauging system has found use in detecting flaws.) Silver plating the test shaft improves the gauge sensitivity and provides a more homogeneous surface. Figures 5 and 6 compare the apparent and true runout on a plated and unplated test shaft when mounted in a low run-out (less than 5 microinch) precision grinder. True runout is measured with an Electrojet contacting probe. The effect of the uniform plating of silver is to mask the flaws or inhomogeneities which produce errors in the apparent gap. Figures 7 and 8 illustrate the improvement obtained in the static calibration curve by silverplating a test shaft. To obtain these curves, a constant gap is held between the probe tip and shaft, and the shaft is rotated to present a different surface in front of the sensing probe. The maximum variations in probe output for fixed gaps are shown in the figures. Plating reduces the maximum error (curve-shift) from about 300 to less than 50 microinches.

3. the gap between probe tip and sensed surface (shaft). The output voltage from the distance detector unit in general is nearly linear with gap change only over a restricted range of shaft displacement. As the sensitivity increases, the linear range becomes smaller. Figure 9 is a typical family of calibration curves of an amplified voltage vs. gap setting for one sensing unit and distance detector.
4. amplification and read-out system. The output voltage of a detector-sensing head combination may also be affected by the read-out system, all other things being equal. For example, the calibration curves of Figure 9 were obtained using a differential voltmeter operating on a null-balance principle. The impedance of this instrument as used is essentially infinite since no current is drawn. The reduction in signal is determined by the ratio of measuring circuit impedance to the sum of instrument and sensing impedance. The output impedance of the distance detector is 10,000 ohms nominal for the D152 and 25,000 ohms for the D252R model. Thus, in order to keep the signal at 99% of its infinite impedance value, the measuring device must provide an impedance of about 1 megohm for the D152 and 250 K ohm for the D252 model detector. Read-out systems with lower impedances will change the basic calibrations (volts per mil displacement). Therefore, other factors being equal, different measuring instruments can produce different calibrations.
5. probe environment. The output voltage of an unprotected probe for a fixed gap between probe and shaft is affected by the presence of water, as shown in Figure 10. It has been found, however, that the probe may be protected by a Teflon cap on the sensing head about

0.005 inch thick at the end. Figure 11 is a calibration curve for such a protected probe when immersed in various media. It can be seen from Figures 10 and 11 that, for example, a gauge output of say, 1.7 volts corresponds to a gauge-to-shaft gap of 0.0402 inches in air and silicone fluid, 0.0455 inches in water, and 0.014 inches when the gauge is covered by a teflon cap. Temperature also affects the probe calibration, although the effect is not large for the temperature range over which the test device operates. Calibration tests with the shaft at 157°F and the probe at 120°F have shown a decreased in sensitivity of about 0.04% per °F.

From the preceding discussion, it will be seen that the opposed gauge calibration requires several steps.

1. The nominal gap between probe tip and centered shaft must be selected. The gap must not be so small that the probe tip is in danger of being rubbed by the orbiting shaft; neither can it be so far away that the curve is highly non-linear or the sensitivity reduced. To find a reasonable compromise between these alternatives, a family of unamplified calibration curves may be drawn such as shown in Figure 9.

Figures 12 and 13 are calibration curves for individual Bently probes, both before and after signal amplification. Signals were amplified by a chopper stabilized d.c. amplifier, Donner Scientific Co. Model No. 3101. It will be seen that the voltage-gap relationship is linear over the anticipated range of measurement. When the individual probe gap and potentiometer setting have been selected in a bench calibration set up, these same values must be achieved in the test device. In practice, the distance detector potentiometer setting is fixed; the probe sensing head is then manually adjusted toward the shaft until the output voltage corresponds to the calibration range.

2. A desired overall sensitivity is selected for the opposed probe pair so that suitable amplification of the signals can be obtained. For example, an amplified calibration sensitivity of 1 volt per 1000 microinch displacement is an acceptable input value for operating read-out instrumentation such as the Tektronix oscilloscope Type 561 A with 3A72 Dual Trace, plug-in amplifier units. This instrument is capable of 3% accuracy over an input range from 10 millivolts per division (10 microinches) to 20 volts per division.
3. To achieve the desired overall sensitivity and eliminate symmetrical effects between the opposed probes of a pair, each probe signal must be separately amplified to produce one-half the total desired sensitivity. Figure 12, for example, illustrates how the basic output of one probe may be amplified from a sensitivity of 0.48 to 0.97 volts per mil. Similarly, the opposed probe for this gauge pair is adjusted from an unamplified sensitivity of 0.377 to 1.00 volts per mil, as shown in Figure 13.
4. The signal voltages from the opposed probes must be combined to produce a continuous curve of output voltage versus shaft displacement. To insure that the combined calibration curve is valid for the opposed probes as installed in the test rig, it is essential to insure that each probe has been mechanically adjusted so as to establish a probe-shaft gap in its calibrated operating range. For example, Figure 14 shows the combined calibration curve obtained by summing the amplified output signals from the opposed probes of Gauge Pair No. 1.

Each gauge of the pair is first adjusted to its proper "gauge zero."

The resulting summed signal for the gauges at their zero is then electrically biased to produce zero output voltage.

All probe pairs are calibrated using a contacting, electronic displacement device to measure change of displacement. Figure 15 is a photograph of the static calibration device. The test shaft is held on centers in a lathe; both the Bently probe sensing head and the reference contacting probe are fixed to a movable, micrometer stage which moves probes relative to the shaft in small increments. The electronic, contacting gauge system consists of a Sheffield Corp. Electrojet Cartridge together with an Accutron amplifier. The Electrojet Cartridge in turn was calibrated against Pratt and Whitney Hoke blocks.

To verify the repeatability of calibration using the eddy-current inductance system, sufficient calibration data were taken in the previous program (3) to permit a statistical evaluation. It was found that a given voltage change represented a shaft position change with an accuracy of ± 11 microinches at the 95% confidence level. Other occasional checks made after a month of gauge operation in a humid environment have not indicated any deterioration.

Static tests were carried out to verify the ability of opposed gauges to compensate for thermal expansion of the gauge holders. In these tests, the position of a silver-plated shaft segment was sensed by opposed gauges attached to the sides of an aluminum box structure with an open top. The shaft segment was inserted into the box through the open top and fixed in position. The position of the shaft relative to the gauges was measured at ambient temperature conditions. Hot water (125°F) was then poured into the box and the

measurements repeated. The combined, amplified probe signals showed a change of shaft position of 57 microinches. Individual probe measurements showed changes in probe-to-shaft gaps of 385 and 281 microinches in different directions. Thus, symmetrical thermal growth effects can be substantially reduced by using opposed gauges. The data for this test is shown graphically in Figure 16. It should also be noted that no protecting air supply was used or necessary during this test. The probe tips were protected by Teflon caps and with a silicone rubber seal filling the radial gap between the Teflon cap and the probe holder.

3. Dynamic Gauge Evaluation

One consideration in the evaluation of the eddy-current inductance gauge is whether a static probe calibration is valid for dynamic conditions. A test was carried out to determine whether this was a valid concern. A variable speed, ball-bearing mounted spindle was fitted with a 1 1/2 inch diameter stainless steel shaft segment. The part was made from the same steel lot as the test shaft used in the previous bearing program. A capacitance probe and a Bently eddy-current gauge were individually calibrated and set up on opposite sides of the shaft to sense shaft run-out. Photographs were taken of the oscilloscope traces produced by both the inductance and capacitance gauges. Figure 17 is typical of these traces. It will be seen that the Bently probe senses a shaft flaw or non-homogeneity in each revolution of the unplated shaft. It is this effect which is attenuated by silver-plating the new test shaft.

Figure 18 compares the shaft run-out at different speeds as seen by both the capacitance and inductance probes. Reasonable agreement exists between the two methods of measurements. It can be concluded, therefore, that shaft surface velocity itself does not affect the probe static calibration, at least over the range of interest in the current program.

In the previous program conducted for the NASA, it was found that the dynamic "gauge zero" shifted from the value obtained under static conditions. The "gauge zero" is the output voltage of a probe produced when the test shaft is centered in its bearings. Gauge zero is established for the static situation (non-rotating shaft) by displacing the shaft back and forth in its bearing clearance. A change in the gauge zero from the static situation therefore results in an error in the determination of eccentricity ratio (film-thickness) for the bearing.

An example of this zero shift is shown in Figure 19 for the test shaft of the previous program supported in water-lubricated, cylindrical bearings. Two oscilloscope traces of the shaft orbit at different speeds are shown. Each of the traces represents approximately the maximum shaft center locus within the bearing clearance. This was achieved by producing a half-frequency whirl at each of the two speeds. Thus the center of each nearly circular orbit may be regarded as indicating the gauge zero at each speed. It will be seen that a change in gauge zero of 1100 microinches occurred in one direction. This value is nearly equal to the radial clearance of the test bearing. The change in gauge zero experienced previously therefore was large and erratic, although it appeared to be speed dependent. In order to establish bearing eccentricity ratio accurately, it is essential to reduce or eliminate this detrimental zero shift.

For the dynamic gauge evaluation tests, two basic improvements were made to the displacement gauging system. Teflon tips were added to the sensing heads of Fig. 2 covering the coils with a thickness of approximately 0.005 inches at the end; gauges were grouped in opposed pairs to eliminate the zero shift due to symmetrical, temperature-induced expansion of the gauge holders and associated parts.

In order to evaluate whether these modifications to the gauges resulted in substantial improvement in the gauge zero shift, a test under simulated environmental conditions is desirable. One additional requirement, however, is that the shaft axis must be fixed within the test rig to a greater degree than provided by fluid-film bearings. Accordingly, preloaded angular contact bearings (MRC No. 7207) were selected to hold the shaft axis in position, as shown in Figure 20. These bearings were oil-mist lubricated. The test shaft used in the previous program was modified by the addition of sleeves and seals to protect the rolling element bearing from the water environment; the bearing housing was similarly modified to accept this selected bearing size. The shaft was silver-plated to a thickness of 0.00495 inch in the displacement gauge measuring areas. Careful control of the grinding resulted in a plate uniformity within ± 30 microinches. Figure 21 gives the details of the shaft measurements.

Initial dynamic gauge evaluation tests were carried with four probe pairs arranged as shown schematically in Figure 22. Shaft orbits were observed in two measuring planes, adjacent to the upper and lower cylindrical bearings. Figure 23 is a photograph showing opposed probe installation adjacent to the upper ball-bearing. Individual probe pair calibration data is given in Table 1 and also in the previous Figures 12, 13 and 14.

Figure 24 shows some shaft orbit amplitudes of the ball-bearing mounted shaft. The probe signals were initially centered on the scope at zero speed. Picture #1 shows a small orbit amplitude at both shaft ends. In subsequent pictures it will be seen that one shaft orbit in the plane adjacent to the lower test bearing exhibited a drifting in the No. 3 probe pair direction. Little drifting occurred for any other probe pair under these test conditions. Pictures No. 5 and 6 show the lower probe signal returning to its initial position $\frac{1}{2}$ hour after shutdown. Subsequent to this test, the sensor head #15287 forming part of the No. 3 gauge pair was found to have a small crack in the protecting Teflon cap. Disregarding this one defective probe signal, picture No. 4 shows the apparent change in gauge zero from the initial setting for the remaining three probes to be about 50 microinches. Figure 24 also illustrates the importance of the protection offered by an undamaged Teflon cap in preventing gauge error due to water.

Figure 25 shows some further measurements of shaft orbit amplitudes at differing speeds (3600, 9000 and 12,000 rpm) and with different conditions to the test device and gauges. Each photograph is a double exposure showing any change in shaft orbit over a period of time. The probe arrangement and calibration were the same as in Figure 22 and Table 1. From the final picture No. 9, taken after 3 hours testing at 12,000 rpm, the gauge zeros for No. 1 and No. 3 probes have changed from the initial, static reference position by about 150 microinches; the No. 2 and No. 4 probes show an even smaller shift.

Following these test runs, the probes were recalibrated to produce a larger "gauge zero" gap between probe and shaft. A larger gap can provide more protection against an orbiting or distorted shaft. It was considered desirable, therefore, to evaluate the gauges with such a larger gap (13 mils nom).

Table 2 contains the basic calibration data for the subsequent tests for which only two pairs of probes at the upper bearing location were used. The nominal probe sensitivity was 1 volt per mil displacement. Figure 26 shows the calibration curve for the No. 2 probe pair.

Figure 27 shows the oscilloscope photographs of the shaft orbits at several speeds up to 21,000 rpm. During these tests, the shaft orbit appeared to move primarily in the direction of one gauge pair. The change in "gauge zero" for the No. 2 probe from the initial static reference position was about 300 microinches. The final picture of Figure 27 shows that the probes 1 and 2 return to their initial set position relative to the shaft after the shaft is stopped. When the initial test rig conditions are reproduced, the gauge readings are restored. Thus the gauges themselves show little or no drifting. When rotating, the shaft axis moves slightly relative to the probes. Apparently the ring holding the probes undergoes a non-uniform expansion at higher speeds which cannot be cancelled completely by opposed probes.

Figure 28 shows some further oscilloscope photographs of the upper end shaft orbit at speeds up to 27,000 rpm. For these tests, the positions of probe pairs No. 1 and 2 in the test rig had been interchanged. The object of switching the probe positions was to determine whether the previously observed change of gauge zero was associated with a particular probe itself or with the probe location in the test rig. For this test, however, the orbit shift on the oscilloscope was not predominantly in one direction. At 27,000 rpm, for example, the No. 1 probe zero had changed approximately 100 microinches and the No. 2 probe about 200 microinches.

In the previous tests, the signals from the gauges were displayed on an oscilloscope so as to produce a picture of the shaft orbit near the test bearing location. Ideally, with the shaft held by perfect rolling element

bearings, the amplitude of shaft orbit is zero and the orbit would appear as a dot on the oscilloscope screen. In practice, however, even with a preloaded angular contact bearing some radial play must be expected. If the play is not uniform in all directions, a distorted orbit will appear on the oscilloscope, making the individual gauge zero change somewhat difficult to establish.

An alternate display of the gauge signals was used for subsequent tests to permit the individual "gauge zeros" to be established for each probe pair. For these later gauge evaluation tests, each probe pair signal was displayed against time on the horizontal oscilloscope axis. The gauge signals were initially electrically biased to coincide with a horizontal reference trace produced by the oscilloscope with no input signal.

To avoid the possible problem of oscilloscope drift masking probe drift, before each photograph was taken the initial reference time was re-established with no input signal. Each photograph therefore contains the initial reference line for each of the two probe pairs as well as the varying voltage signal produced by the probe when the shaft is rotating. The mid-position or average value of the probe signal may be taken as the dynamic gauge zero; the change in this position from the static reference position may be regarded as the gauge zero shift.

It must be remembered, however, that this gauge zero shift does not necessarily imply an error in the gauge reading. The actual gap between probe and shaft may change for a number of reasons, such as: unsymmetrical temperature expansion of the gauge holding fixtures; forces acting on the rotating shaft assembly which tend to deflect the "fixed" axis of the shaft to a different equilibrium position than the static, or no load condition.

Figures 29-31 show some typical traces of gauge voltages against time at several different speeds. Figures 32-36 show the apparent zero shift with time from the initial static reference position. Generally, it will be seen that an immediate signal shift occurs from the static reference position when the shaft is rotating. The magnitude of this shift, however, is five to ten times smaller than experienced with the single gauge installation as used in the previous program. After the shaft has been rotating for a period of time, the gauge zero position usually appears to stabilize at one value for a specific speed. This suggests that in actual testing, the gauge zero position should be determined after the test rig has been run for at least one-half an hour at the desired speed.

Based on the dynamic gauge evaluation tests which have been described, the following conclusions are drawn:

1. The probe static calibration is unaffected by shaft surface speed.
2. The probe "zero shift" occurring in the previous program probably resulted from two causes: temperature gradients within the test rig which changed the gap between probe and shaft, and the presence of water droplets. The former can be minimized by opposed probes, the latter shielded by Teflon caps on the probe ends. With properly sealed Teflon caps, no air curtain is required around the probe sensor head.
3. The dynamic "gauge zero" for opposed gauges, with Teflon caps, will be within ± 150 microinches of the static gauge zero. This assumes that the test rig has been brought to temperature equilibrium by the shaft rotating at the particular test speed before the static gauge zero is obtained. Gauge zero shifts of this magnitude are $\pm 6\%$ of the radial clearance of the test bearings.

4. Further improvements in accuracy of dynamic film-thickness measurement is presently limited by differential thermal expansion of the assembly holding the gauges in the test device rather than by inherent gauge limitations. To reduce thermal gradients in the test device, room temperature water should be used, or the ambient temperature external to the test rig kept at the lubricant temperature.
5. Shaft vibration amplitudes can be measured to an accuracy within ± 50 microinches using the Bently eddy-current inductance gauges. Such an accuracy ($\pm 2\%$ of the bearing radial clearance) is adequate for the anticipated use of this data.

Following the dynamic gauge evaluation tests, the sensing heads were installed in the new gauge holders, shown in Figure 37. Sixteen probes were calibrated individually and grouped into 8 opposed pairs. Typical calibration curves for these probes are shown in Figures 38 and 39 for individual and combined probes, respectively. Table 3 summarizes the calibration data. The Teflon caps on these probes were sealed with an RTV silicone rubber compound after the initial calibration. To determine whether the calibration was affected by this seal, the combined probes were then recalibrated. Little change was noted, as shown in Table 3.

Loader Bearing Friction Torque Determination

A second task in test preparation was the determination of friction torque produced by the partial arc loader bearings. These water lubricated bearings are used to supply the steady, unidirectional load to the test shaft. During such tests, total input torque will be measured which will therefore include both loader and test bearing friction torques and shaft windage torque. To separate the torque of the various test bearings from total input torque, it is desirable to make independent measurements of friction loss with the partial arc loader bearings.

Figure 40 gives the details of the loader bearings and Figure 41 is a photographic view.

Friction torque for these bearings was determined in a special test device shown in Figure 42. Two opposed partial arc bearings are loaded against a variable speed shaft (1.2530 inch. diam.) projecting from a spindle. The two partial arc bearing assemblies, including air pistons, are attached to a box-like structure which is free to rotate about an axis coincident with the shaft axis. The box structure is supported by low-friction, rolling element bearings.

Load is provided on both partial arc bearings simultaneously by pressurizing the air pistons through flexible hoses. The opposed loader bearing arrangement produces a net zero load on the rotating shaft, minimizing bending effects on the cantilevered test shaft. Bearing friction torque is measured by a strain-gauge cantilever beam producing a restraining torque on the box structure. Water is supplied to the two loader bearings through flexible hoses. Figure 43 is a photograph showing an overall view of the torque test rig; Figure 44 is a close-up view.

Data was taken over a speed range from 1000 to 30,000 rpm. Lubricant supply pressure was kept at 20 psi with ambient temperature water as the lubricant. Bearing load was varied over a range from 17 to 122 lbs. Test data is presented in Table 4 and in Figure 45. Figure 45 also contains the theoretical shaft moment coefficient for the loader bearing in laminar flow. The hydrostatic effect of the supply pressure as well as cavitation effects have been neglected in the theoretical solutions which were obtained with a computer program.

Force-Gauge Dynamic Evaluation

For the direct determination of bearing fluid-film spring and damping coefficients, measurements of transmitted radial force are essential. Provision has been made in the modified test rig to measure such forces using preloaded strain gauge load cells. Figure 46 illustrates the principle involved. Opposed load cells are arranged radially in each of two orthogonal directions to transmit rotor loads to the test rig casing. The forces sensed by these load cells are shown as force vectors in Figure 46. The signals from opposed gauges are electrically subtracted to produce a single signal proportional to one component of the total force; the remaining gauges are similarly combined to produce the other component of the transmitted force. Each of the components of the transmitted force signal may be varying with time. The average (d.c.) value of the signal is proportional to the steady or unidirectional load on the bearing. The alternating signal is proportional to the dynamic force.

An identical scheme had been previously used at the General Electric Company (ref. 4) to measure bearing reactions for a much larger rotor. To verify whether the technique was adequate for a smaller rotor and lower dynamic forces, a special force-gauge checkout device was designed, built and operated. A cross-section of this device is shown in Figure 47.

A shaft which is supported on rolling element bearings has unbalance discs attached outboard of the bearings. The shaft is rotated at different speeds by a flexible rod inserted into a hole and pinned near the center so as to provide a minimum of radial restraint. The outer-race of the supporting ball-bearings are held in a housing which in turn is supported on load cells in the manner previously described.

The assembly is driven by a variable speed d.c. motor through a belt and pulley arrangement, as shown in Figure 48. Figure 49 is a partially disassembled view of the device.

The rotating elements of the test shaft were dynamically balanced as a unit to 0.035 gram-inches of residual unbalance. The device was then deliberately unbalanced to predetermined levels by adding screws to each of the end discs. Unbalance force transmitted from the rotating shaft assembly is calculated from the shaft rotational speed and the known unbalance. The calculated value can then be compared with the measured value of dynamic load to evaluate the measurement technique. During tests, an unbalance of 7.8 grams was added to each of the discs at a radial distance of 1.25 inches.

Figure 50 shows some oscilloscope photographs of the signals obtained with such a rotating unbalance in the force gauge checkout rig. The force signal is plotted on the vertical axis of the oscilloscope against time on the horizontal axis. The force signal is obtained as the net output from four individual force gauges, arranged as shown diagrammatically in Figure 51. A typical, combined static calibration for the four assembled gauges is shown in Figure 52. Assuming no damping in the force buttons, the force button signal will be in phase with the unbalance below the system critical speed.

Figure 53 is a typical calibration curve for an individual load cell showing apparent strain vs. applied load at different plate thickness values. A plate thickness value of 0.050 inch was selected for the remaining load cells. Calibration data for other load cells is given in Table 5. The stiffness of the load cell design was also evaluated by measuring deflection of the plate under various loads. The stiffness of the individual load cells

is approximately 60,000 lbs. per inch. An assembly of four preloaded cells produces a stiffness four times that of the individual cell, i.e., 240,000 lbs. per inch.

Figure 54 is a comparison between the theoretical and measured values of transmitted radial force values using the technique described. The rig was run to the upper limit of the drive system. It will be seen that the agreement is reasonable and that the technique appears adequate for the measurements required, and no vibratory resonances occurred over the speed range tested.

II. MECHANICAL DESIGN

During this quarter a critical speed analysis of the test rig was performed. Fabrication of the hardware for the new high speed test rig was completed and delivered. In addition, the design of a self-aligning pivoted pad journal bearing was initiated, the layout design of which has been finished and the detail manufacturing drawings 30% completed. Also, the shaft unbalance disks were redesigned for better assembly and control of rotor balance, and the fabrication of these new components was completed.

Critical Speed Analysis

A critical speed analysis of the shaft-bearing assembly has been performed (based upon the design as shown in Figure 55). The computer program used was based on the balance of potential and kinetic energy, and is entitled System Vibration and Static Analysis (VAST). This is a General Electric Company program which follows the Rayleigh-Ritz method of analysis.

An important assumption in this program is that all bearings act as springs of constant stiffness, regardless of speed. Also, no damping of the bearings or in any mechanical parts is considered. While it is recognized that the spring constants change with speed and other dynamic conditions, the present analysis was made to determine generally where critical speeds will occur, as a guide to test planning, and to determine the first bending critical speed of the shaft.

The analysis identified the two rigid body modes of vibration (conical and cylindrical) within the operating range, and also identified the beam bending mode of the shaft as illustrated in Figure 58.

In the analysis, the model is broken down into spans, and subsequently into segments which are considered as connected beams mounted in the supporting springs or bearings; (see Figure 59). Weight and area properties of these short beam segments, in addition to the linear values of the spring constants comprise the major calculations inputs. A speed range of 100 to 40,000 rpm was investigated.

The analytical model for the shaft system was investigated in six different cases. At first the shaft was assumed to be supported in extremely soft supports, or a free-free condition. Linear spring constant values of 4 lb/in. and 0.001 lb/in. were assigned to spring numbers 101, 102, 106 and 107 in Cases I and II respectively; (see Table #6). Cases III, IV, V and VI were then evaluated with progressively stiffer values of the spring constants for springs 101 and 102 (the test bearings), while maintaining the no-load condition in the loader bearings.

The results of the analysis are shown in Table 7. In considering the shaft as free-free, a first shaft bending critical speed of 28,802 rpm was obtained. The analysis of the shaft pinned at the test bearing locations yielded similar results since the free-free nodal points actually occur almost at the bearing centers. The total range of shaft

critical speeds varied from 28,282 to 31,311 rpm. When the spring constants for the test bearings were assumed to be 50,000 lb/in. (Case III), two additional critical speeds were encountered. These are of the conical mode type and occur at 20,332 and 21,156 rpm with the principal vibrating members being the upper and lower test bearings respectively. It is apparent from these findings that the critical frequency of the test bearings, and the range of shaft critical speeds lie very close to the maximum proposed testing speed of 30,000 rpm.

It can be concluded from this analysis that the critical speed range of the shaft in this test rig is essentially independent of the test bearing stiffness, since the bearings are located near the natural nodal points of the shaft in the free-free condition. The shaft bending first critical speed is between 28,000 and 33,000 rpm, depending upon bearing stiffness and load. The critical speed range of the shaft may be raised above the maximum proposed testing speed of 30,000 rpm if a stiffness value for the loader bearings of 17,000 lb/in. is realized.

Parts Procurement and Fabrication

During this quarter, the manufacture of all test rig components was completed, with the exception of a new pivoted pad test bearing, to be discussed later. Figure 60 shows an exploded view of all test rig components, corresponding to the assembly drawing shown in Figure 55. All parts were manufactured to the required tolerances, and were fabricated without major difficulty or required design changes. The entire test rig was delivered from the manufacturing shops on December 20, 1965. Some of the individual test rig parts are shown in Figures 61 through 65b and 67 through 68. Figure 61 is a view of the inner bearing housing, which holds the test bearing. In it can be seen the threaded ports for insertion of the Bently gage holders, and the flat recesses for insertion of the force buttons which support this entire sleeve and bearing assembly. The main bearing housing support section is shown in Figure 63. The large flange for attaching the adjustable bearing housing can be seen at the bottom. Figure 65a is a view of the Bently gage holder assembly, and Figure 65b shows this component disassembled.

Although good quality machining was required throughout, the major portion of the components did not require the exacting tolerances as did the test shaft. The fabrication of the test shaft required very close engineering, metallurgical, and manufacturing follow-up to insure that it would be completed per schedule and meet blueprint tolerances. The shaft design specified that four diameters be silver plated (in the vicinity of the Bently gages). The thickness of which had to be maintained uniform within a total of 50 micro-inches variation. The grinding and plating technique

was developed and evaluated on a sample specimen. A lapping versus grinding process for obtaining the required surface finish was evaluated, and it was found possible to complete the shaft to the tolerances and surface finish indicated below by grinding.

<u>CONDITION</u>	<u>SPECIFICATION (in.)</u>	<u>ACTUAL (in.)</u>
Roundness	0.000050 FIR	0.000030 FIR
Concentricity	0.000050 FIR	0.000030 FIR
Taper	0.000050 FIR	0.000040 FIR
Plating Thickness	0.0050 Nominal	0.005 + 0.0001 Max.
Surface Finish	8AA	4.5AA

Figure 66 shows superposed traces of the shaft at several critical diameters, indicating the above roundness, and concentricity.

Figure 67 (a) is an overall view of the test shaft, and Figure 67 (b) shows a close-up of the plated section on either side of the test bearing location.

The required supporting structure is shown in Figure 68. This comprises three "clam-shell" removable doors, which make a cylinder when closed and which are insulated to maintain a controlled temperature environment around the test rig. Electric resistance wire is used to maintain a prescribed temperature around the test rig. The three supporting columns act as air manifolds to provide flow to the Bently gages and for actuation for the loader bearing pistons. Temperature control of air, lubricating water, and operating environment will be maintained on the test rig during operation.

Unbalance Disks

The unbalance disks used at each end of the test shaft to produce specified amounts of unbalance have been redesigned to employ single disks rather than the previously employed pair of eccentric disks (Reference Figure 69). Two tapped holes located 180° apart on a 2.000 inch diameter bolt circle will provide a means for locating various weights. Screws of various weight differences will be fabricated, and when installed at assembly, provide the desirable amounts of unbalance. The holes in these new unbalance disks have been fabricated on the same radial centerline as the notch in the O.D. of the disk which provides the signal for the Z input to the bearing oscilloscope traces, thereby directly defining the direction of the unbalance forces.

Two axial slots have been fabricated 180° apart on the I.D. of the disk. Locating pins will be assembled into the modified shaft and once the disks are mounted, provide a means of positively locating the disks. These pins will be employed in addition to using the locking nut on each end of the shaft (Reference Figure 69).

In addition, keyways and locking pins have been installed in addition to the previously used locking nut to lock the disks against shifting during operation.

Self-Aligning Pivoted Pad Bearing

The contractual requirements of this program require testing bearings at both transverse and/or angular misalignments of the values indicated

in the Introduction. Figure 70 interprets these misalignments in terms of loss of diametral clearance within the test bearings. It can be seen that the angular misalignment requirements of 400 seconds provides a consumption of diametral clearance of approximately 6 times that produced by the 0.004 inch transverse misalignment, and that under the worst combination of transverse and angular misalignment, as much as 2.78 of the total 5 thousandths of an inch diametral clearance is consumed by misalignment.

In addition to testing the fixed geometry bearings (two axial groove bearing for calibration of the test assembly and the 3-lobed bearing) which were originally defined for testing in this program, the decision has been made to investigate and test a bearing designed to accommodate such misalignment as indicated above, without adversely affecting bearing performance. Such a bearing is a self-aligning pivoted pad bearing, which will be designed, built, and tested instead of the originally intended pivoted pad bearing with cylindrical pivots (this bearing would have allowed pivoting in the radial plane, but would not accommodate axial misalignment).

The pivoted pad bearing is chosen for the self-alignment design, since it easily accommodates adjustment to a misaligned shaft, and also, the pivoted pad bearing has shown itself to be a leading contender for suppression of half frequency whirl. The bearing layout design has been completed, and is shown in Figure 71. The pads are mounted on spherical pivots, allowing universal alignment capabilities within the limits of angular and transverse bearing displacement defined in this program. The requirements for the design

of this bearing not only required the self aligning feature, but also the ability to lock a pad or all pads, and thereby simulate the condition of a frozen pivoting joint.

About 30% of the detailed manufacturing drawings are completed, with the remaining details expected to be finished in February. The design characteristics of the bearing are as follows:

O.D. - 2.5001 - 2.5004

Machined I.D. = 1.2549 - 1.2550

Length of Pads (Axial) - 1.2500

L/D = 1.0

Number of Pads - 4

Pivot Point - 55% of Pad length (Circumferential) from leading edge.

Type of Lubrication - Flooded

Assembly Configurations:

<u>Number</u>	<u>Diameter (I.D.)</u>	<u>Preload</u>	<u>Diametral Clearance</u>
1	1.2549 - 1.2550	0	5 mils
2	1.2529 - 1.2530	0.4	3 mils

Roundness Requirement of bore - 0.000050 FIR

Concentricity of bore to O.D.
of retaining ring - 0.0002 FIR

Taper of bore - 0.0001 FIR

Surface finish of bore - 8 AA

The bearing is a "flooded" design, wherein the water lubricant is injected into the general bearing cavity which is created by two close-running shaft screw seals. The bearing has been designed for operation both with and without preload, as indicated above.

The bearing consists of an outer retaining ring, pivoting pins, clearance adjusting washers, four partial arc pads, and the end plates. The inner bore of the bearing will be final machined with the bearing assembled, during which the pads will be secured into position on the pivoted pins and located by the use of four cylindrical pins and 8 locking bolts, and with the retaining ring functioning as a tooling fixture. This same pad holding technique will be used to lock individual pads during testing to simulate frozen pivoting joints. The water lubricant will be introduced into the bearing cavity through four passages which enter between the partial arc pads. The outer retaining ring is made from 304 stainless steel, while the four pivot pins will be fabricated from Stellite 3, and the pads will be SAE 660 bronze. The design of the pivots is hard-vs-hard, wherein the spherical pivoting pins seats against a corresponding Stellite 3 washer inserted into the recessed hole on the back of each pad. The sides of the Stellite pivot pin contact the soft 660 bronze for a maximum lubrication between these members during operation.

The pivot point of the pad was established at 55% of the pad length from the leading edge. To insure that the grinding assembly can be reproduced, all components will be match marked relative to the retaining ring pivot pin holes.

Preload is accomplished by varying the washer mounted between the pivot pin and the outer ring.

The screw threads in the side seal plates have been designed to pump the lubricant against the pressurized cavity. Four water exit ports have been designed into each seal plate in addition to four small pins. These pins fit into oversized holes in the pads and will inhibit the pads from falling during handling, but will not retard pad movement during testing.

A pad may be fixed or locked into position during testing simulating a failed or frozen pad by simply installing the match marked roll pins used during fabrication behind the pad and installing the locking bolts. All four pads can be locked in this manner if desired.

REFERENCES

1. J. D. McHugh, "Low Viscosity Bearing Stability Investigation,"
Final Report, NASA-CR-54039 under NASA Contract No. NAS 3-2111
2. "Low Viscosity Bearing Stability Investigation," Contract NAS 3-2111
Quarterly Report No. 4 for period ending November 9, 1962
3. "Low Viscosity Bearing Stability Investigation," Contract NAS 3-2111
Quarterly Report No. 6 for May 9, 1963
4. J. D. McHugh and J. W. Lund, "Bearing Attenuation - Experimental
Evaluation," August 1961, General Electric Report prepared for the
Bureau of Ships under Contract NObS78930

TABLE 1
DISPLACEMENT GAUGE CALIBRATION DATA 10/15 - 10/22/65

Calibrated Against Silver Plated Shaft (0.005 in. Plate)

GAUGE PAIR IDENT. NO.	DISTANCE DETECTOR MODEL AND SERIAL NO.	GAUGE SENSOR HEAD MODEL H-1-084-3 SERIAL NO.	PROBE TO SHAFT GAP AT GAUGE ZERO MILS (NOMINAL)	UNAMPLIFIED GAUGE OUTPUT AT GAUGE ZERO VOLTS	AMPLIFIED INDIVIDUAL GAUGE SENSITIVITY AT GAUGE ZERO VOLTS/MIL	COMBINED GAUGE SENSITIVITY VOLTS/MIL
1	D152R #3459	#15288	7	7.43	.972	1.97
	D252R #5522	#14438	9	7.63	.996	
2	D152 #3447	#15296	6	7.728	.852	1.843
	D252R #5519	#15289	6	6.275	.998	
3	D152 #3462	#15280	10	7.169	0.906	1.887
	D252R #5518	#15287	8	5.570	0.995	
4	D152 #3458	#14770	7	8.442	0.801	1.796
	D252R #5521	#15279	12	6.603	0.991	

TABLE 2
DISPLACEMENT GAUGE CALIBRATION DATA Nov. 20-22, 1965

Calibrated Against Silver Plated Shaft (0.005 in. Plate)

GAUGE PAIR IDENTIFICATION NO.	DISTANCE DETECTOR MODEL AND SERIAL NO.	GAUGE SENSOR HEAD H-1-084-3 SERIAL NO.	UNAMPLIFIED GAUGE OUTPUT AT 13 MILS NOM. GAP VOLTS	AMPLIFIED INDIVIDUAL GAUGE SENSITIVITY AT 13 MILS NOM. GAP VOLTS/MIL	COMBINED (OPPOSED) GAUGE SENSITIVITY AT 13 MILS NOM. GAP VOLTS/MIL
1	D152 #3459	#15288	5.417	0.469	0.977
	D252 R #5522	#14438	5.169	0.497	
2	D152 #3447	#15296	10.26	0.469	.976
	D252 R #5519	#15289	8.098	0.511	

TABLE 3
DISPLACEMENT GAUGE CALIBRATION DATA Jan. 10-14, 1965

GAUGE PAIR IDENTIFICATION NO.	DISTANCE DETECTOR MODEL AND SERIAL NO.	GAUGE SENSOR HEAD - MODEL H-1-084-3 SERIAL NO.	PROBE TO SHAFT GAP AT GAUGE ZERO MILS	UNAMPLIFIED GAUGE OUTPUT AT GAUGE ZERO VOLTS	UNAMPLIFIED GAUGE SENSITIVITY VOLTS/MIL	AMPLIFIED GAUGE SENSITIVITY AT GAUGE ZERO VOLTS/MIL	COMBINED GAUGE SENSITIVITY VOLTS/MIL
1	D152 3459	15273	9	6.574	0.395	0.487	1.008
	D252R 5522	14439	9	6.674	0.441	0.497	*1.003
2	D152 3447	15284	9	7.683	0.419	0.483	1.000
	D252R 5519	14444	9	6.925	0.410	0.483	*0.992
3	D152 3462	15296	9	7.750	0.394	0.478	0.984
	D252R 5518	14438	9	6.700	0.421	0.497	*0.994
4	D152 3458	15287	8	9.940	0.437	0.499	1.002
	D252R 5521	15281	9	7.038	0.384	0.504	*0.999
5	D152 3451	15292	12	9.467	0.424	0.472	0.961
	D252R 5515	15289	9	7.778	0.419	0.472	*0.954
6	D152 3453	15288	13	10.404	0.455	0.491	0.993
	D252R 5516	15279	9	6.596	0.398	0.494	*1.001
7	D152 3454	15280	9	8.453	0.456	0.493	0.987
	D252R 5520	14770	7	7.479	0.5034	0.503	*0.980
8	D152 3464	16763	9	7.863	0.403	0.481	0.980
	D252R 5517	16758	9	7.851	0.448	0.478	*0.979

* Teflon Caps Sealed with RTV Adhesive Recalibrated Combined Gauges 1/22/64

TABLE 4
LOADER BEARING FRICTION TORQUE DATA SUMMARY

RUN NO.	SPEED RPM	WATER		BEARING LOAD		FRICTION TORQUE LB-IN	FRICTION FORCE LBS	COEFFICIENT OF FRICTION	SOMMERFELD NO.	SHAFT MOMENT COEFFICIENT	FLOWRATE GPM
		TEMP. °F	VISCOSITY ₂ LB-SEC/IN	LBS	PSI						
1	1020	64	15.3x10 ⁻⁸	17.5	7.45	.0996	.159	.00908	.1306	2.31	.71
2				35.0	14.9	.1164	.186	.00531	.0653	2.70	.555
3				52.5	22.3	.1350	.216	.00412	.0436	3.14	.435
4				70.0	29.8	.1526	.244	.00349	.0327	3.54	.35
5				87.5	37.1	.1701	.273	.00312	.0262	3.96	.30
6				105.0	44.7	.1870	.299	.00285	.0218	4.34	.27
7	2040	65	15.1x10 ⁻⁸	17.5	7.45	.1236	.198	.0113	.284	1.32	.735
8				35.0	14.9	.1393	.223	.00637	.142	1.49	.60
9				52.5	22.3	.1598	.256	.00487	.0947	1.71	.495
10				70.0	29.8	.1765	.283	.00399	.0663	2.00	.41
11				87.5	37.1	.1923	.308	.00352	.0568	2.10	.35
12				105.0	44.7	.2040	.327	.00311	.0473	2.18	.32
13	4000	65	15.1x10 ⁻⁸	17.5	7.45	.1157	.185	.01057	.527	.665	.75
14				35.0	14.9	.1465	.234	.00664	.263	.838	.63
15				52.5	22.3	.1730	.277	.00528	.175	1.000	.535
16				70.0	29.8	.1933	.310	.00443	.132	1.12	.45
17				87.5	37.1	.2092	.334	.00381	.105	1.21	.395
18				105.0	44.7	.2214	.354	.00337	.0878	1.27	.345
19				122.5	52.0	.2346	.376	.00301	.0753	1.32	.31
20	7973	66	14.9x10 ⁻⁸	35.0	14.9	.1913	.306	.00874	.517	.561	.635
21				52.5	22.3	.2100	.336	.00640	.345	.616	.535
22				70.0	29.8	.2232	.357	.00510	.259	.654	.46
23				87.5	37.1	.2390	.383	.00438	.207	.703	.40
24				105.0	44.7	.2532	.405	.00386	.172	.745	.36
25				122.5	52.0	.2620	.419	.00342	.148	.767	.33
26	10060	67	14.7x10 ⁻⁸	35.0	14.9	.2136	.341	.00974	.643	.502	.635
27				52.5	22.3	.2286	.366	.00697	.429	.540	.525
28				70.0	29.8	.2444	.392	.00561	.322	.578	.45
29				87.5	37.1	.2630	.421	.00482	.257	.623	.39
30				105.0	44.7	.2902	.465	.00443	.214	.687	.35
31				122.5	52.0	.3018	.483	.00394	.184	.711	.32
32	15100	69	14.4x10 ⁻⁸	52.5	22.3	.3620	.579	.0111	.631	.583	.535
33				70.0	29.8	.3816	.610	.00872	.473	.600	.455
34				87.5	37.1	.408	.654	.00747	.379	.654	.395
35				105.0	44.7	.424	.679	.00646	.315	.681	.34
36				122.5	52.0	.443	.709	.00578	.270	.710	.30
37	20060	70	14.2x10 ⁻⁸	52.5	22.3	.634	1.013	.01929	.828	.774	.54
38				70.0	29.8	.637	1.020	.01459	.622	.780	.48
39				87.5	37.1	.641	1.026	.01172	.497	.784	.43
40				105.0	44.7	.641	1.026	.00977	.414	.784	.375
41				122.5	52.0	.641	1.026	.00836	.355	.784	.315
42	25000	70	14.2x10 ⁻⁸	52.5	22.3	.775	1.240	.0236	1.030	.761	.53
43				70.0	29.8	.786	1.259	.0180	.773	.775	.51
44				87.5	37.1	.796	1.274	.01456	.618	.783	.48
45				105.0	44.7	.800	1.280	.01219	.514	.786	.46
46				122.5	52.0	.805	1.289	.01053	.441	.795	.435
47	29880	72	13.8x10 ⁻⁸	52.5	22.3	.880	1.409	.0268	1.197	.745	.56
48				70.0	29.8	.900	1.440	.0206	.899	.759	.56
49				87.5	37.1	.914	1.461	.0167	.720	.771	.55
50				105.0	44.7	.946	1.512	.0144	.598	.813	.54
51				122.5	52.0	.946	1.512	.01235	.514	.798	.525

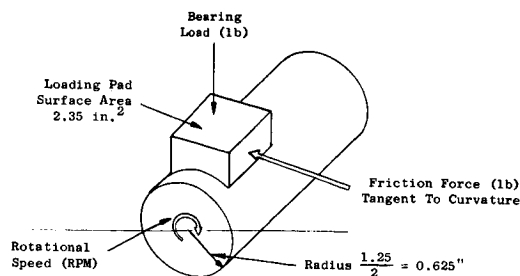


TABLE 5
CALIBRATION DATA FOR LOAD-CELLS
Load Cell Drawing 115A4384 with 0.050 in. Plate Thickness

LOAD CELL NO.	* LOAD CELL SENSITIVITY MICRO-INCHES STRAIN PER LB. LOAD	** SHUNT RESISTANCE FOR APPARENT 50 LB. LOAD OHMS	CALIBRATION DATE
2	8.4	144,000	11-4-65
3	10.4	116,000	11-1-65
4	12.6	95,000	11-17-65
5	10.2	118,000	11-4-65
6	9.34	128,000	11-4-65
7	10.4	116,000	11-6-65
8	12.7	94,000	11-4-65
9	10.4	116,000	11-6-65

* USING BALDWIN SR4 STRAIN METER, GAUGE FACTOR AT 2.0

** SHUNT RESISTANCE ACROSS ONE LEG OF LOAD CELL BRIDGE CIRCUIT

TABLE 6

ASSUMED SPRING CONSTANTS FOR VARIOUS
ANALYTICAL CRITICAL SPEED CASES

CASES RUN	K VALUES OF SPRING #/IN.				REMARKS
	101	102	106	107	
I	4	4	4	4	Shaft Only (Free-Free)
II	1×10^{-3}	1×10^{-3}	1×10^{-3}	1×10^{-3}	Shaft Only (Free-Free)
III	5×10^4	5×10^4	4	4	Shaft Only (Pinned-Pinned)
IV	1×10^5	1×10^5	4	4	Shaft Only (Pinned-Pinned)
V	2×10^5	2×10^5	4	4	Shaft Only (Pinned-Pinned)
VI	1×10^6	1×10^6	4	4	Shaft Only (Pinned-Pinned)

TABLE 7
RESULTS OF CASES CONSIDERING SHAFT MODEL

Cases	Critical Mode Shape	CRITICAL SPEED OF PRINCIPAL VIBRATING MEMBERS (RPM)						REMARKS
		Upper Force Buttons (104)	Lower Force Buttons (103)	Upper Test Brg. (102)	Lower Test Brg. (101)	Shaft	Support Hsgs.	
I	1st	-	-	-	-	-	-	Shaft Model only-soft Springs
	2nd	-	-	-	-	-	-	
	3rd	-	-	-	-	28,802	-	
II	1st	-	-	-	-	-	-	As Above
	2nd	-	-	-	-	-	-	
	3rd	-	-	-	-	28,802	-	
III	1st	-	-	20,332	21,156	-	-	Shaft Model Only-stiff Springs
	2nd	-	-	-	-	-	-	
	3rd	-	-	-	-	29,122	-	
IV	1st	-	-	-	-	-	-	As Above
	2nd	-	-	-	-	-	-	
	3rd	-	-	-	-	31,311*	-	
V	1st	-	-	-	-	-	-	As Above
	2nd	-	-	-	-	-	-	
	3rd	-	-	-	-	28,282	-	
VI	1st	-	-	-	-	-	-	As Above
	2nd	-	-	-	-	-	-	
	3rd	-	-	-	-	28,486	-	

* The mode shape at this critical speed was of the bending beam type. However, the lower test bearing is responsible for 53% of the total potential energy.

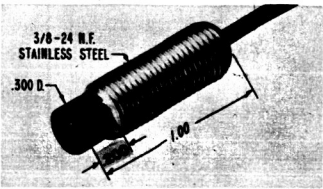


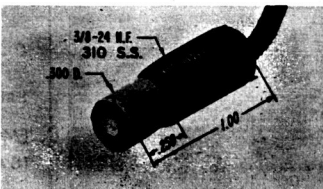

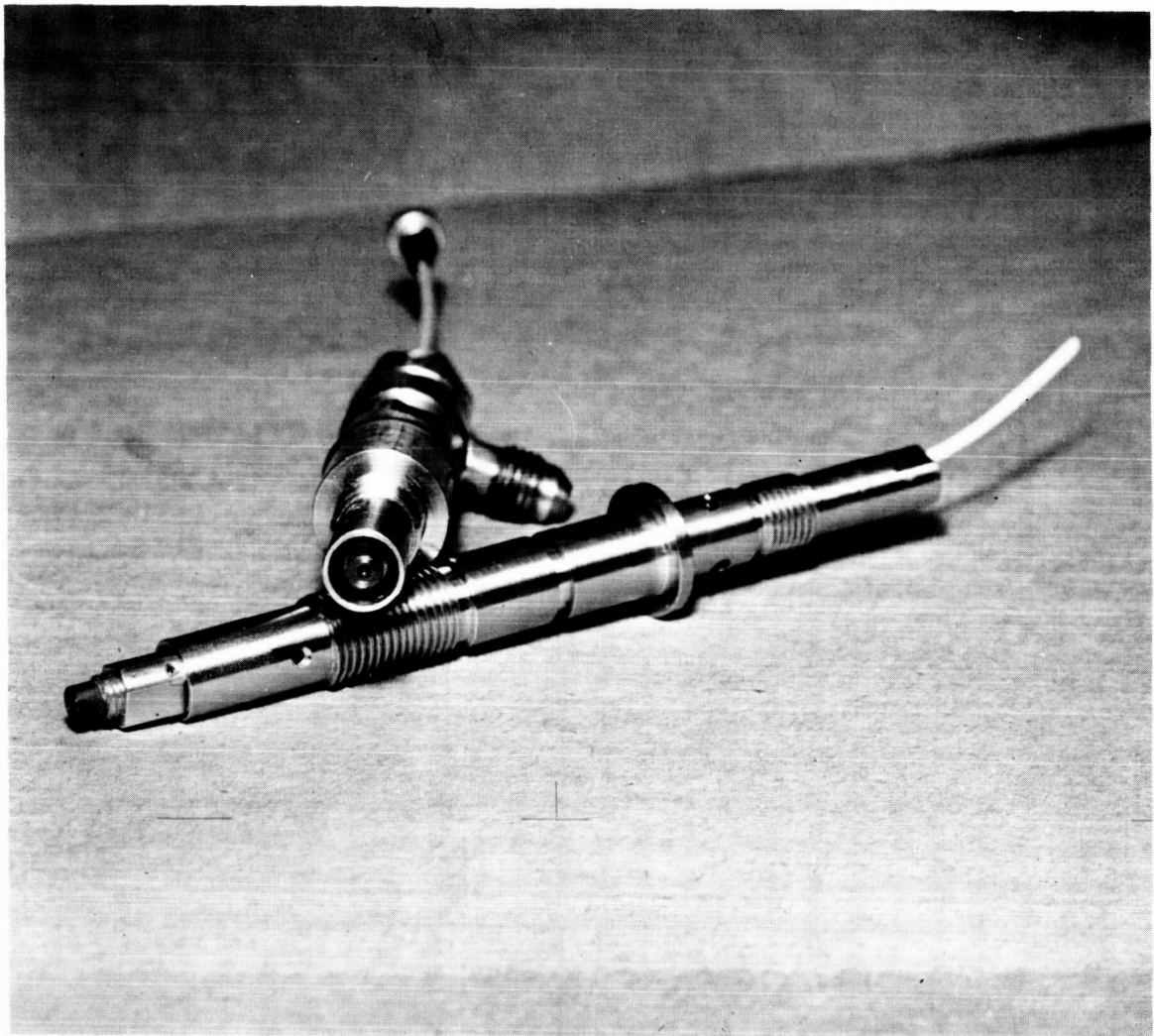
BENTLY SENSING HEADS				BENTLY NEVADA CORPORATION MINDEN, NEVADA	
	MODELS			CHARACTERISTICS	
RANGE	H-1			SHORT RANGE (0 TO 0.025") HIGH SCALE FACTOR	
	H-3			UTILITY RANGE (0 TO 0.100") GENERAL PURPOSE	
	H-8			SILVER COIL H-3, LEAST SHIFT WITH TEMPERATURE	
	H-4			LONG RANGE (0 TO 0.250")	
CABLE			- 1	-3 CABLE FOR USE WITH D-15 ONLY	
			- 3	30 IN., 50 OHM TEFLON CABLE.	
			- 4	72 IN., 95 OHM TEFLON CABLE.	
			- 5	2 IN., 50 OHM TEFLON CABLE (FOR USE WITH EXTENSION CABLES).	
			- 6	9 IN., 50 OHM FLEXIBLE CERAMIC COAX.	
PHYSICAL DATA	H-1 H-3 H-8	-021-	1 3 4 5		RECOMMENDED FOR GENERAL PURPOSE APPLICATIONS
	H-1 H-3 H-8	-022-	1 3 4 5		RECOMMENDED FOR GENERAL PURPOSE APPLICATIONS HEX HEAD END FOR EASY ADJUSTMENT.
	H-1	-084-	1 3		RECOMMENDED FOR SMALL AREA RESOLUTION. HIGH SCALE FACTOR
	H-3	-042-	6		RECOMMENDED FOR HIGH TEMPERATURE AND/OR HIGH VACUUM APPLICATIONS (710°C/1300°F) METAL-CERAMIC CONSTRUCTION (SEE 042 SPECIFICATIONS)
	H-4	-037-	1 3 4		RECOMMENDED FOR LONG RANGE APPLICATIONS

Figure 2. Bently Sensing Heads - Characteristics and Physical Data.



1" \pm 0.89"

Figure 3. Shaft Displacement Probe Holder Assembly.

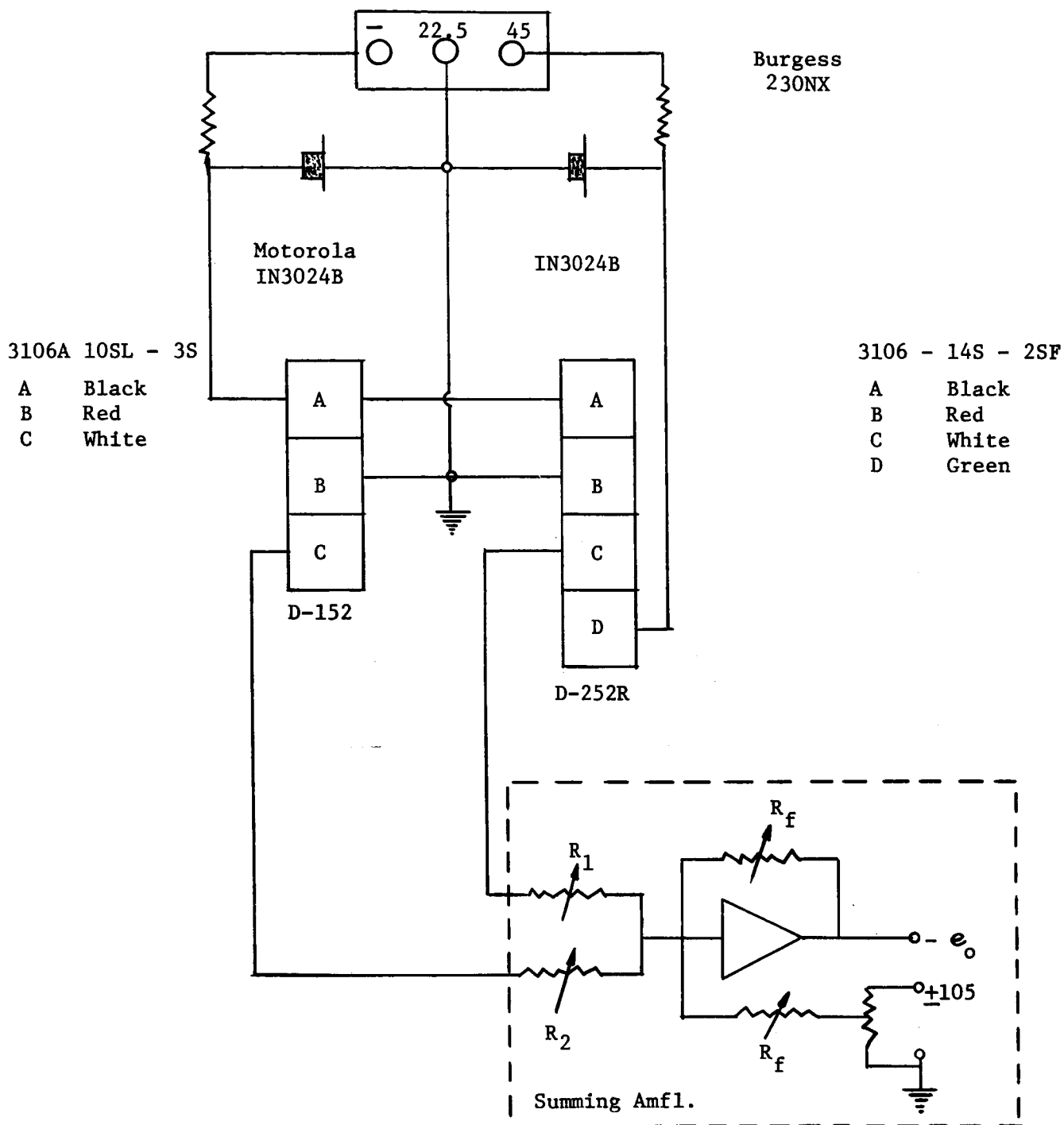


Figure 4. Schematic Diagram Opposed Bently Gauge Distance Detectors.

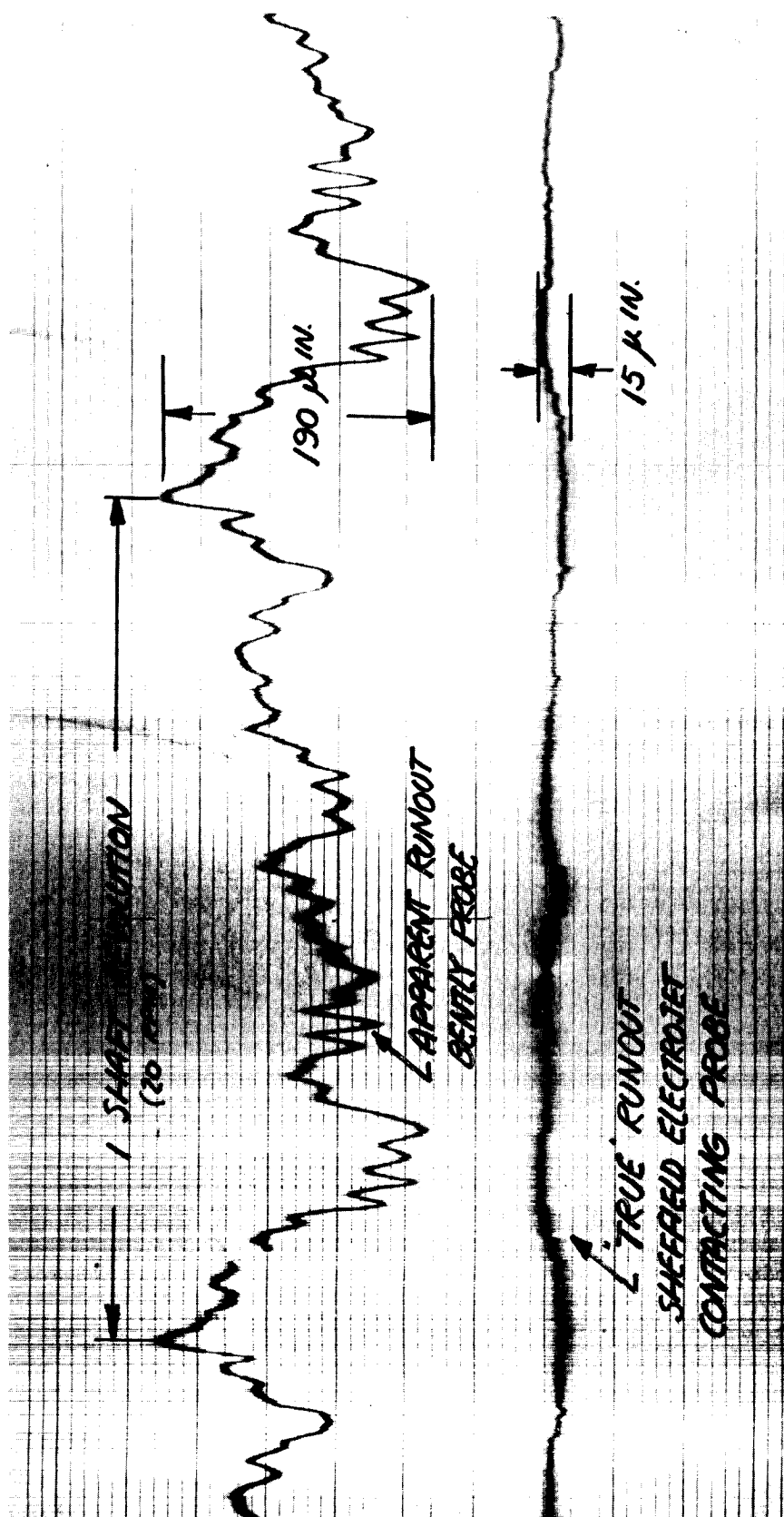


Figure 5. True and Apparent Shaft Runout. Type 420 S.S. Shaft 1.25" Dia.

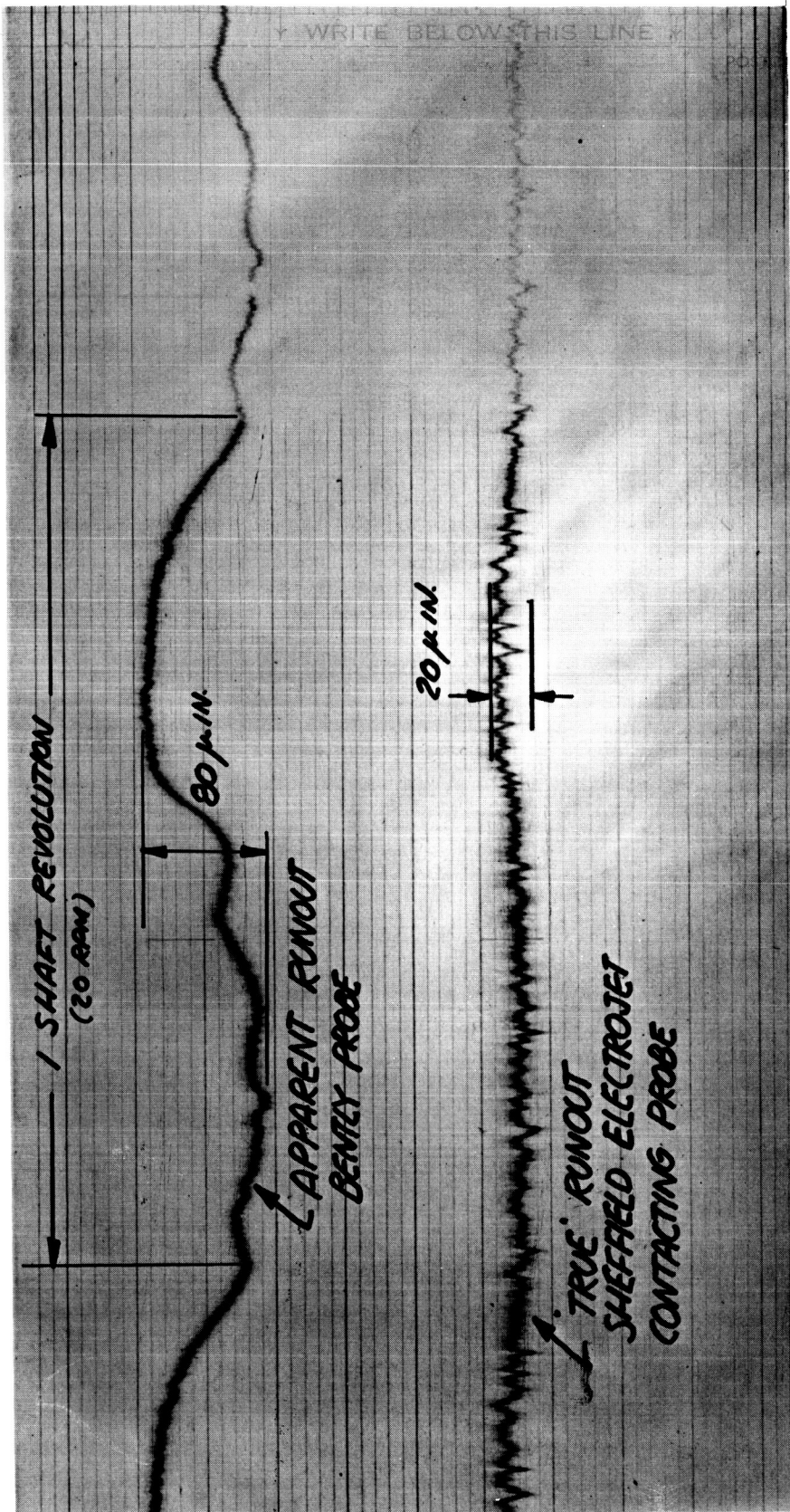


Figure 6. True and Apparent Shaft Runout. Type 420 S.S. Shaft 1.25" Dia.
With Silver Plate 0.010" Thick.

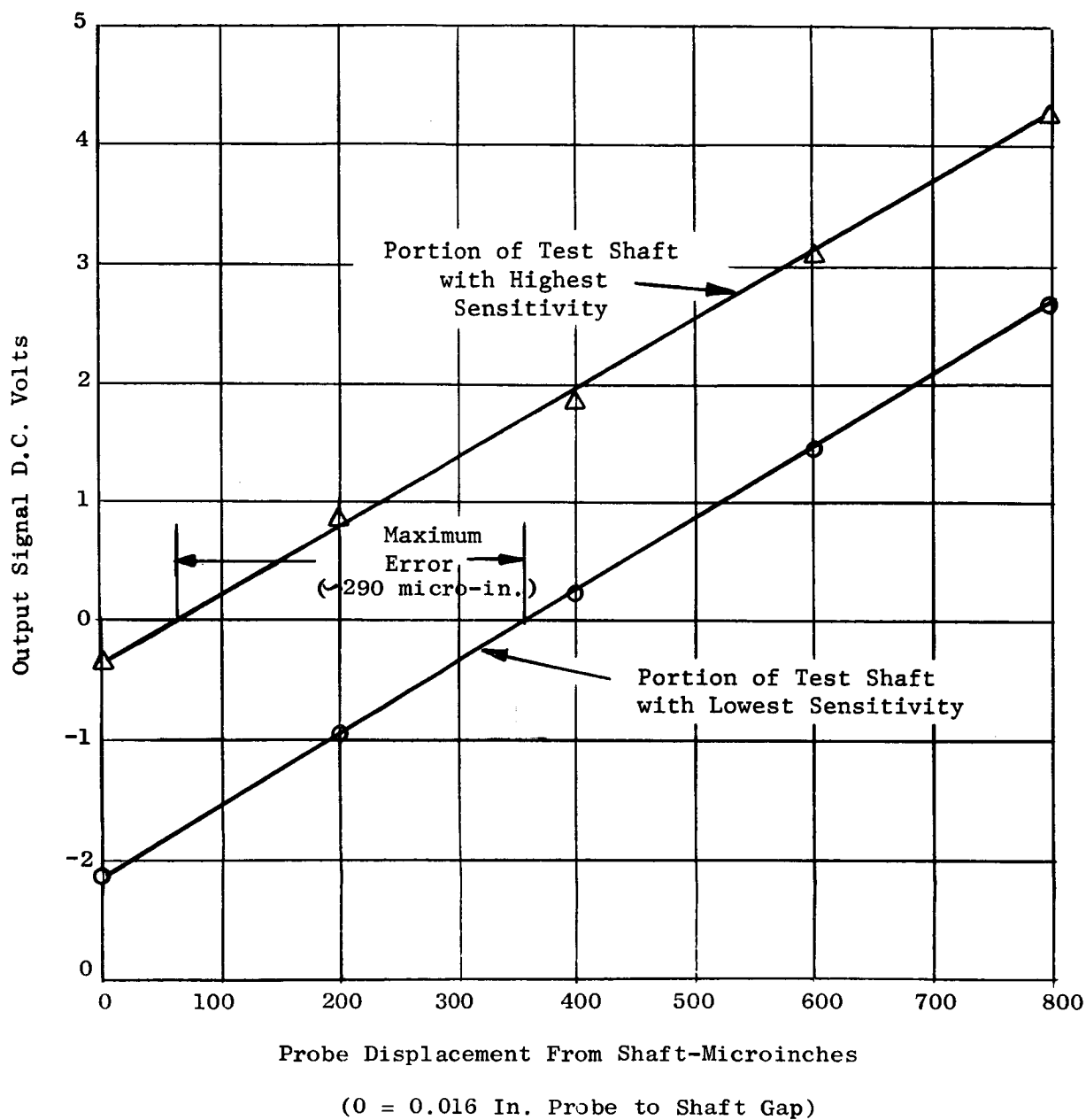


Figure 7. Maximum Variation in Bently Probe Calibration Over the Circumference of a 420 S.S. Shaft Because of Non-homogeneities in the Shaft Material.

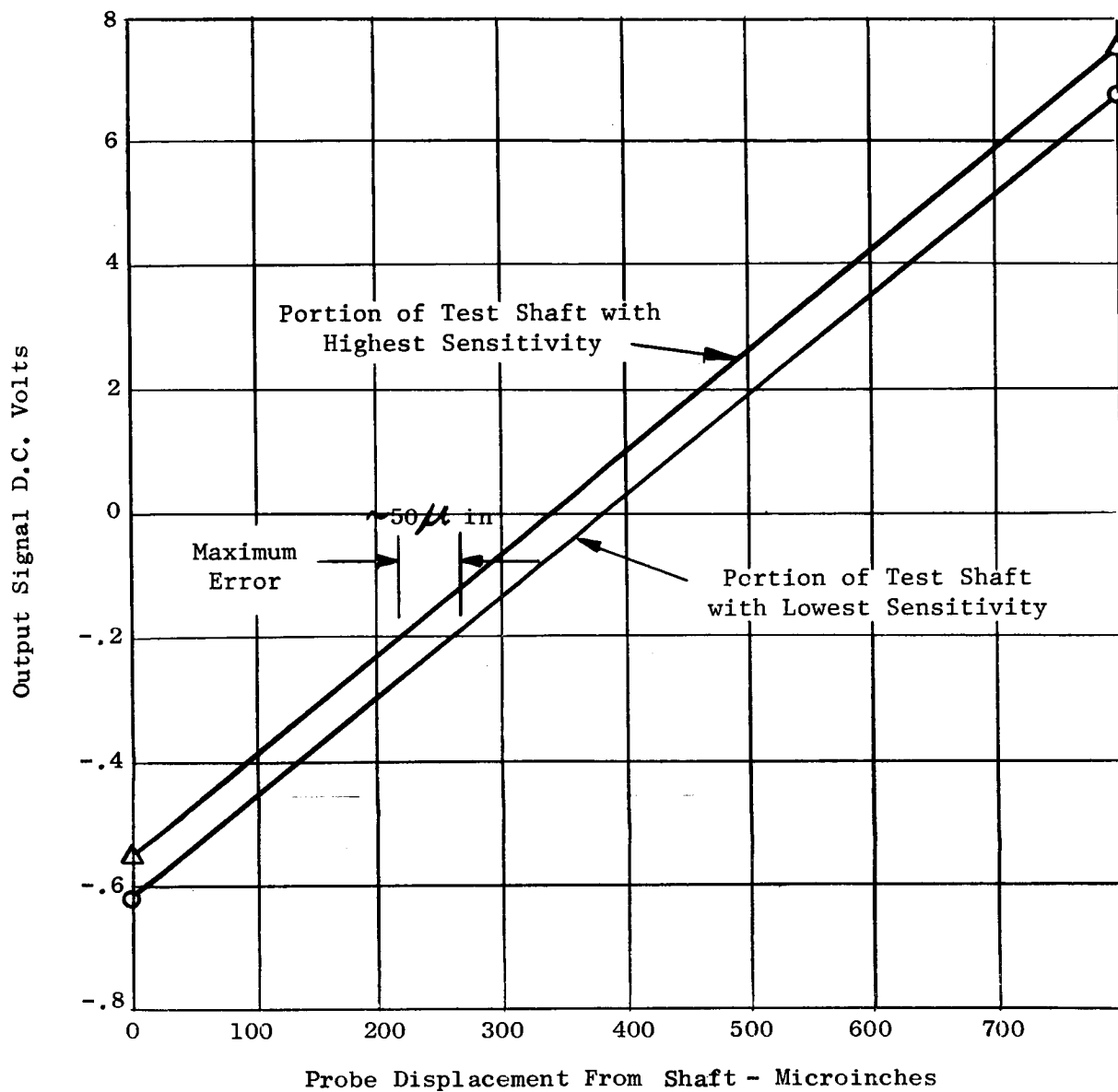


Figure 8. Maximum Variation in Bently Probe Calibration Over the Circumference of a 420 S.S. Shaft Overlaid with 0.005 Inch Silver Plate Because of Non-homogeneities in the Plating.

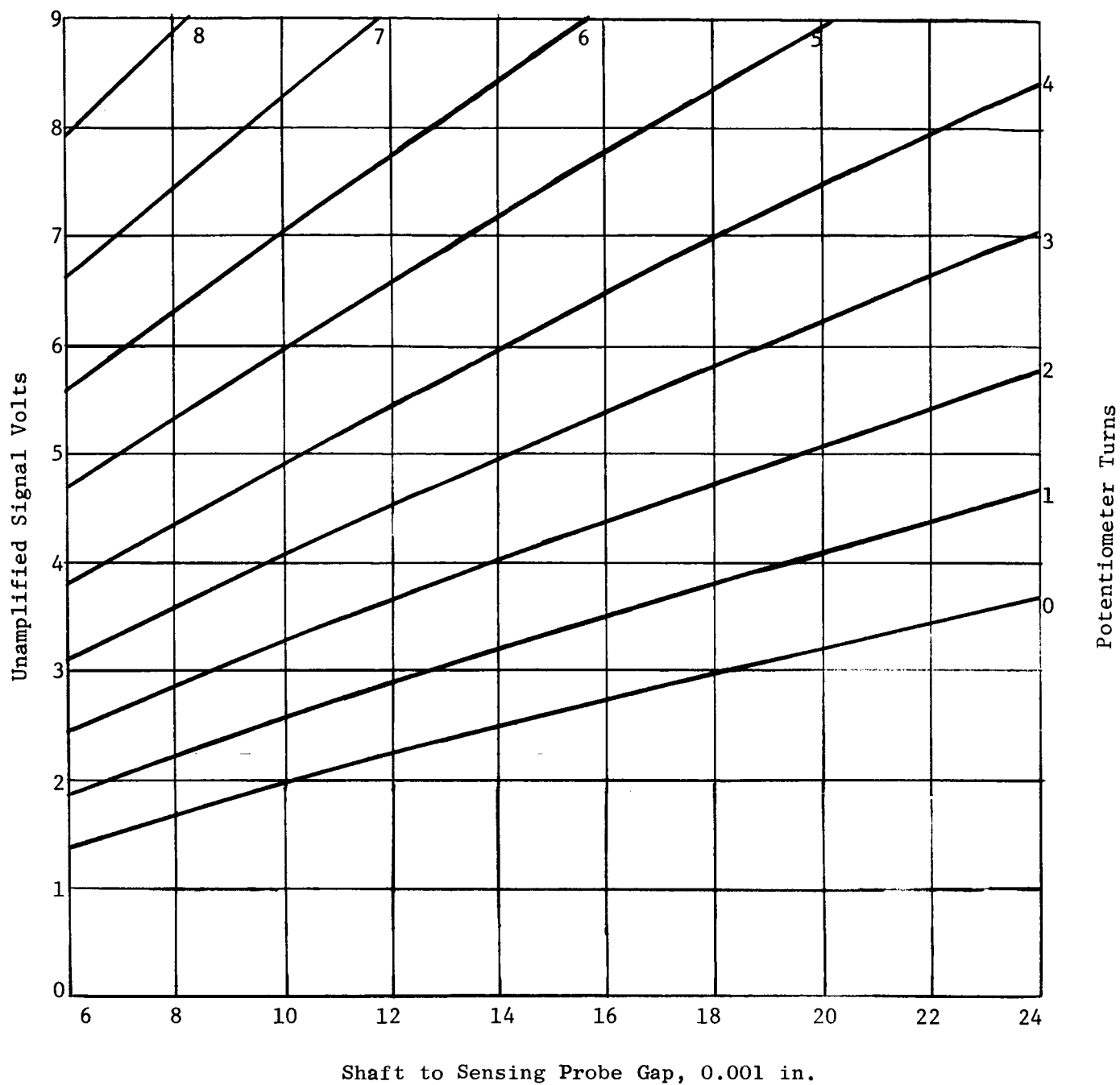


Figure 9. Typical Calibration Curves - Bently Distance Detector.

Probe Head H-1-084-3 Serial No. 15289

Distance Detector D252R Serial No. 5519

Shaft: 0.005 In. Silver Plate Teflon Tip on Probe Head:
0.005 In. Thick

Distance in 0.001 In. Between Probe and Shaft

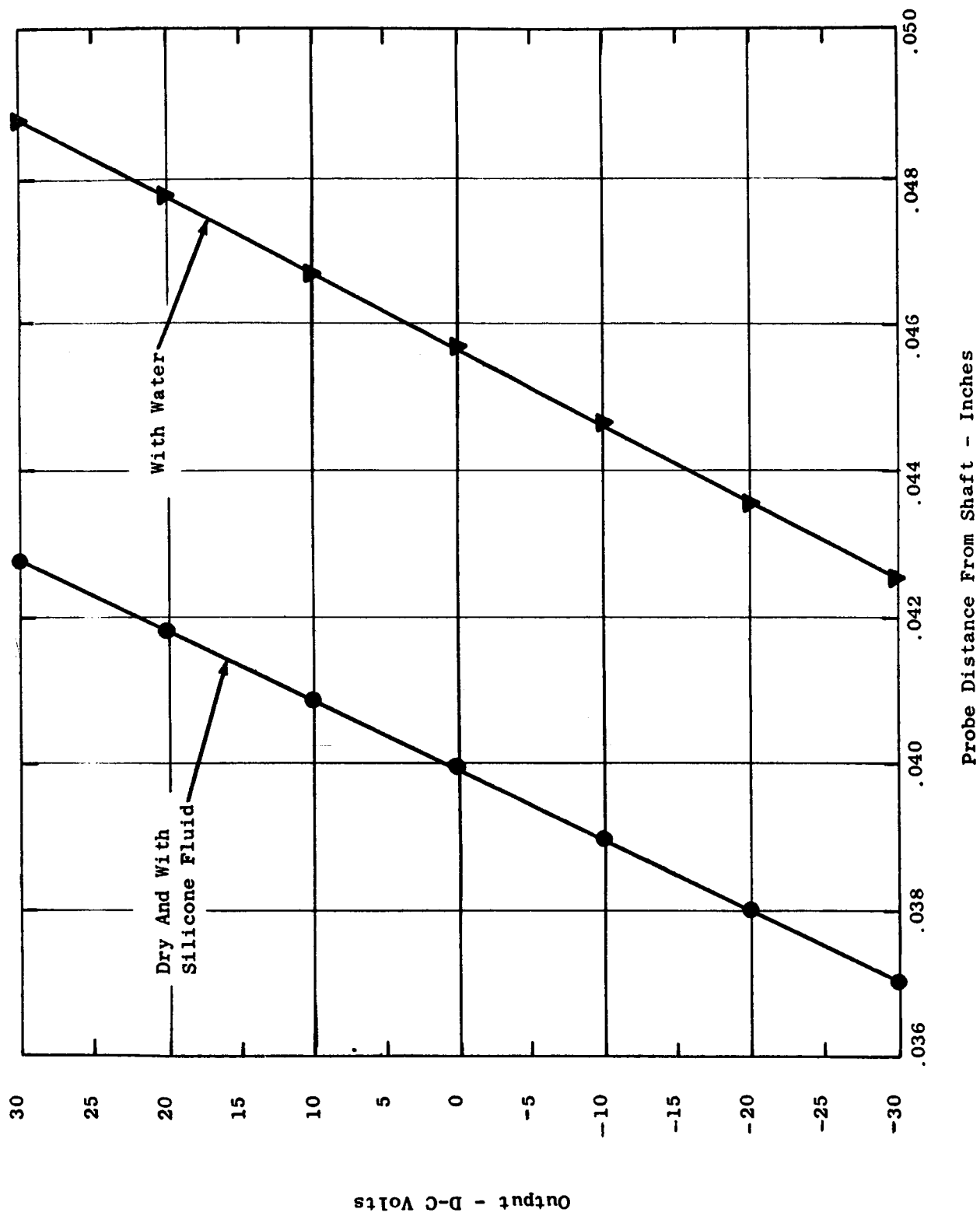


Figure 10. Proximity Gage Static Calibration for Various Media.

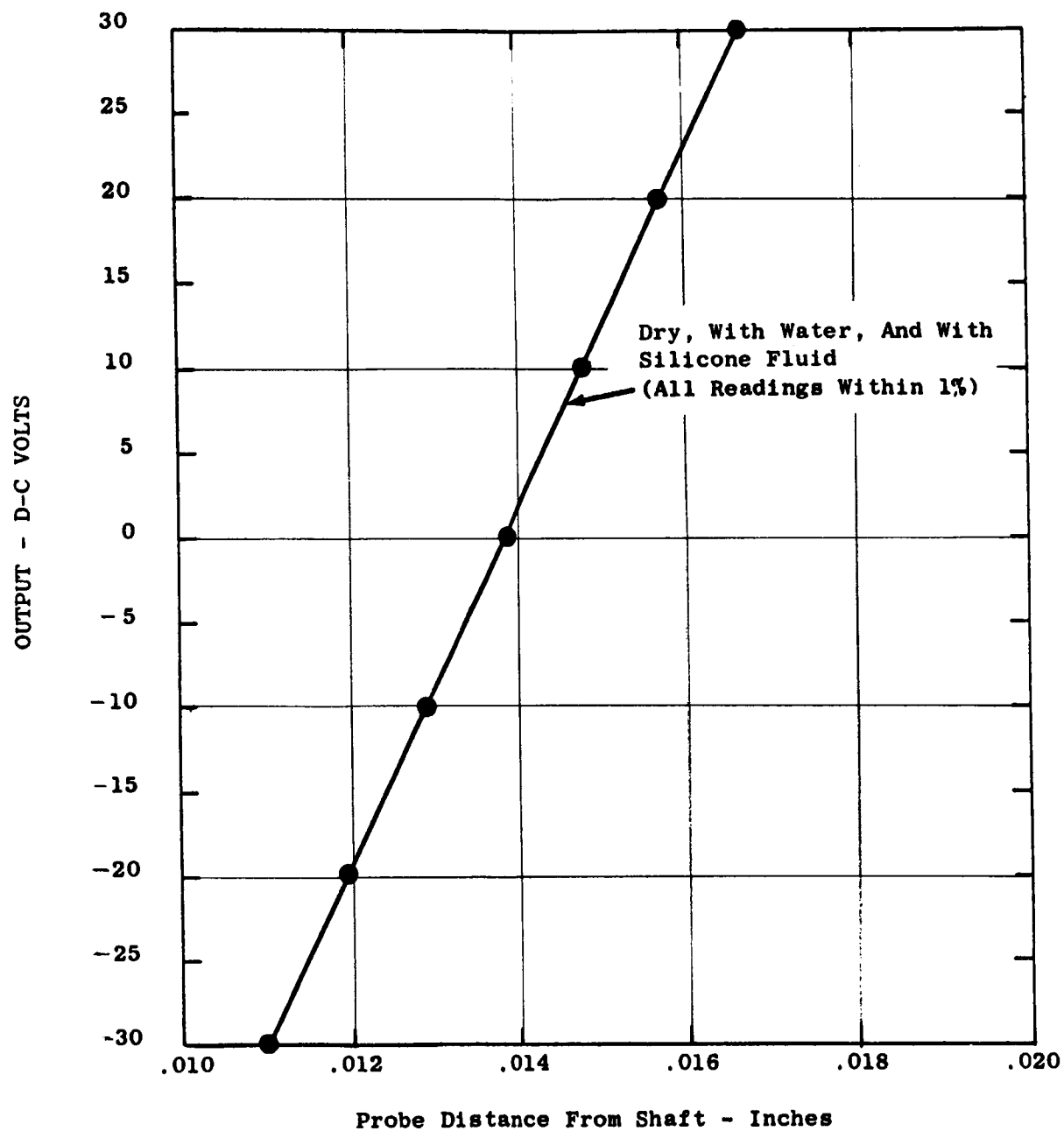


Figure 11. Proximity Probe Static Calibration Curve, Probe Tip is Shielded With a Teflon Cap.

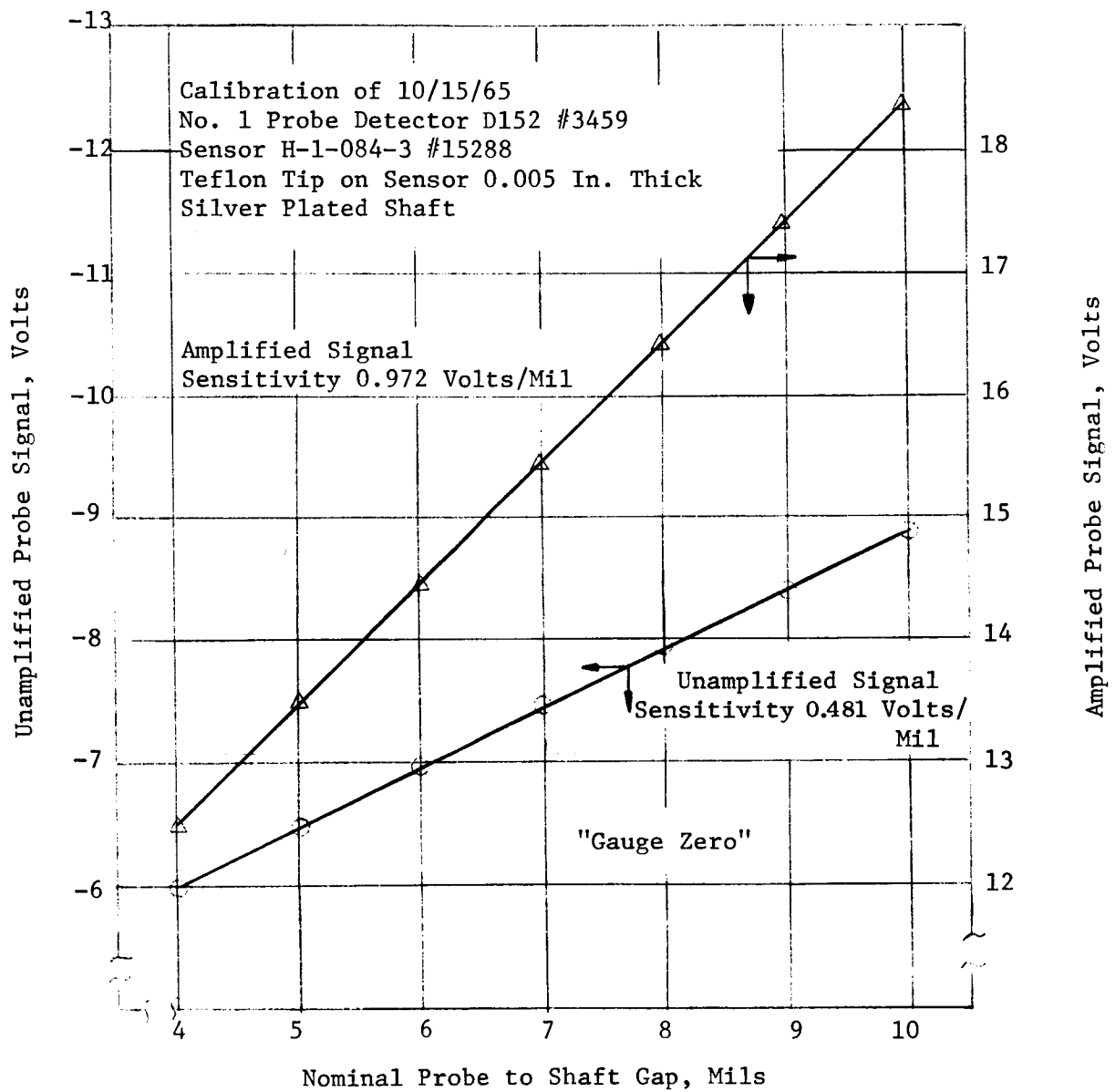


Figure 12. Bently Detection System Calibration No. 1 Probe, Detector D152.

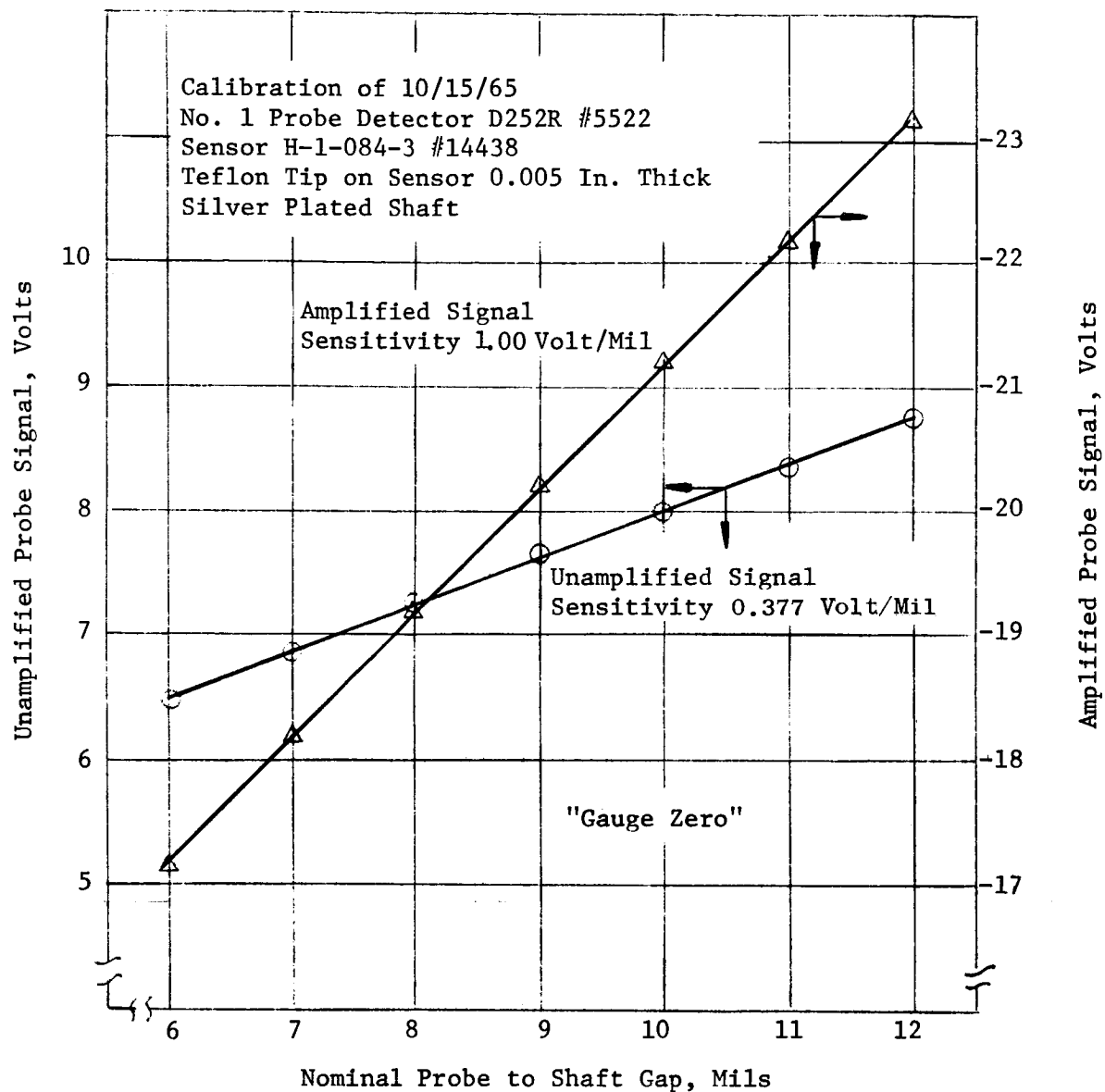


Figure 13. Bently Detection System Calibration, No. 1
 Probe Detector D252R.

No. 1 Probe Pair Calibration of 10/15/65
D152 #3459 Sensor #15288 "Gauge Zero" 7 Mils
D252R #5522 Sensor #14438 "Gauge Zero" 9 Mils

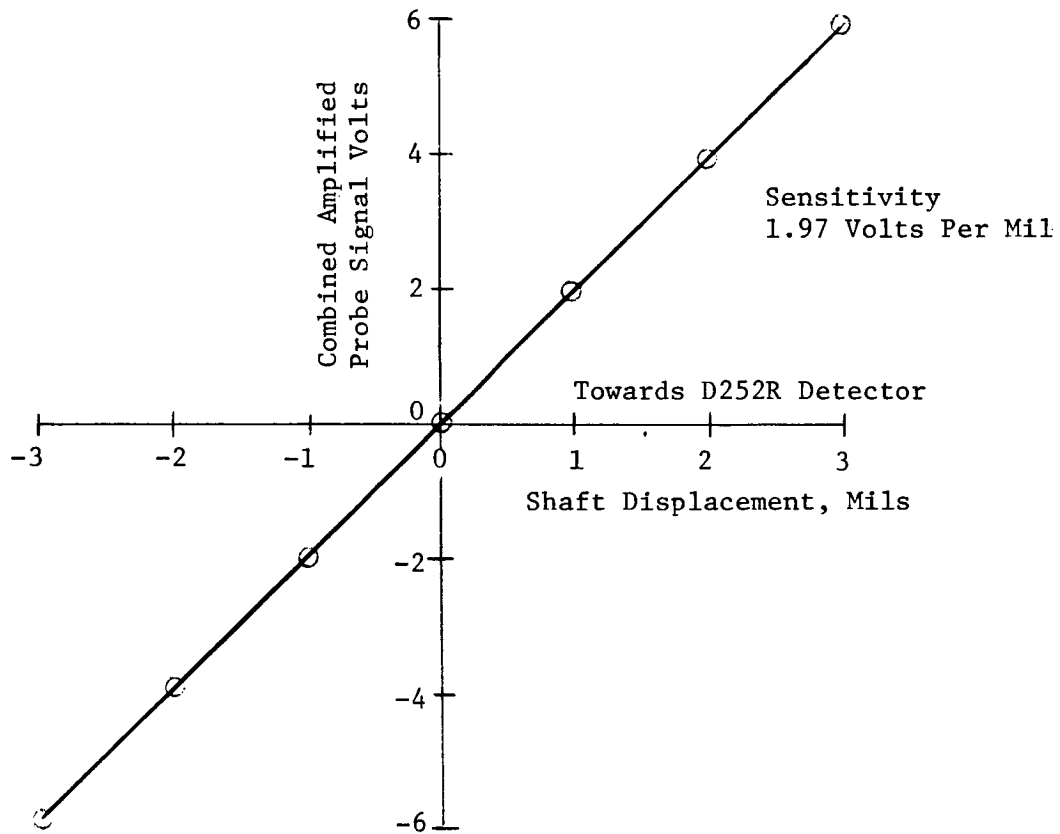


Figure 14. Bently Detection System Calibration, No. 1 Probe Pair, Combined Probes.

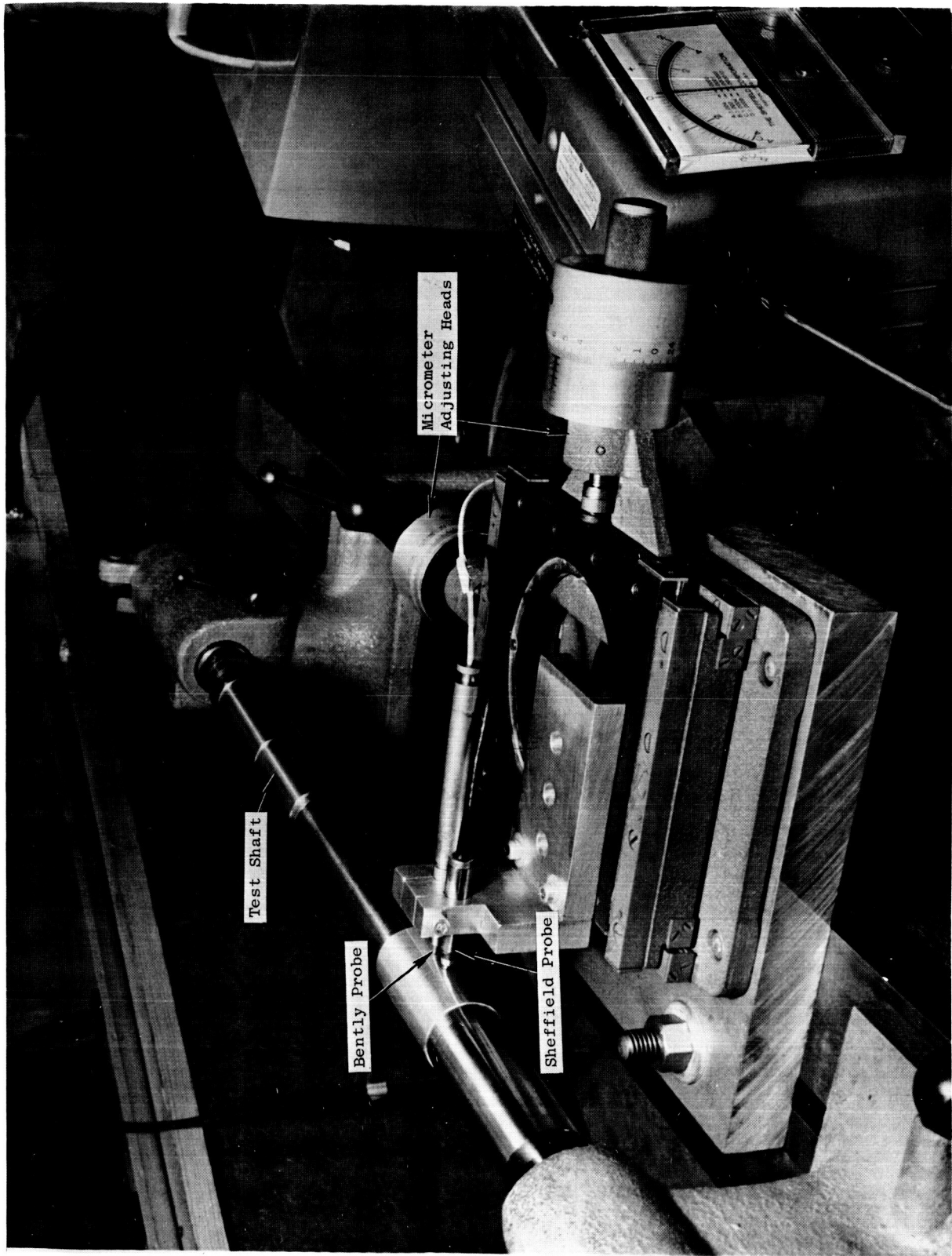
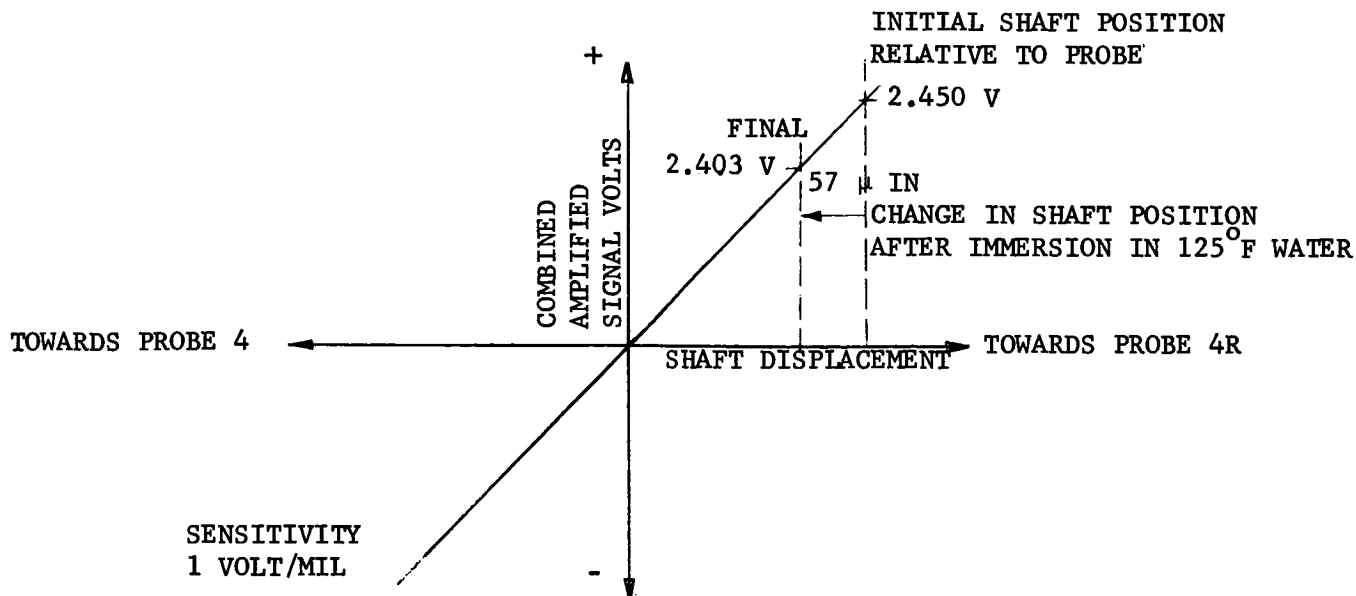
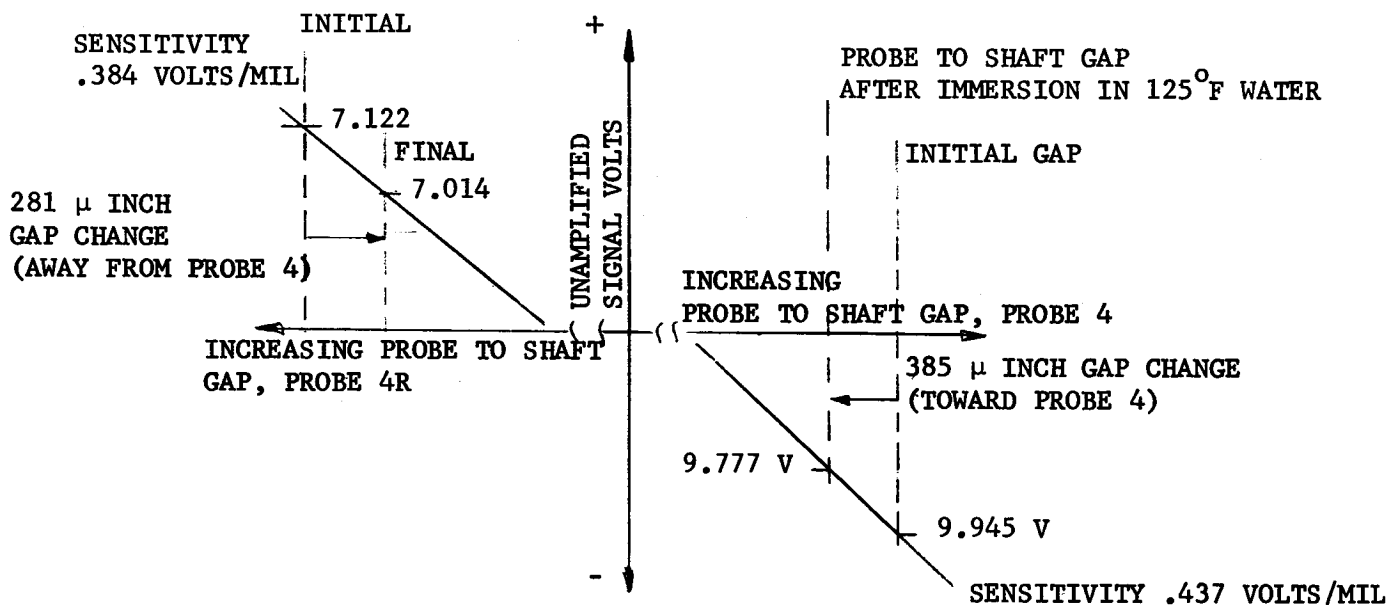


Figure 15. Calibration Test Device

1" = 4.5"



CHANGE IN SHAFT POSITION AS SENSED BY COMBINED GAUGES 4 AND 4R



CHANGE IN SHAFT POSITION AS SENSED BY INDIVIDUAL GAUGES 4 AND 4R

PROBE 4 DIST. DETECTOR NO. 3458, SENSOR NO. 15287
PROBE 4R DIST. DETECTOR NO. 5521, SENSOR NO. 15281

Figure 16. Demonstration of Temperature Growth Compensation
Using Opposed Gauges No. 4 and 4R

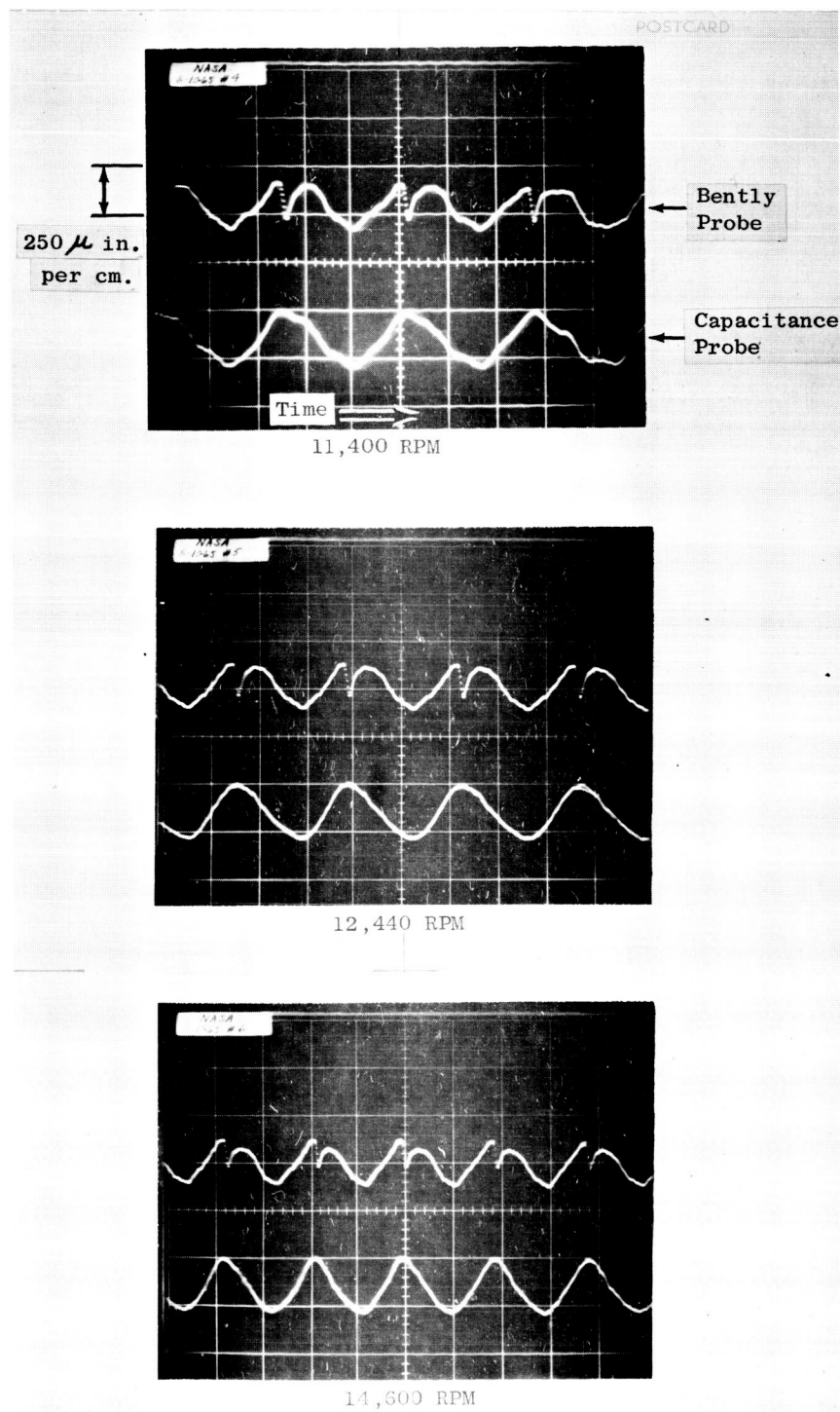


Figure 17. Comparison of Shaft Runout Measurements Bently and Capacitance Probes at Various Speeds.

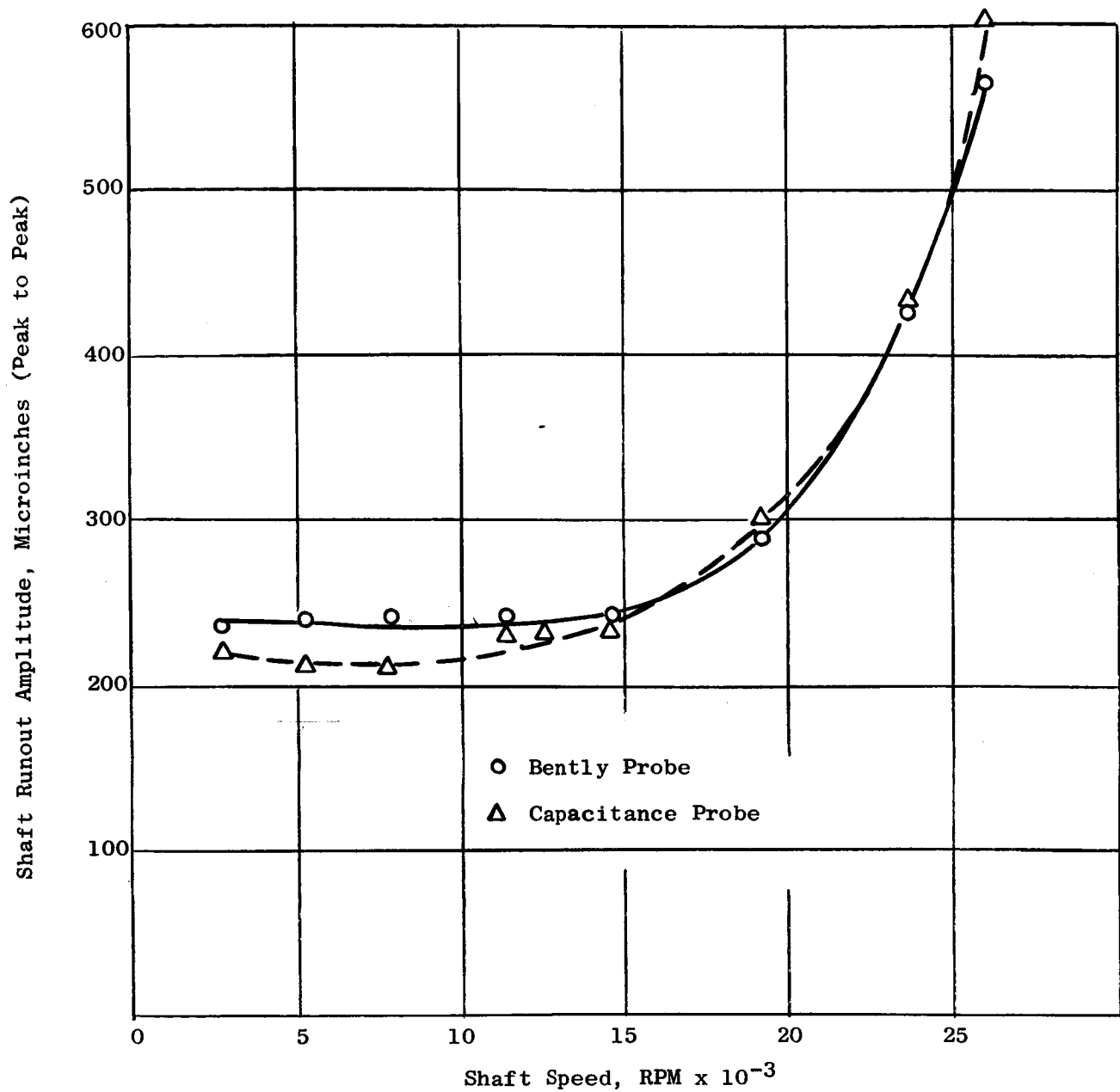
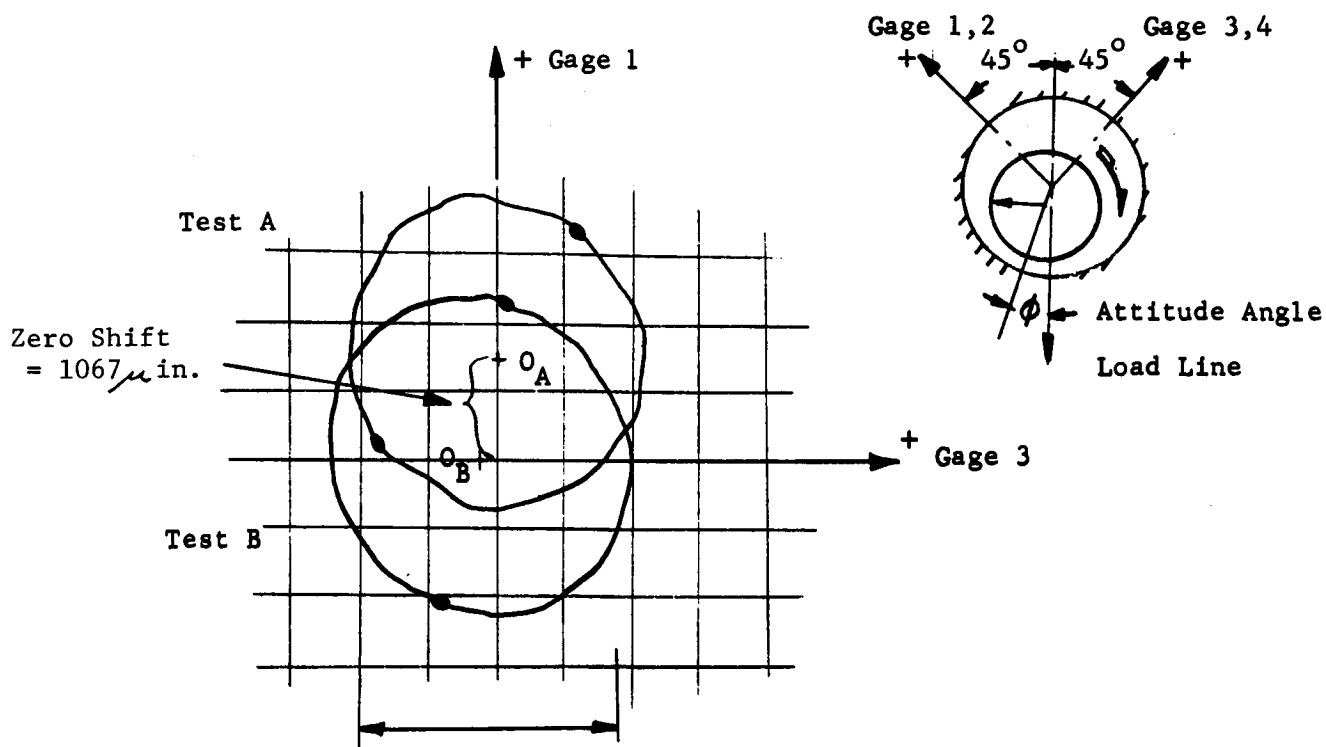


Figure 18. Comparison of Shaft Runout Measurements Using Bently and Capacitance Probes.



Calculated Brg. Diametral Clearance = 3 mils
 0.2 volt/Cm. Scope sensitivity; 0.25 volts/mil gage-scope
 calib.

Gage zero shift with speed

Two axial groove bearing $L/D = 1$

3 mil diametral clearance shaft

Data of November 4, 1963

Test A - Half frequency whirl at 17.5 cps shaft speed

D.C. voltmeter readings

#1 gage - 1.8V calibration .09628 mils/volt

#3 gage - 2.3V calibration .09706 mils/volt

Test B - Half frequency whirl at 168 cps shaft speed

D.C. Voltmeter readings

#1 gage - 13.2V

#3 gage - 3.8V

Figure 19. Gage Zero Shift with Speed.

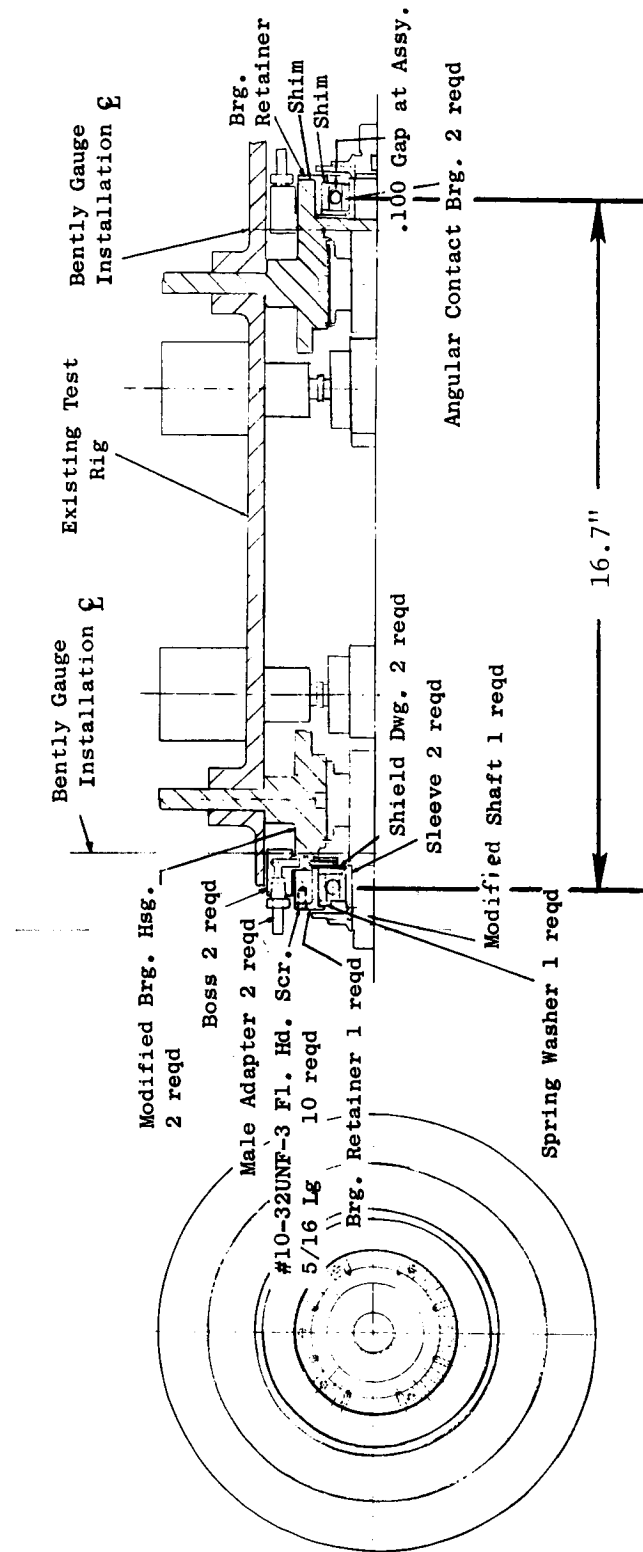
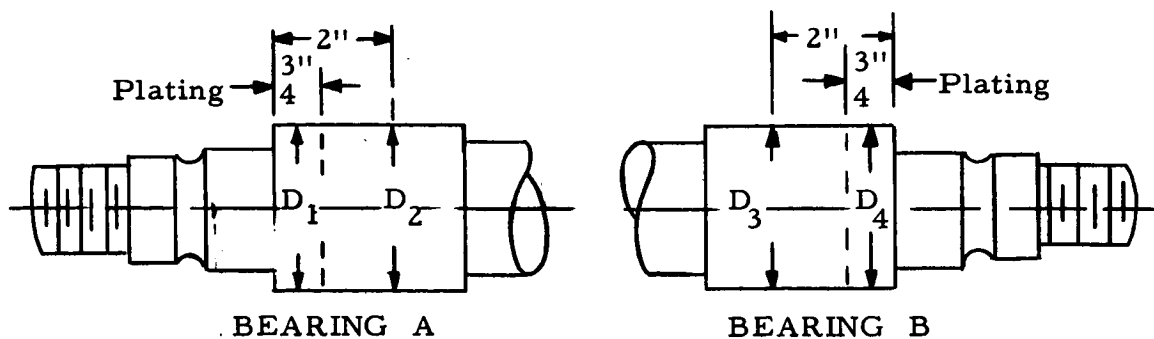


Figure 20. Gauge Check-Out Test Rig.



Test Shaft No. 3

Dwg. 4012000-782
Mod. per Dwg. 119C2948

SHAFT CONDITION	BEARING A	BEARING B
Before Grinding Sections to be Plated (Headstock Center Runout 4×10^{-6} in.)	$D_2 = 1.2499''$ D_2 Runout = $15 \times 10^{-6}''$	$D_3 = 1.2499''$ D_3 Runout = $12 \times 10^{-6}''$
After Grinding Bearing Section to be Plated	$D_1 = 1.2395''$ D_1 Runout = $10 \times 10^{-6}''$	$D_4 = 1.2395''$ D_4 Runout = $10 \times 10^{-6}''$
After Plating Bearing Section and Before Final Grind on Plate	D_2 Runout = $8 \times 10^{-6}''$	D_3 Runout = $13 \times 10^{-6}''$
After Plating Bearing Section and After Final Grind on Plate	$D_1 = 1.2494''$ D_1 Runout = $15 \times 10^{-6}''$ $D_2 = 1.2499''$ D_2 Runout = $25 \times 10^{-6}''$	$D_4 = 1.2494''$ D_4 Runout = $17 \times 10^{-6}''$ $D_3 = 1.2499''$ D_3 Runout = $18 \times 10^{-6}''$

Figure 21. Measurements on Shaft for Dynamic Gage Evaluation Test

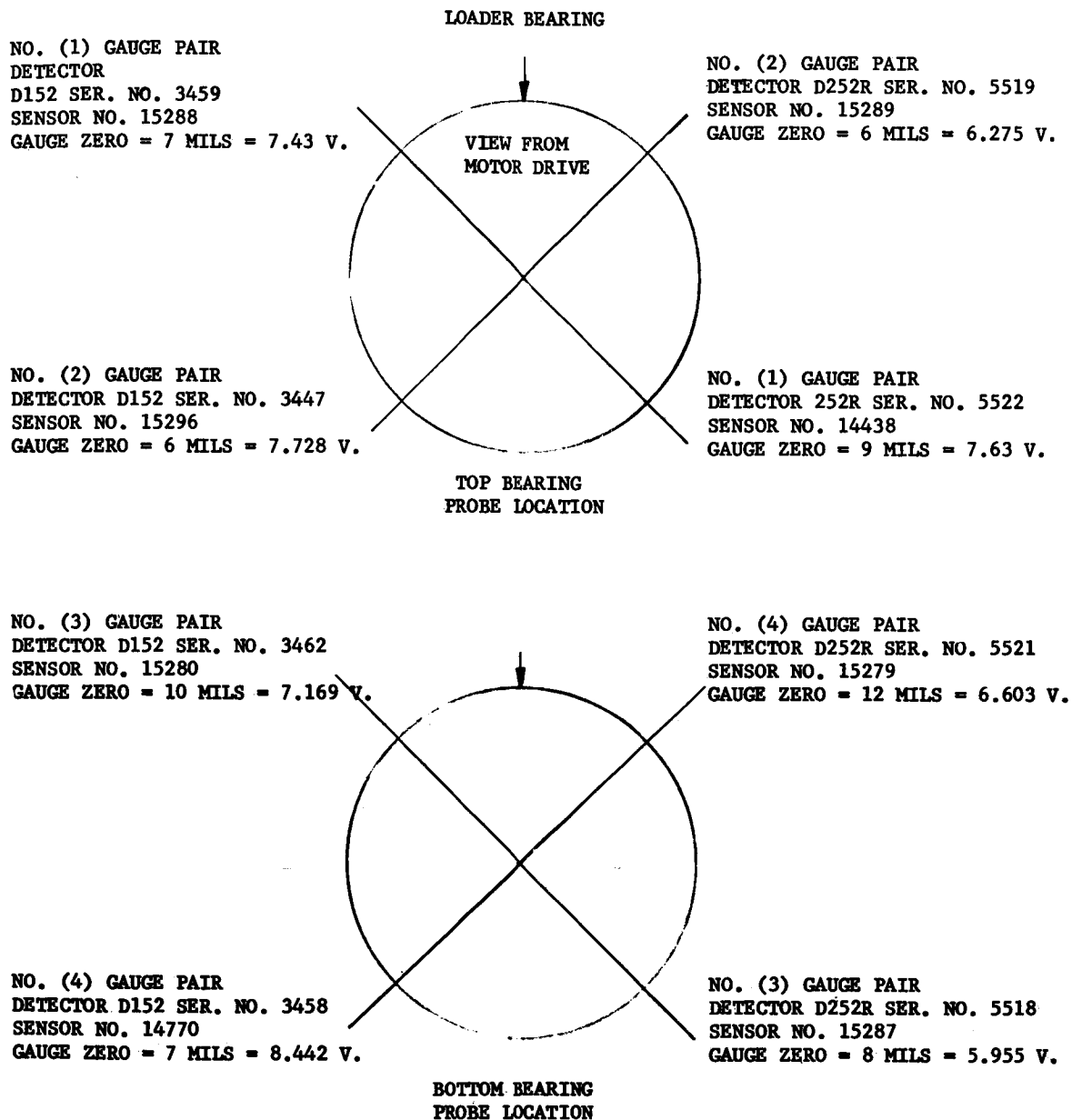
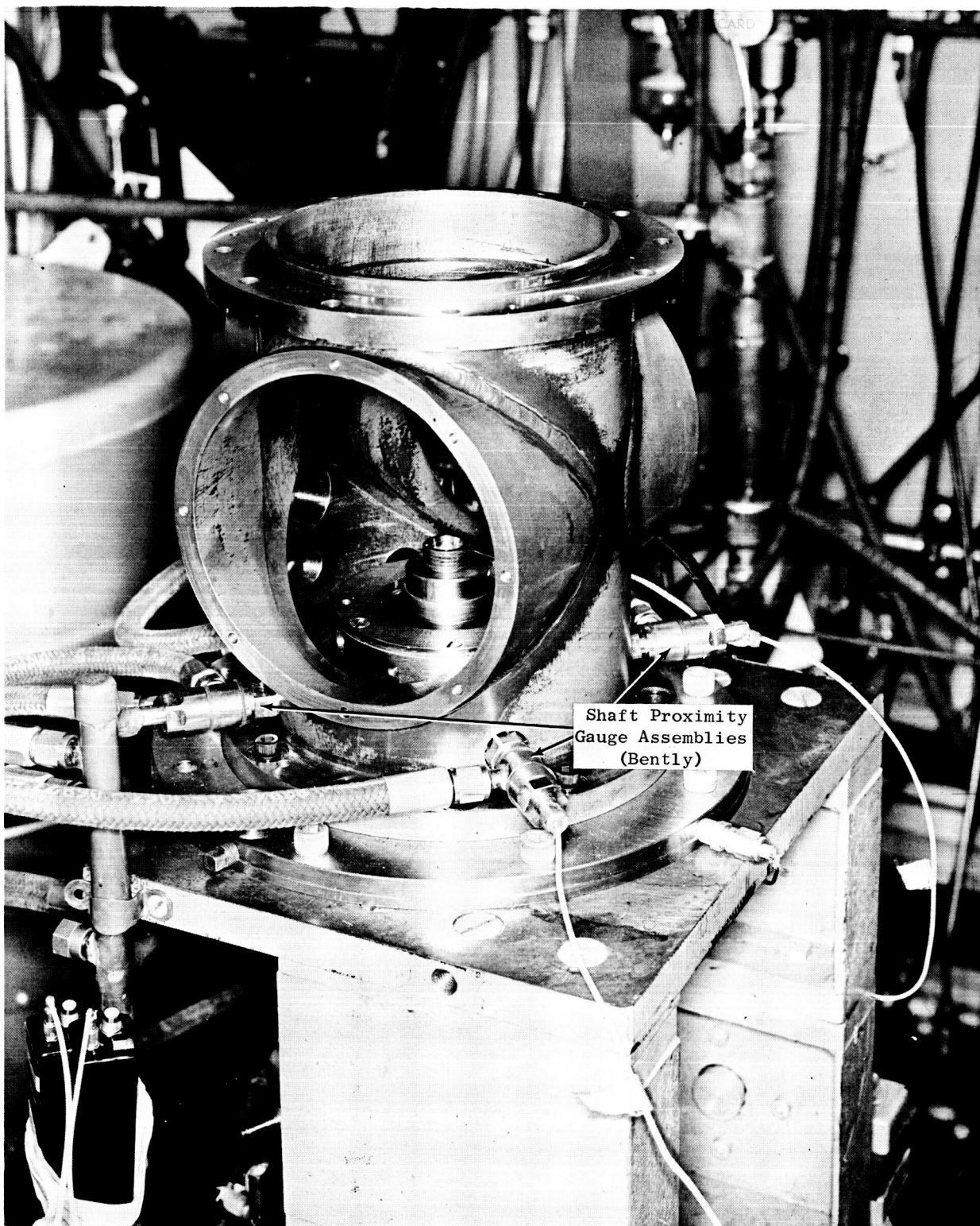


Figure 22. Location of Probes for Dynamic Gauge Tests of 10/22/65.

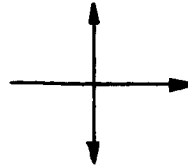


1"=2.5"

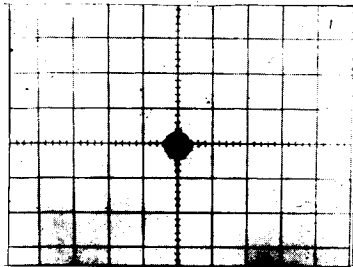
Figure 23. View Showing Opposed Gauge Installation for Dynamic Gauge Evaluation.

DISPLACEMENT GAUGE DYNAMIC EVALUATION
 OPPOSED PROBES MOUNTED IN TEST RIG USING BALL-BEARING MOUNTED SHAFT
 TEST OF 10/22/65 - PROBE CALIBRATIONS OF 10/19/65
 SHAFT ORBITS MEASURED IN TWO PLANES ADJACENT TO UPPER AND LOWER TEST BEARING
 PROBES CENTERED ON SCOPE AT ZERO SPEED

No. 2,4 PROBE PAIRS

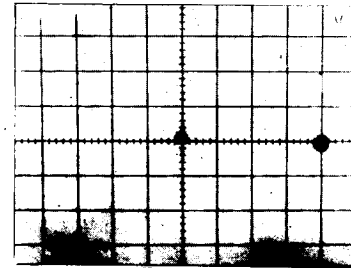


No. 1,3 PROBE PAIRS



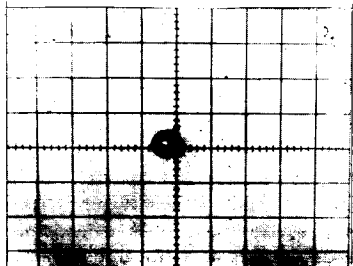
#1

Scope Calibration 250μin./cm
 12,000 RPM
 Oil to Ball Bearings
 No Water to Test Bearings
 No Air to Probe Holders



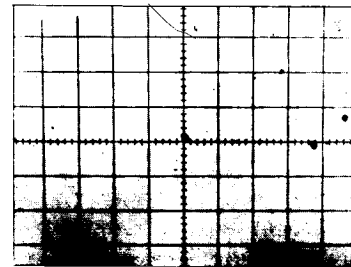
#4

Scope Calibration 500μin./cm
 12,000 RPM
 Conditions Same As #3
 Drifting of Probe Signal in Lower
 Bearing in Direction of #3 Probe



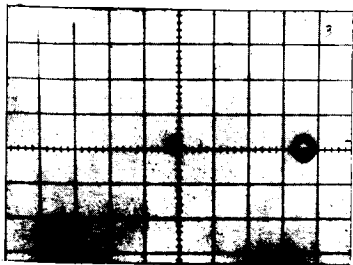
#2

Scope Calibration 250μin./cm
 12,000 RPM
 Oil to Ball Bearings
 No Water to Test Bearings
 Air at 20 psi to Probe Holders



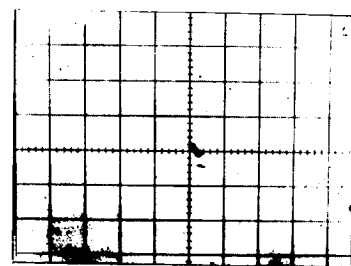
#5

Scope Calibration 500μin./cm
 0 RPM
 Air Only to Probe Holders



#3

Scope Calibration 250μin./cm
 12,000 RPM
 Oil to Ball Bearings
 Water to Test Bearings
 Air at 20 psi to Holder



#6

Scope Calibration 500μin./cm
 0 RPM
 Air Only to Probe Holders
 1/2 Hr. Elapsed Time After Picture
 Probe No. 3 Nearly Returned to Zero

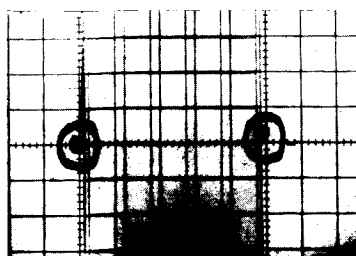
Figure 24. Oscilloscope Photographs - Orbiting of Ball Bearing Mounted Shaft.- Data of 10/22/65.

DISPLACEMENT GAUGE DYNAMIC EVALUATION
 OPPOSED PROBES MOUNTED IN TEST RIG USING BALL-BEARING MOUNTED SHAFT
 TEST OF 11/10/65 - PROBE CALIBRATION 10/19/65
 SHAFT ORBITS MEASURED IN TWO PLANES ADJACENT TO UPPER AND LOWER TEST BEARING
 PROBES CENTERED ON SCOPE AT ZERO SPEED
 SCOPE CALIBRATION 250 μ in./cm

No. 2,4 PROBE PAIRS



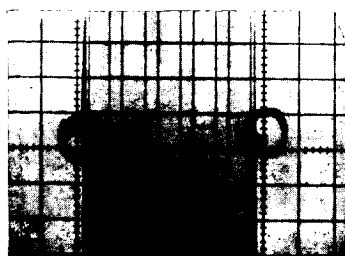
No. 1,3 PROBE PAIRS



#1

1:08 PM 1:23 PM

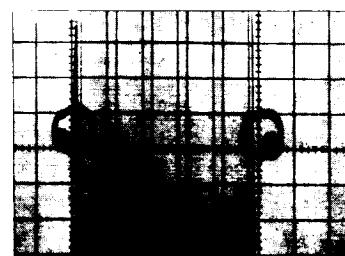
3600 RPM
Oil Only



#2

1:25 PM 1:35 PM

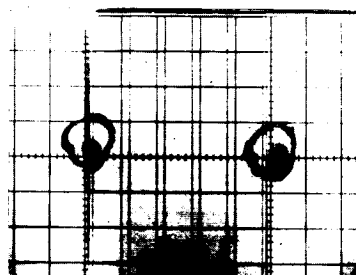
3600 RPM
Oil, Air, Water On



#3

1:26 PM 1:51 PM

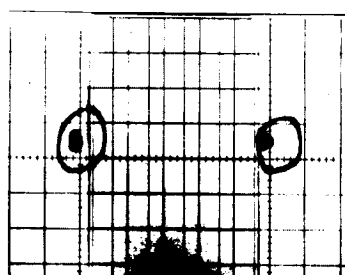
3600 RPM
Oil, Water On



#4

1:55 PM 2:10 PM

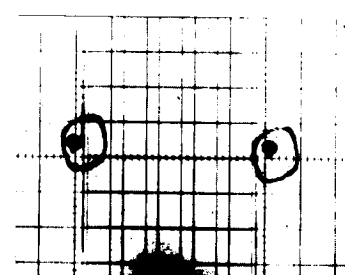
9000 RPM
Oil Only



#5

2:12 PM 2:26 PM

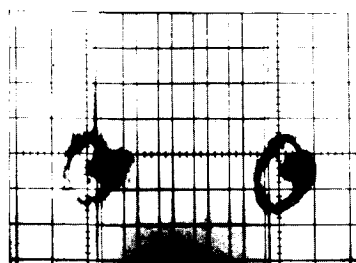
9000 RPM
Oil, Air, Water On



#6

2:28 PM 2:43 PM

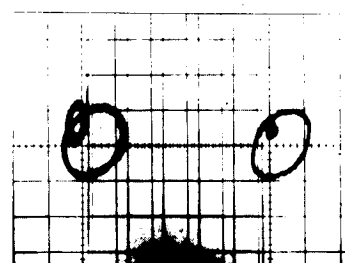
9000 RPM
Oil, Water On



#7

3:17 PM 3:31 PM

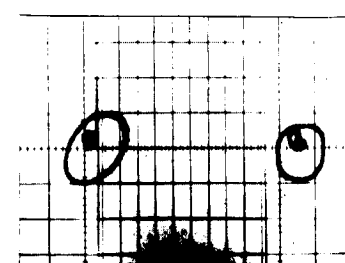
12,000 RPM
Oil Only



#8

3:33 PM 3:47 PM

12,000 RPM
Oil, Air, Water On



#9

3:45 PM 4:03 PM

12,000 RPM
Oil, Water On

Figure 25. Oscilloscope Photographs - Orbiting of Ball Bearing Mounted Shaft.- Data of 11/11/65.

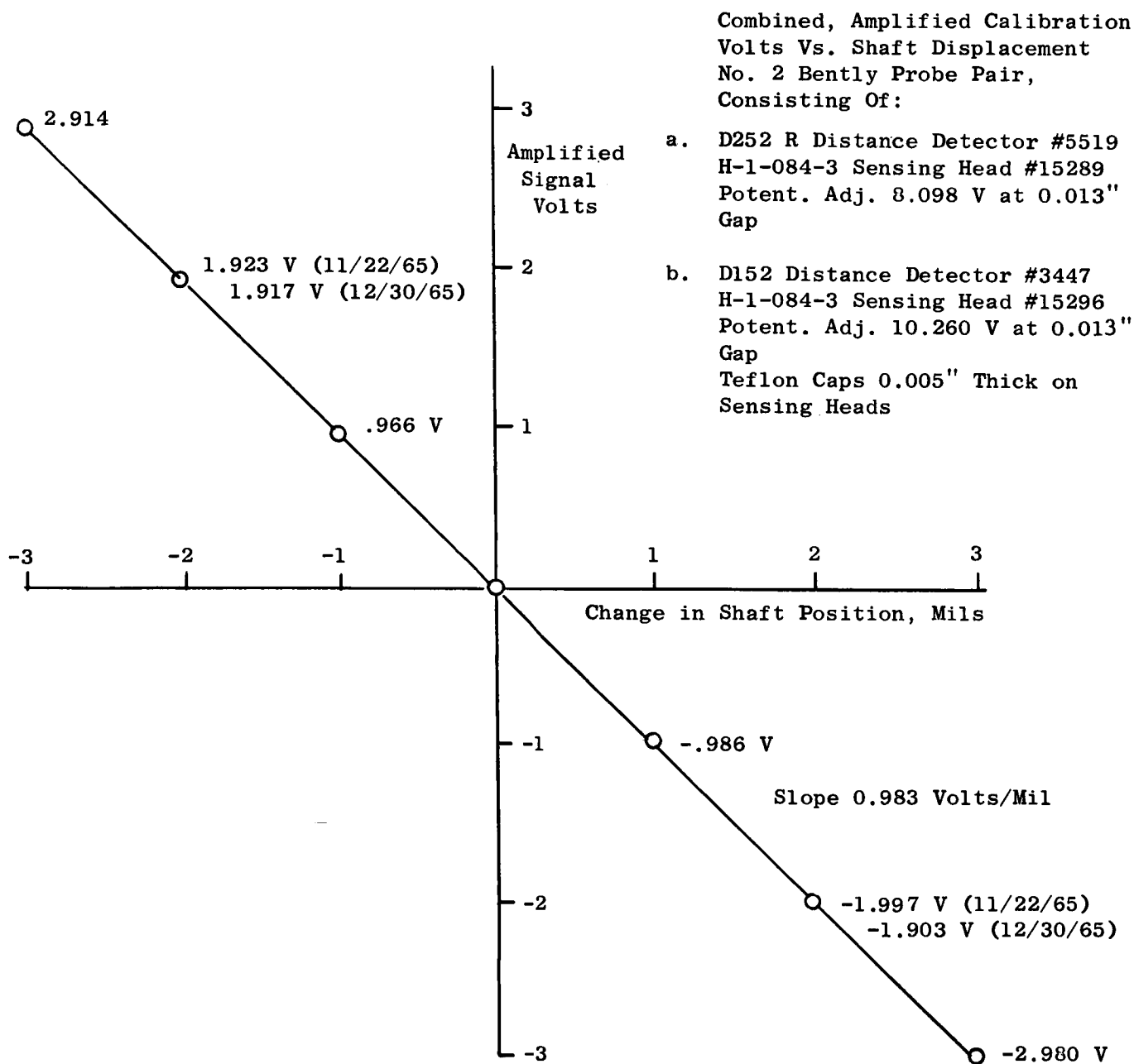


Figure 26. Calibration Curve - No. 2 Bently Displacement Gage Probe Pair.
Data of 11/22 and 12/30/65.

DISPLACEMENT GAUGE
DYNAMIC EVALUATION IN WATER ENVIRONMENT
SHAFT ORBITS AT VARIOUS SPEEDS
PROBES CENTERED ON SCOPE AT START-UP
200 MICROINCHES PER CM SENSITIVITY

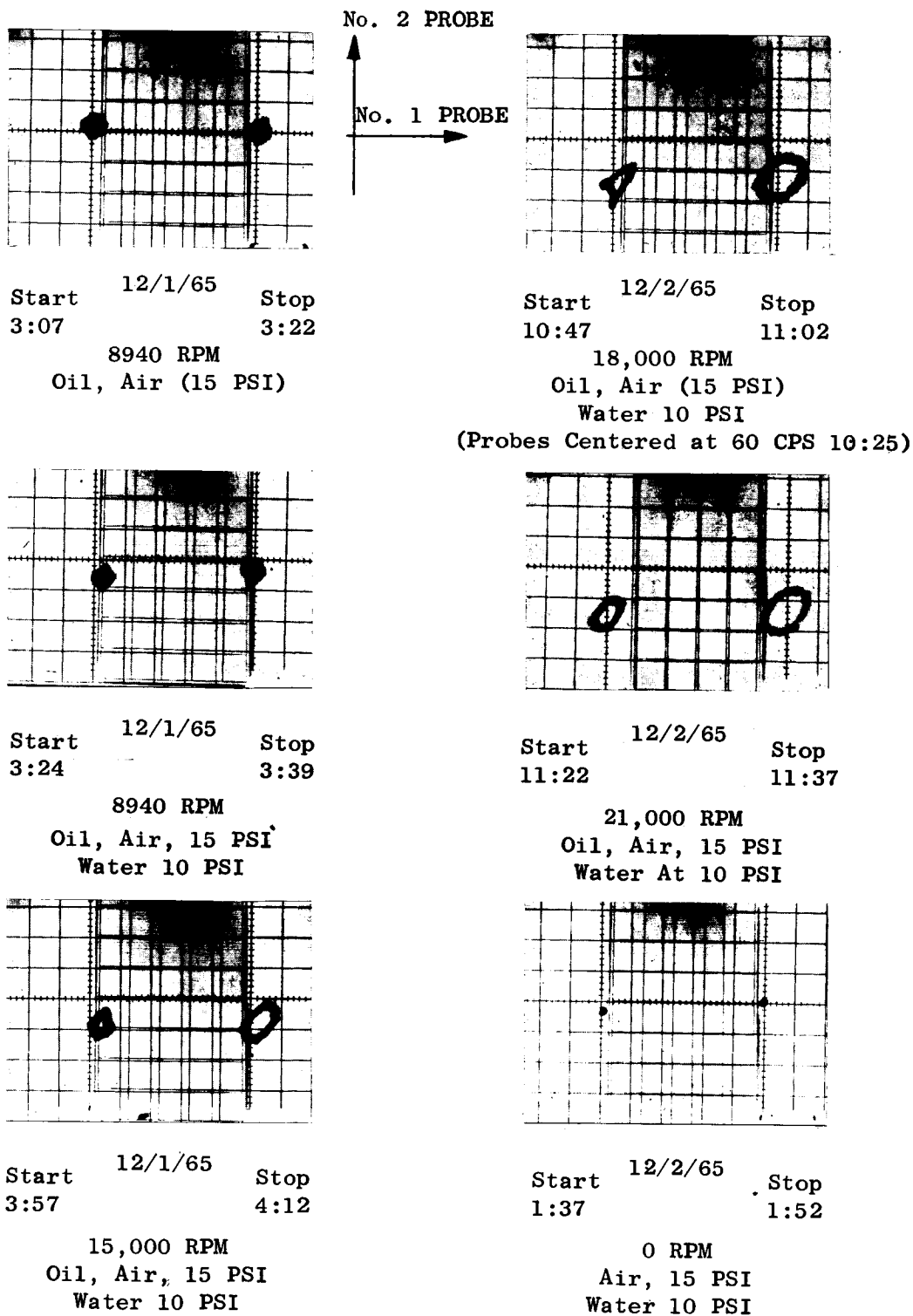


Figure 27. Oscilloscope Photographs - Orbiting of Ball Bearing Mounted Shaft.— Data of 12/1 and 12/2/65.

DISPLACEMENT GAUGE DYNAMIC EVALUATION
OPPOSED PROBES MOUNTED IN TEST RIG USING BALL-BEARING MOUNTED SHAFT
TEST OF 12/2/65, PROBE CALIBRATION OF 11/20-22/65
UPPER BEARING MEASUREMENTS, PROBES CENTERED ON SCOPE AT ZERO SPEED

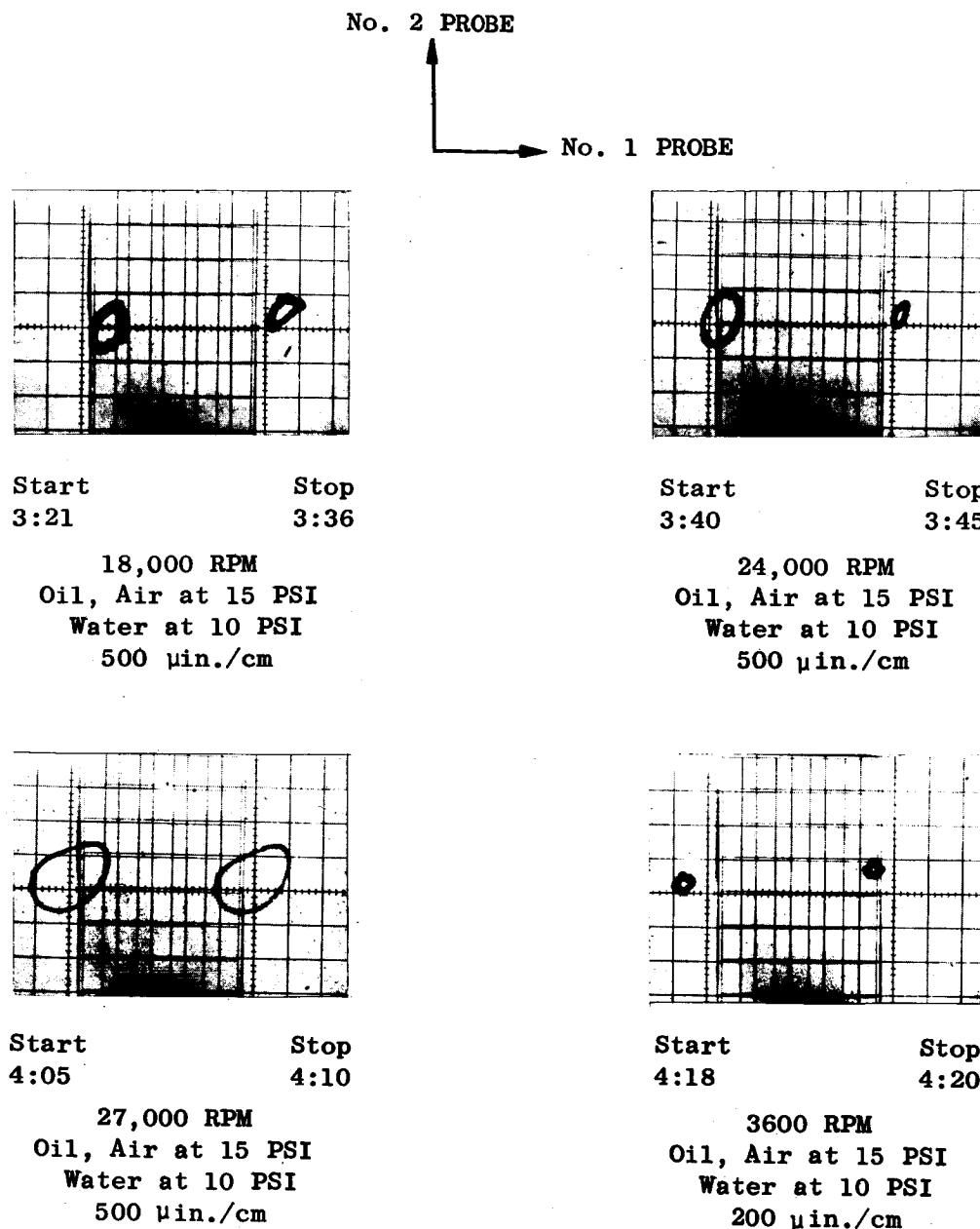


Figure 28. Oscilloscope Photographs - Orbiting of Ball Bearing Mounted Shaft.- Data of 12/2/65,

DISPLACEMENT GAUGE
DYNAMIC EVALUATION IN WATER ENVIRONMENT
BALL BEARING MOUNTED SHAFT

SPEED: 150 CPS (9000 RPM)
200 MICROINCHES PER CM SENSITIVITY
A = VIBRATIONAL AMPLITUDE, MICROINCHES
Z = APPARENT ZERO, MICROINCHES

DATA OF 12/6/65

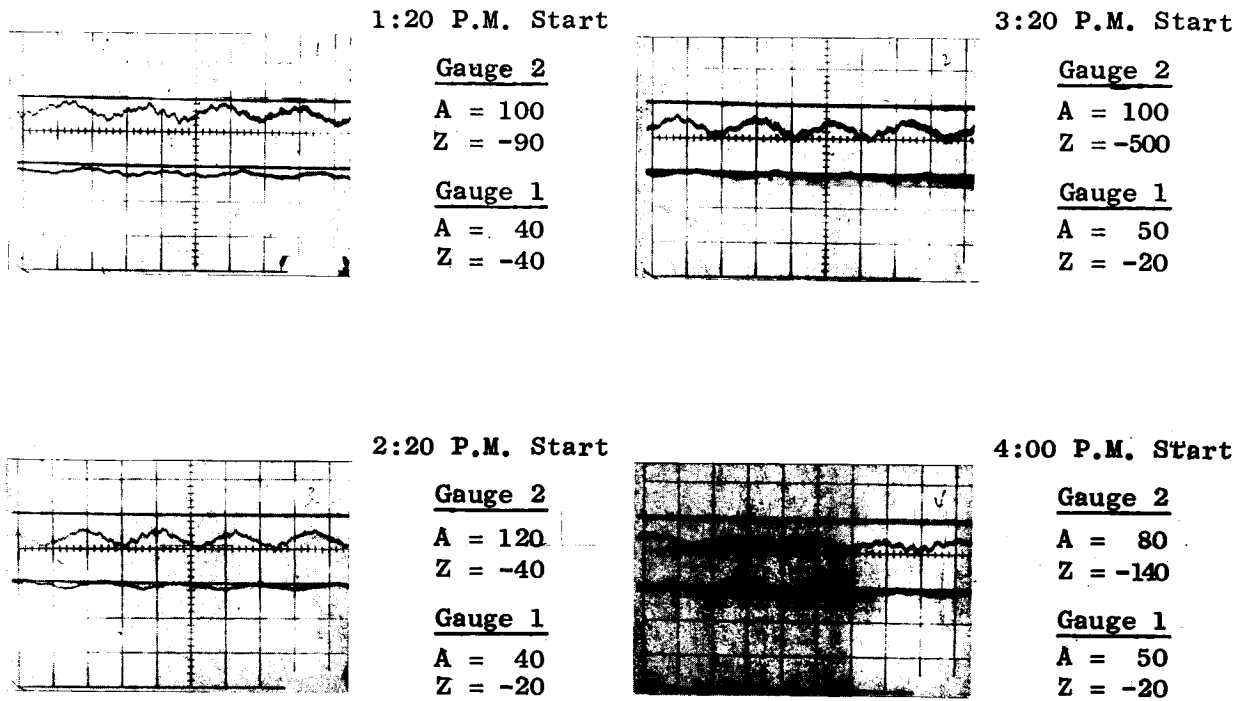


Figure 29. Oscilloscope Traces - Probe Signal vs. Time at 9000 rpm -
Data of 12/6/65

DISPLACEMENT GAUGE
DYNAMIC EVALUATION IN WATER ENVIRONMENT
BALL BEARING MOUNTED SHAFT

SPEED: 15,000 RPM

CALIBRATION: 200 MICROINCHES PER CM SENSITIVITY

A = VIBRATIONAL AMPLITUDE, MICROINCHES

Z = APPARENT ZERO, MICROINCHES

DATA OF 12/7/65

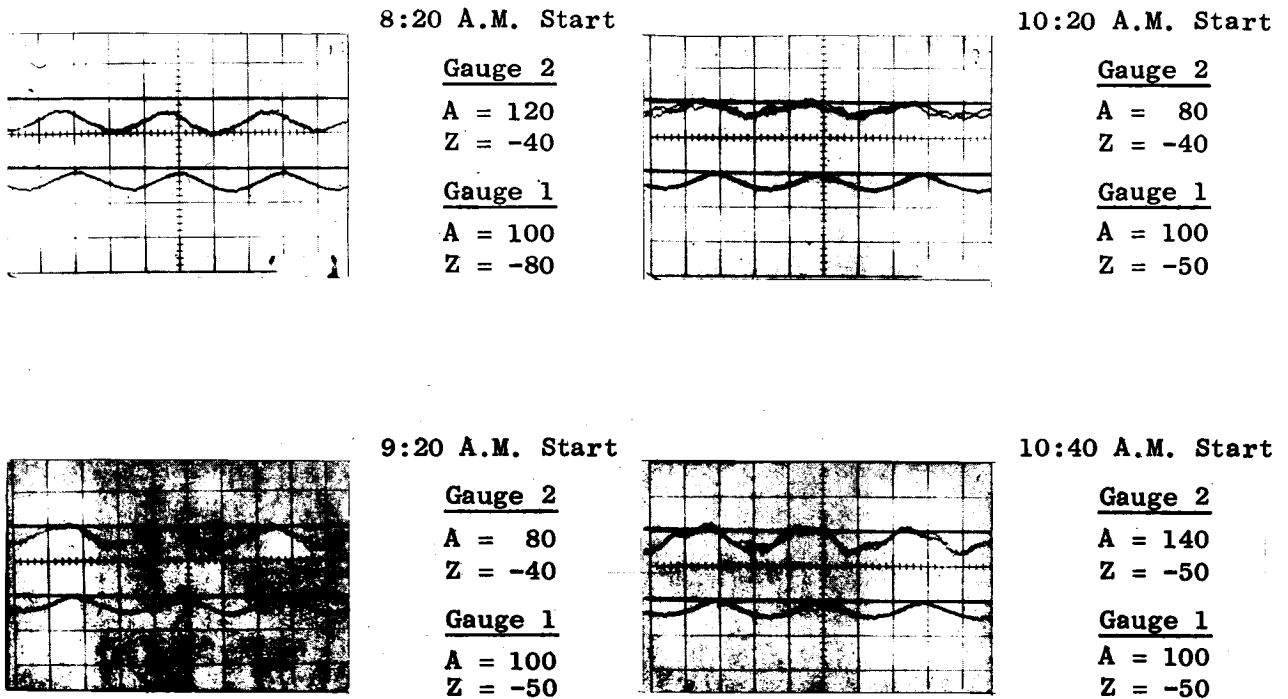


Figure 30. Oscilloscope Traces - Probe Signal vs. Time at 15,000 rpm -
Data of 12/7/65.

DISPLACEMENT GAUGE
DYNAMIC EVALUATION IN WATER ENVIRONMENT

SPEED: 435 CPS (26,100 RPM)
500 MICROINCHES PER CM SENSITIVITY
A = VIBRATIONAL AMPLITUDE, MICROINCHES
Z = APPARENT ZERO, MICROINCHES

DATE OF 12/10/65

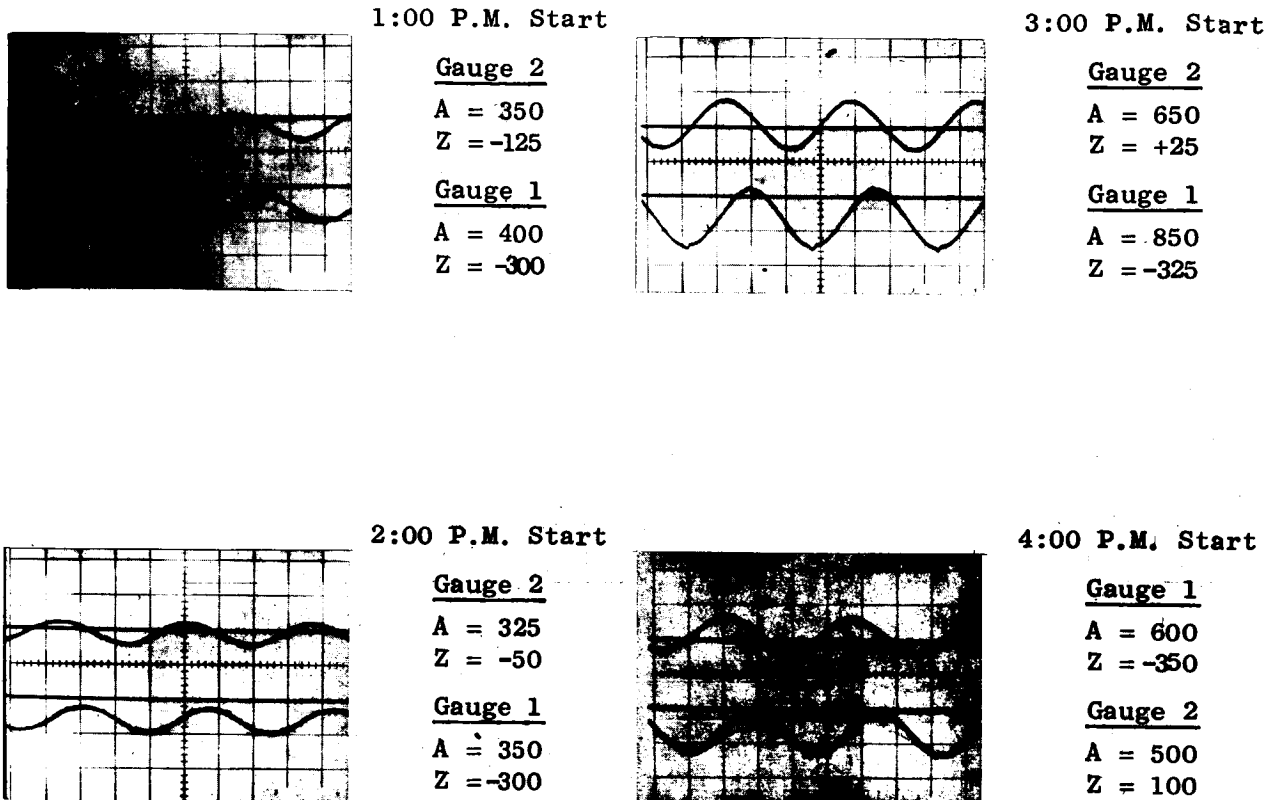


Figure 31. Oscilloscope Traces - Probe Signal vs. Time at 26,100 rpm -
Data of 12/10/65.

Displacement Gage Dynamic Evaluation
 Ball Bearing Mounted Shaft
 10 PSI Ambient Temperature Water to Journal Bearings
 9000 RPM Shaft Speed
 Data of 12-6-65

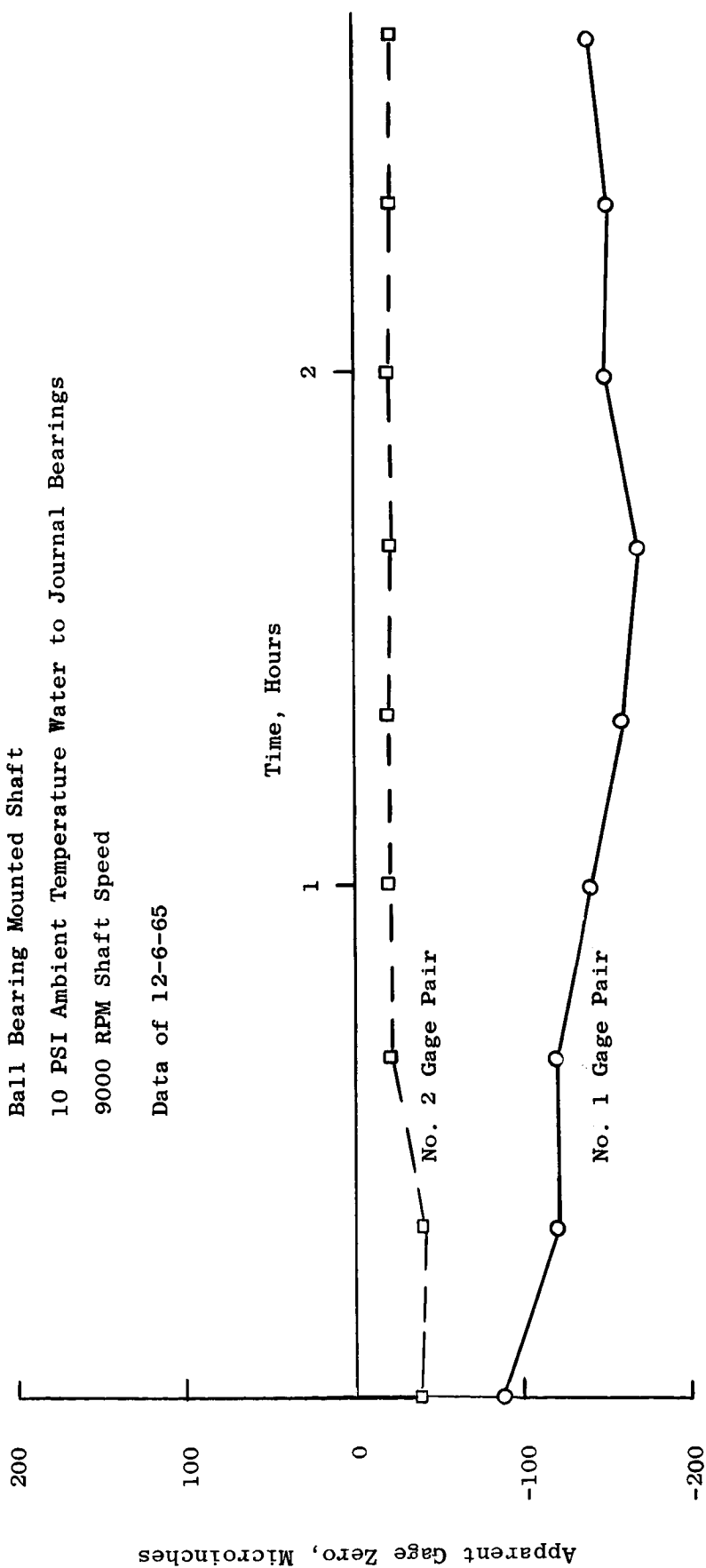


Figure 32. Apparent Gage Zero Shift With Time at 9000 rpm.

Displacement Gage Dynamic Evaluation

Ball Bearing Mounted Shaft

10 PSI Ambient Temperature Water to Journal Bearing

15,000 RPM Shaft Speed

Data of 12-7-65

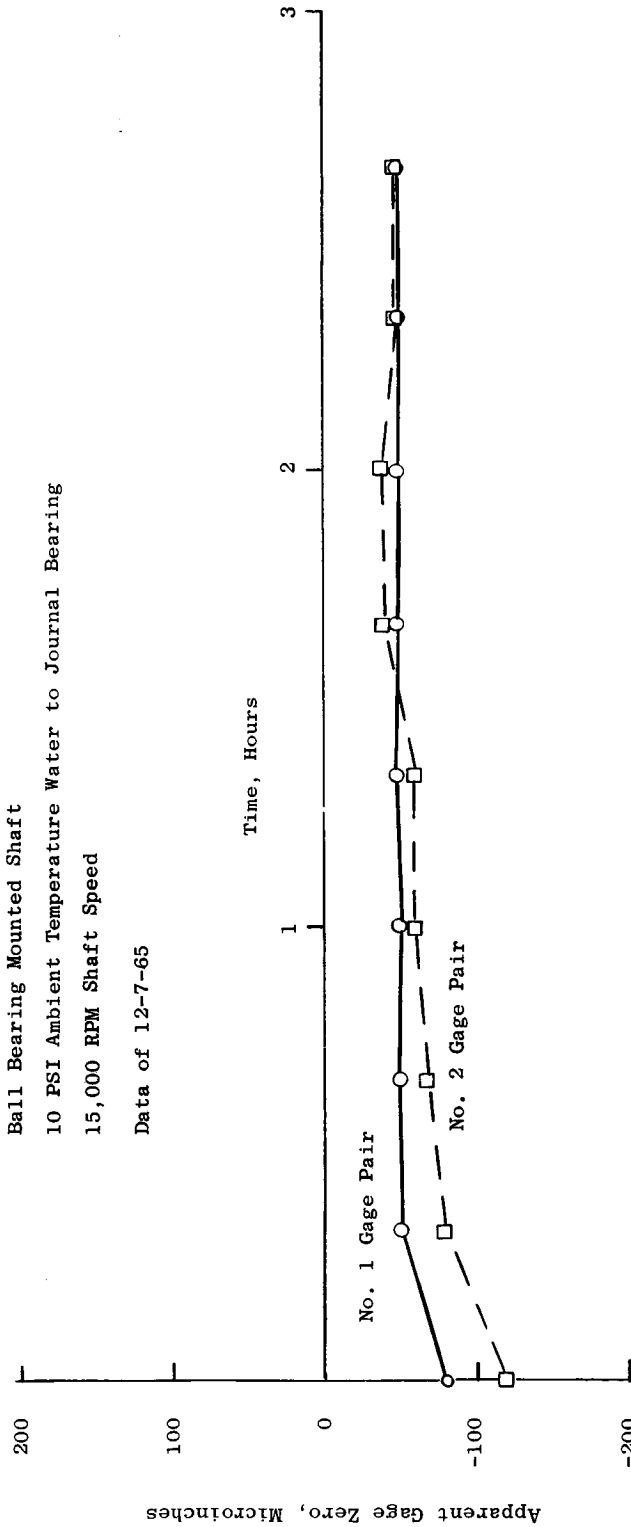


Figure 33. Apparent Gage Zero Shift With Time at 15,000 rpm.

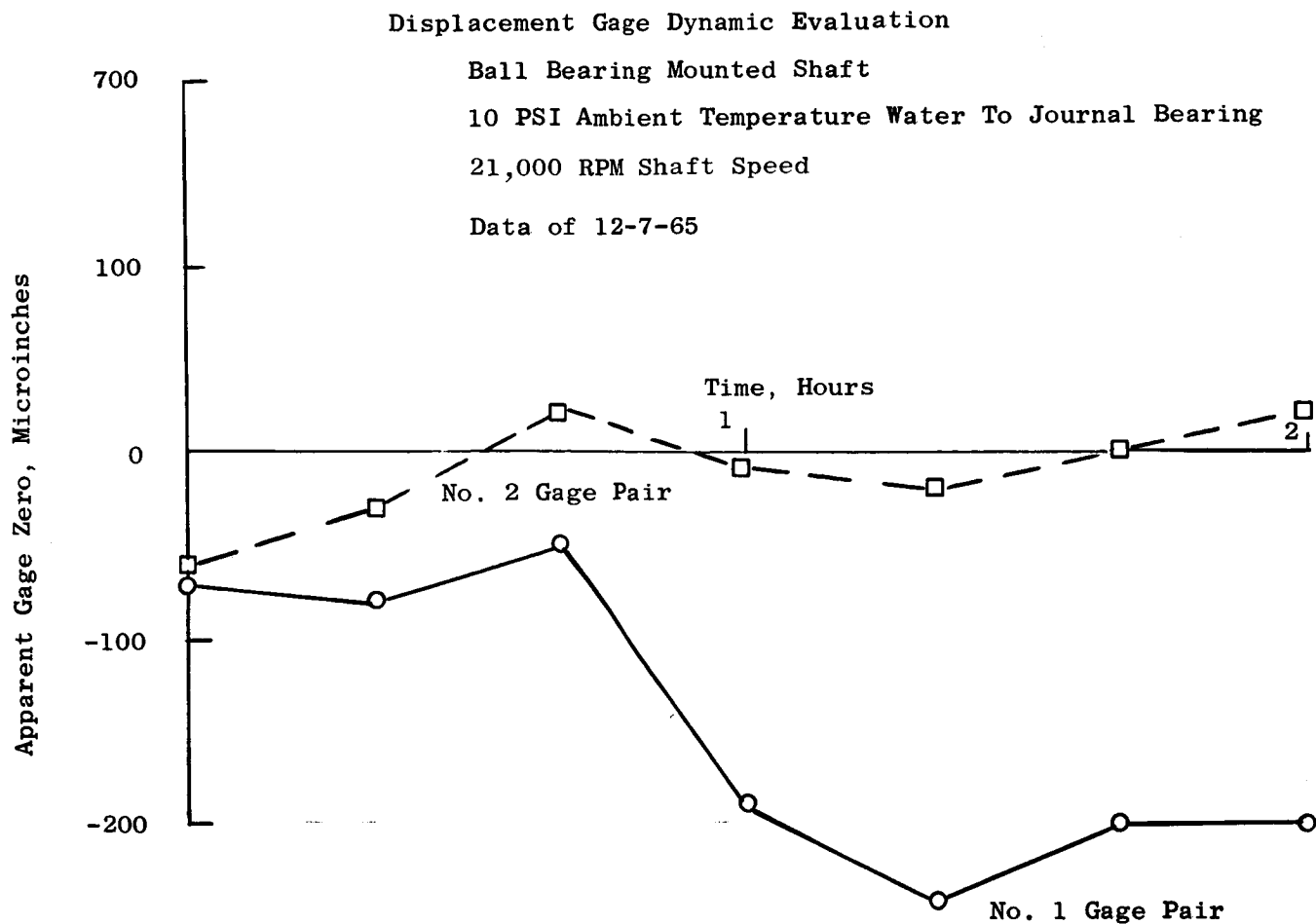


Figure 34. Apparent Gage Shift With Time at 21,000 rpm.

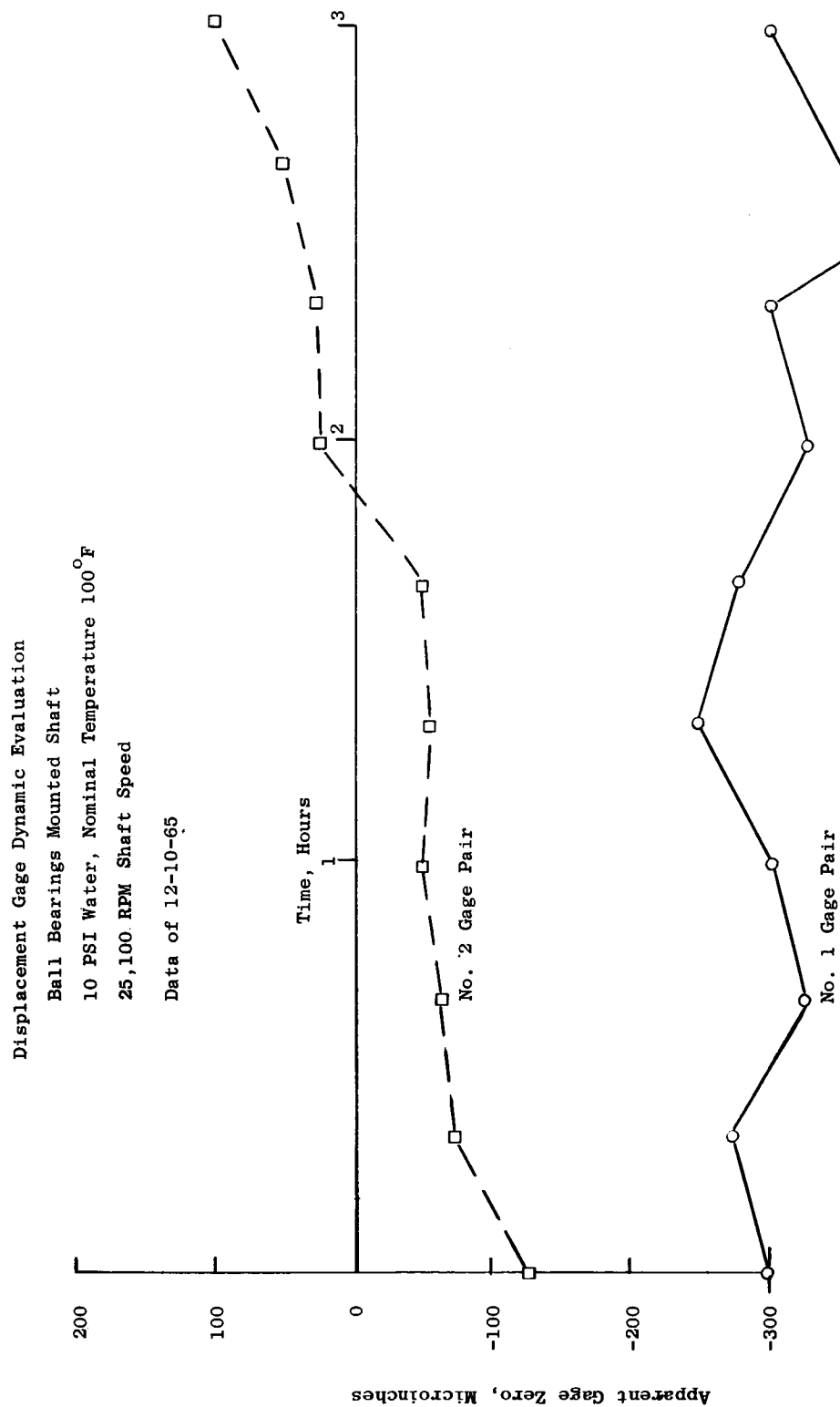
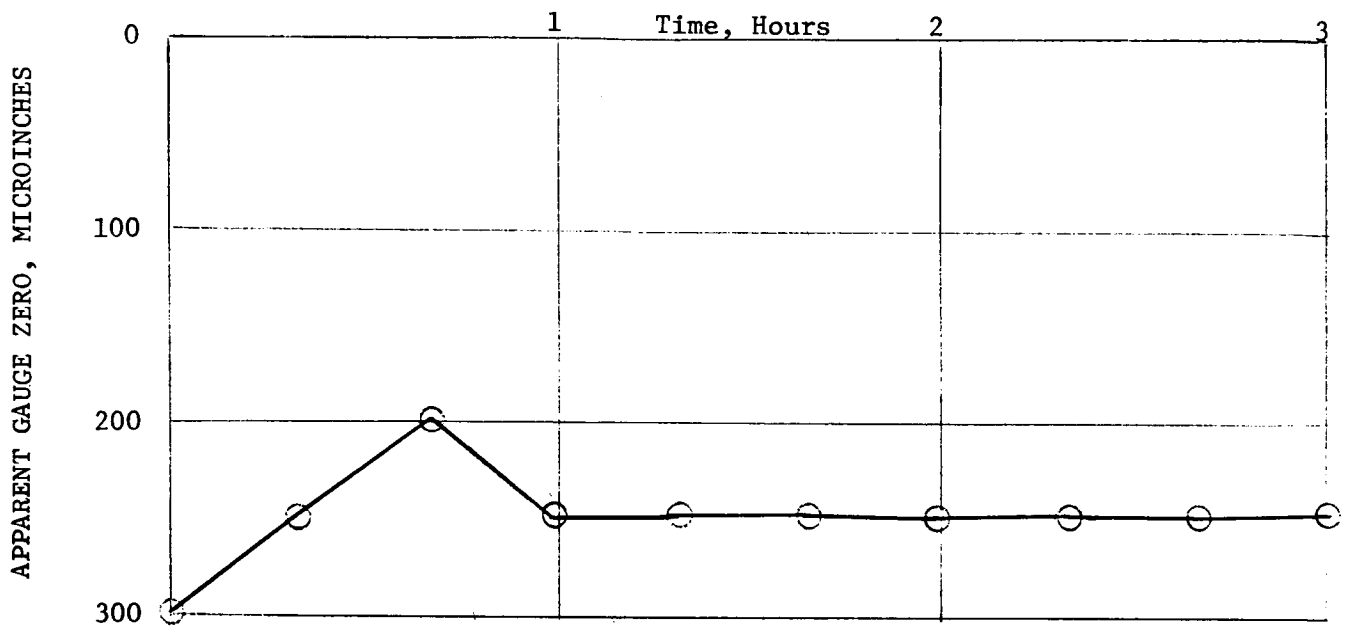


Figure 35. Apparent Gage Zero Shift With Time at 26,100 rpm.



Displacement Gauge Dynamic Evaluation
 Ball Bearing Mounted Shaft at 15,000 RPM
 10 psi Water at 120°F to Journal Bearing
 Data of 12/11/65 on No. 2 Probe Pair

Figure 36. Apparent Gauge Zero Shift With Time at 15,000 rpm.

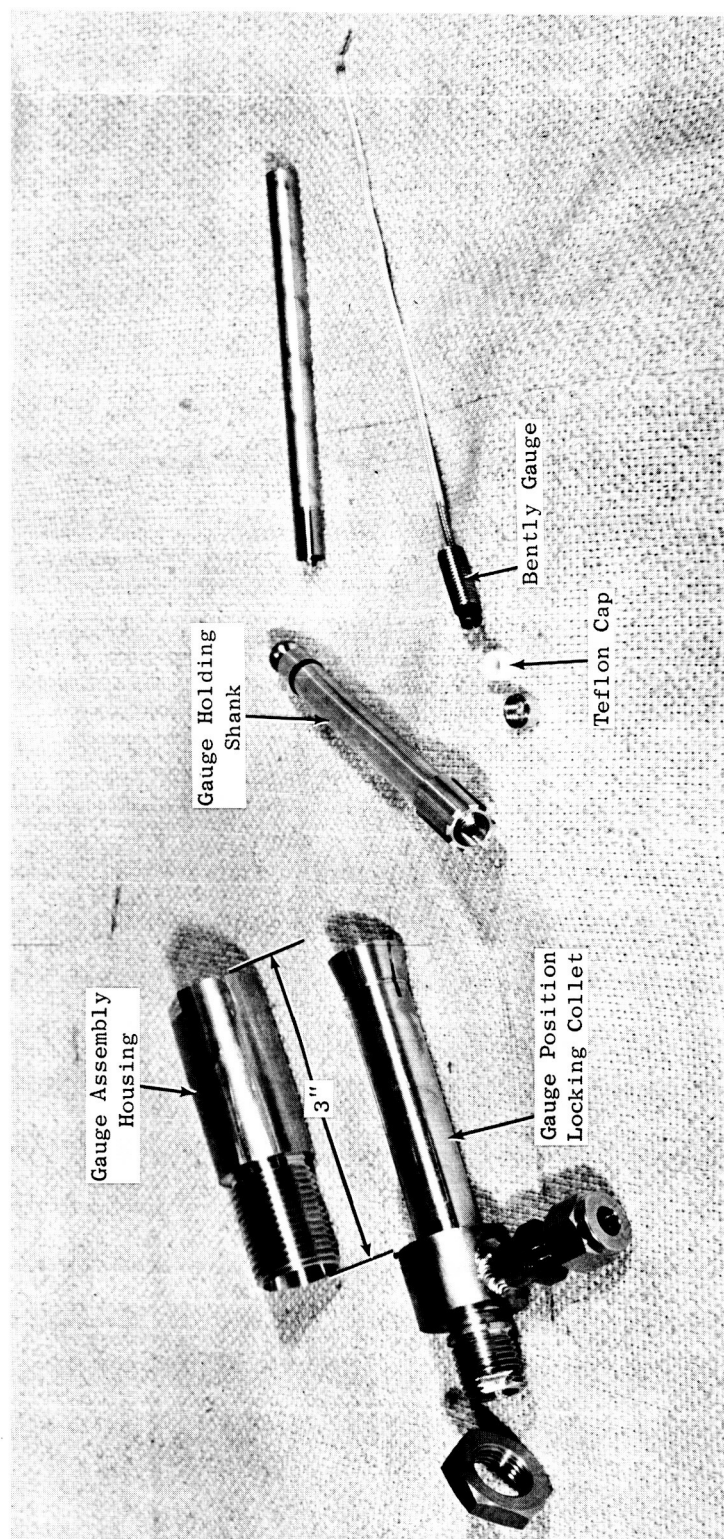


Figure 37. Disassembled View - New Displacement Probe Holders.

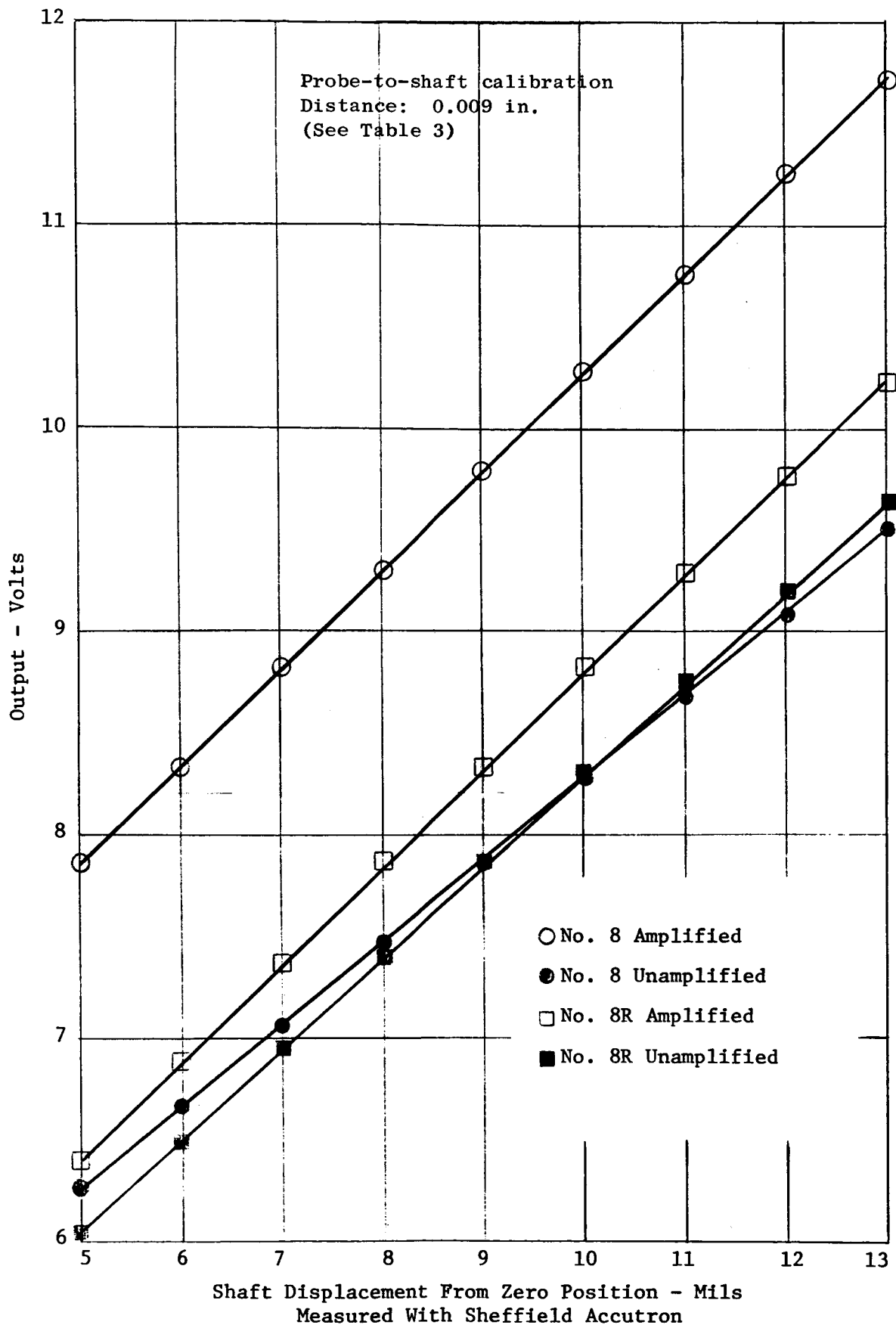


Figure 38. Bently Individual Probe Calibration - Gauge 8 and 8R.

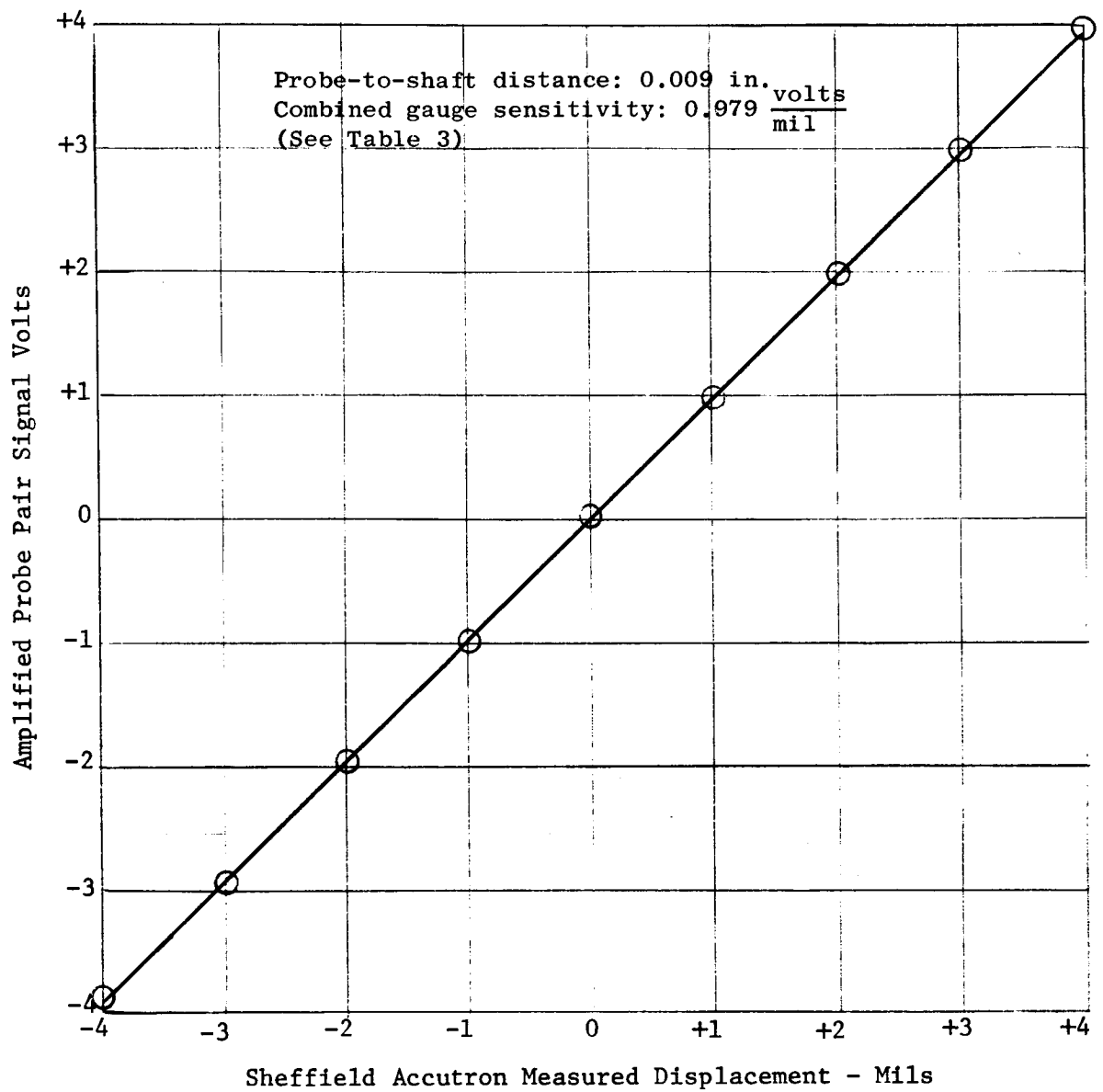
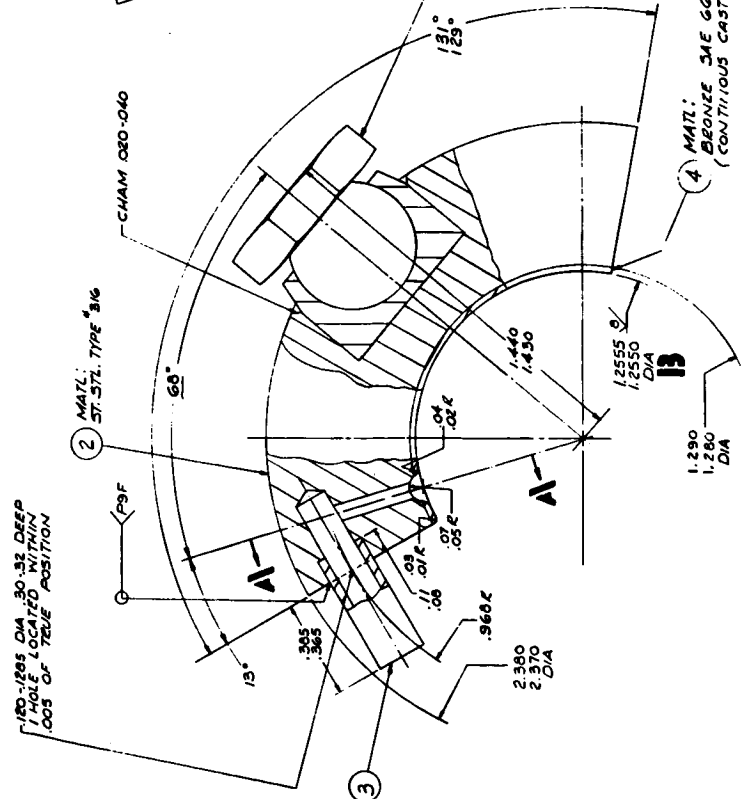
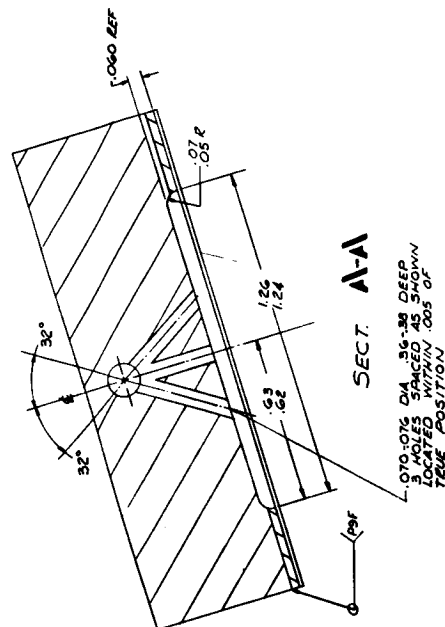
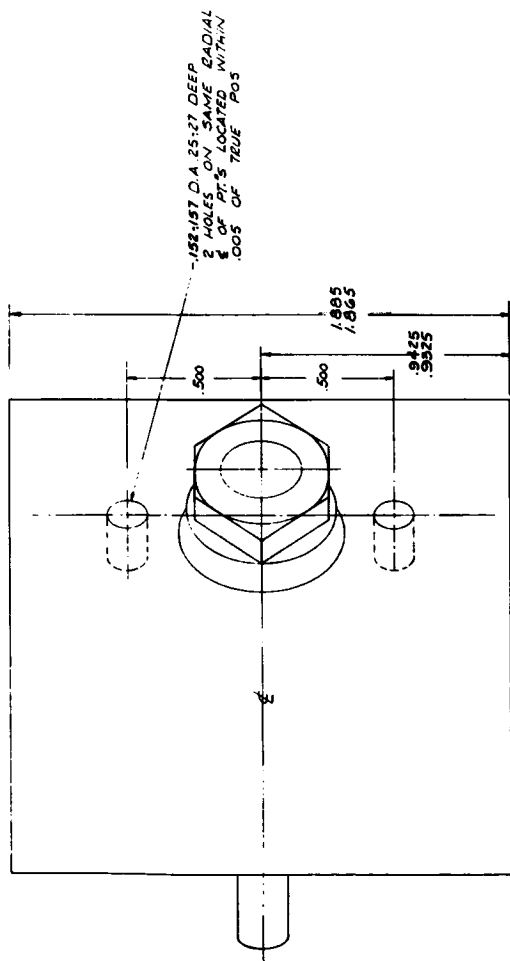


Figure 39. Bently Combined Probe Calibration - Gauge 8 and 8R.

ITEM	IDENTIFICATION NO.	DESCRIPTION OR NAME	ZONE	GROUP NO. & QTY
1			1	2
2	402000-724R	HOLDING	D9	1
3	-724R	TUBE	B1	1
4	-724R	INNER RACE	A8	1
5	CAT. NO. EP-1	TOGGLE PAD	B7	1
6				

* ST. STL. TYPE "316" SEAMLESS
.1875 O.D. .030 WALL THK.
Ø BEID TOOL SUPPLY CO., MUSKOGEE HEIGHTS, MICH. 49809-124



5. SEE PROCESS SPEC "1-2"
 4. FOR BEARING OPERATION SEE PROCESS SPEC DWG. 401000-724
 3. TAPER OF DIA 13 MUST NOT EXCEED .0008
 2. DIA 13 MUST BE ROUNDED WITHIN .0002 FIE
 1. BREAK SHARP EDGES .015 MAX.
- PRODUCT MUST CONFORM TO THE REQUIREMENTS OF THE ABOVE NOTES

Figure 40. Partial Arc Loader Bearing Details.

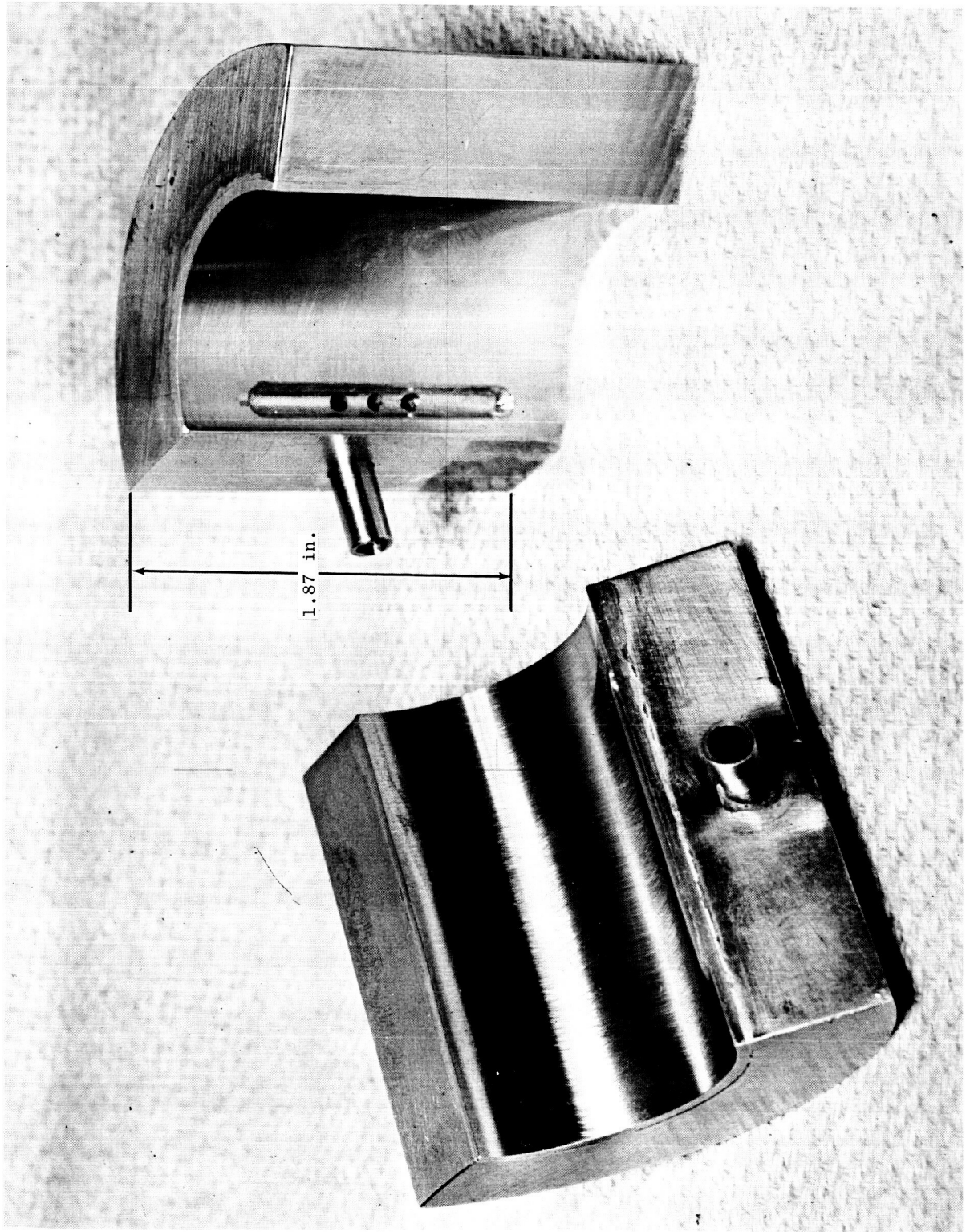


Figure 41. View of Partial Arc Loader Bearing.

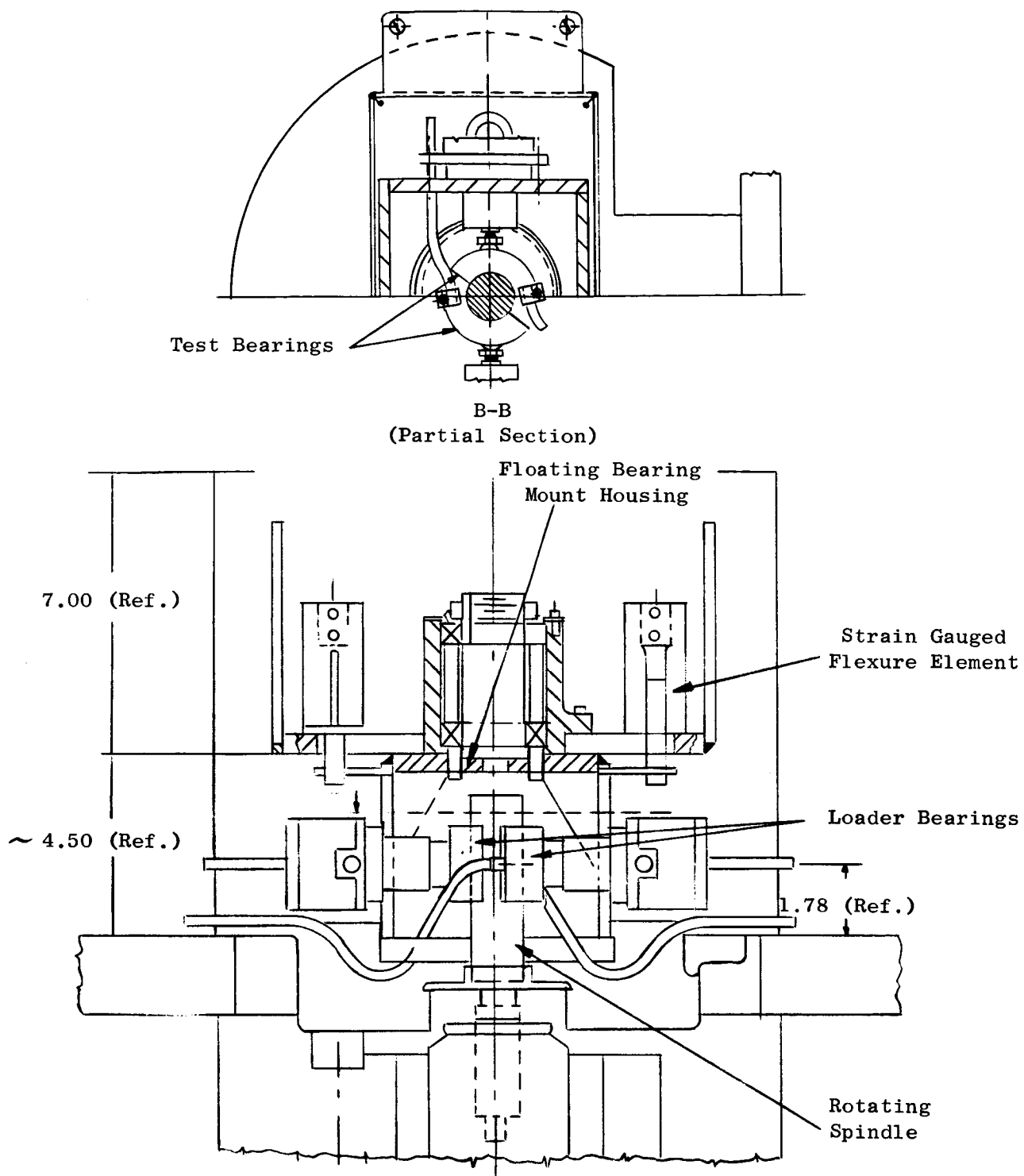


Figure 42. Test Rig for Measuring Loader Bearing Friction Torque.

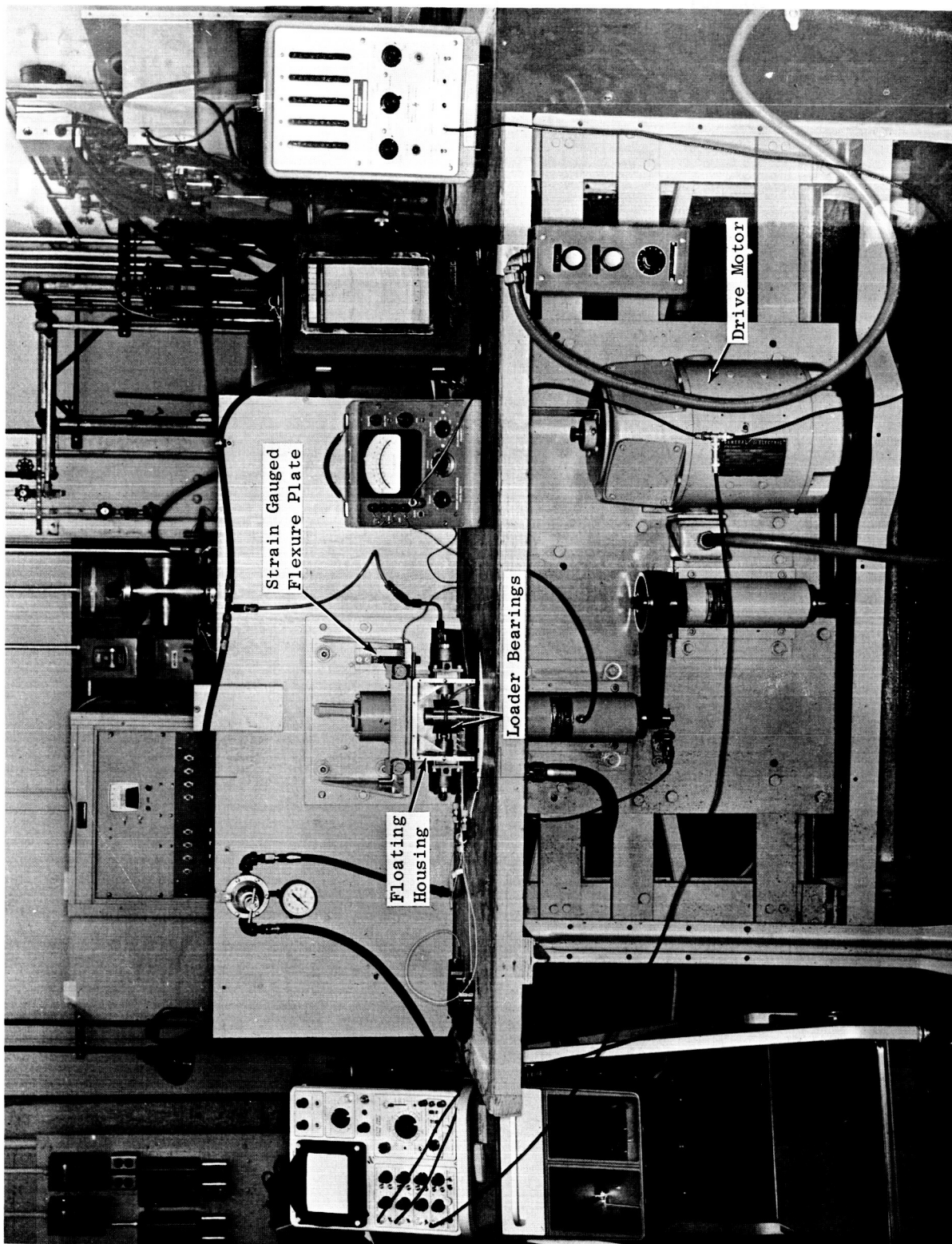


Figure 43. Overall View of Loader Bearing Friction Torque Test Rig.

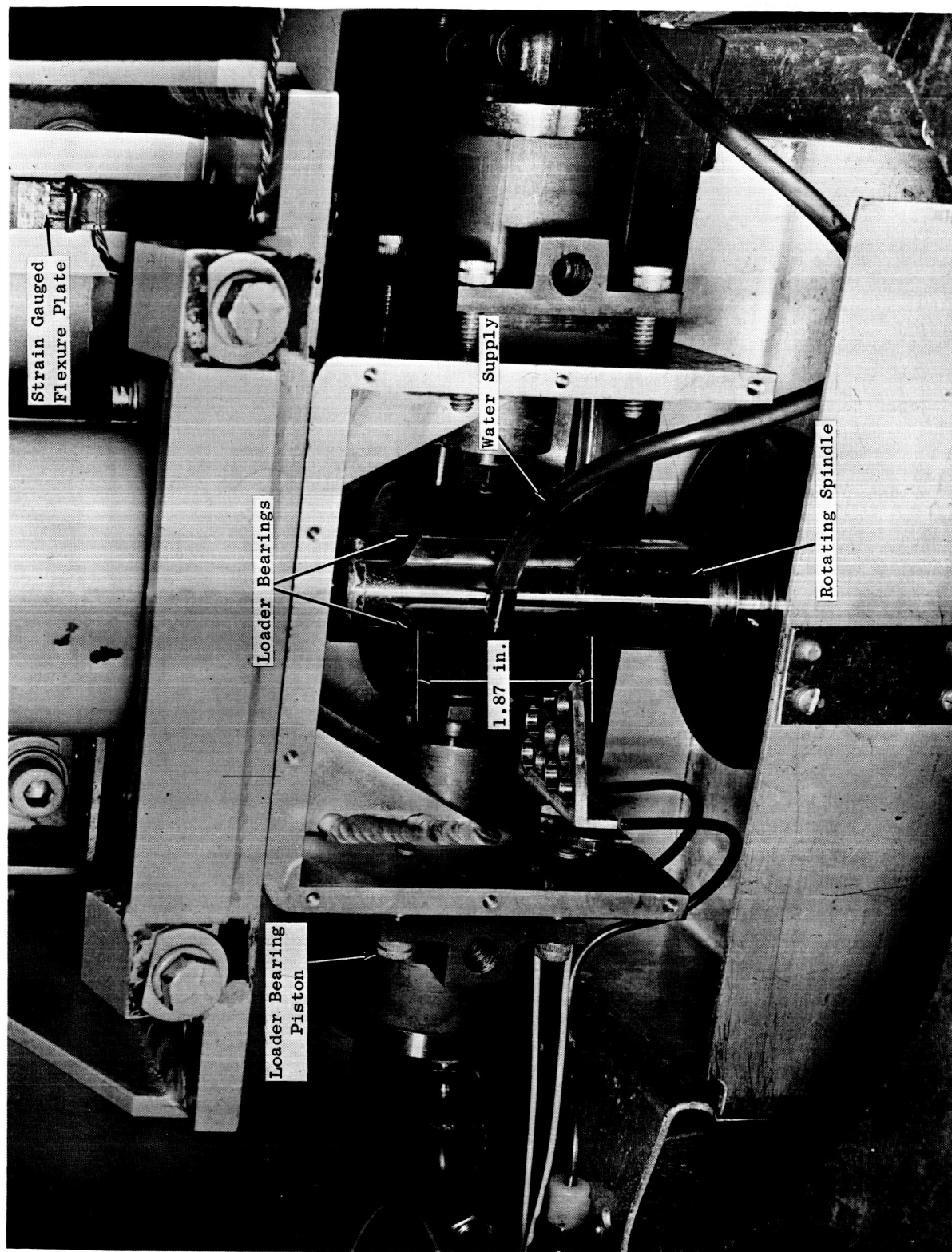


Figure 44. Closeup View of Loader Bearing Friction Torque Test Rig.

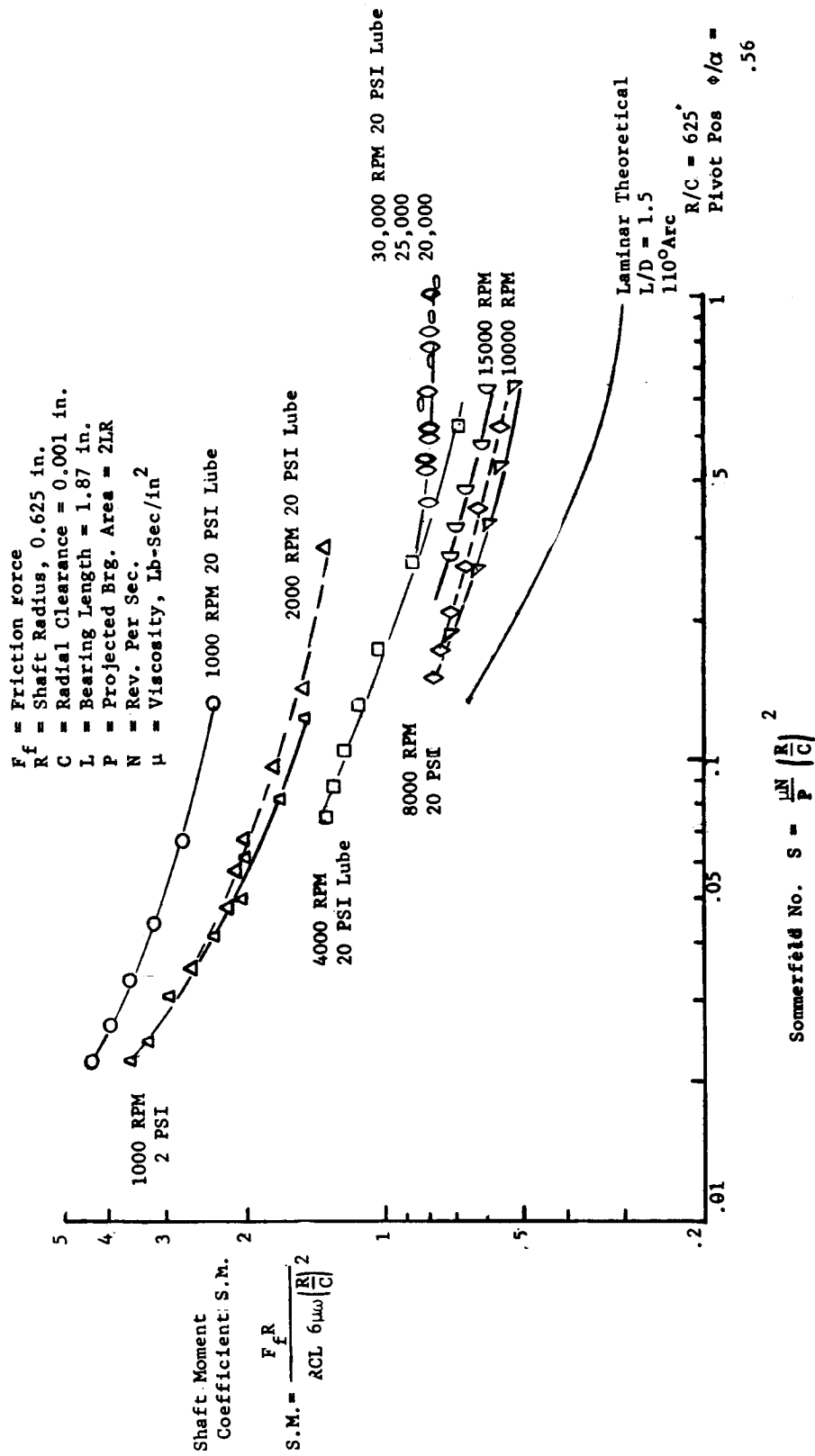


Figure 45. Loader Bearing Shaft Moment Coefficient vs. Sommerfeld No.
 (ϕ , Arc Length from Leading Edge to Pivot; α , Arc Length of Pad)

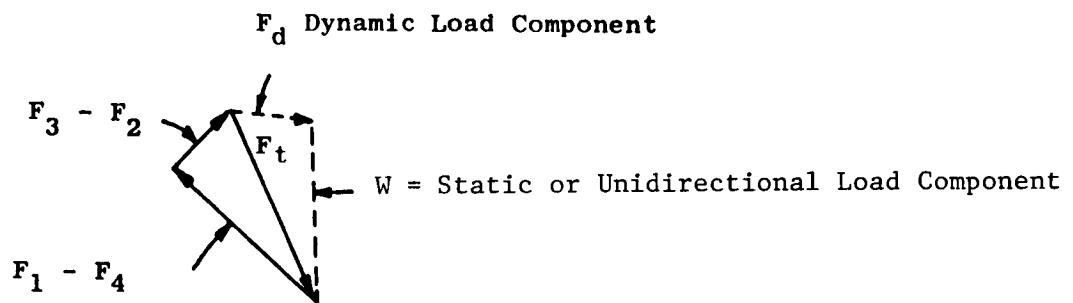
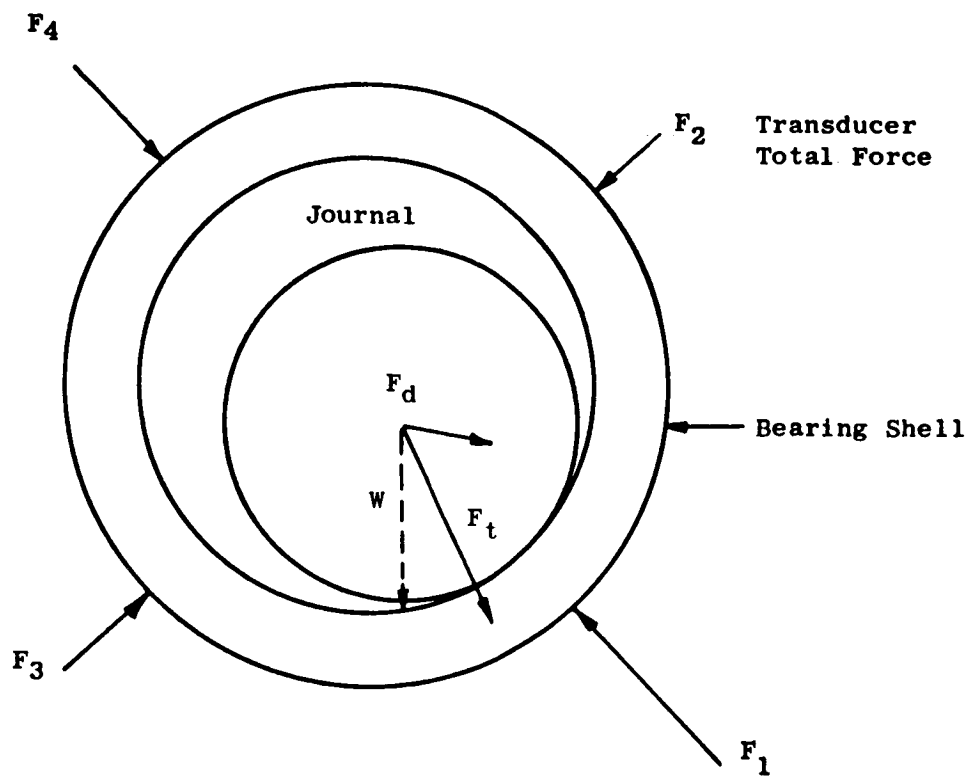


Figure 46. Principle of Radial Force Measuring Technique

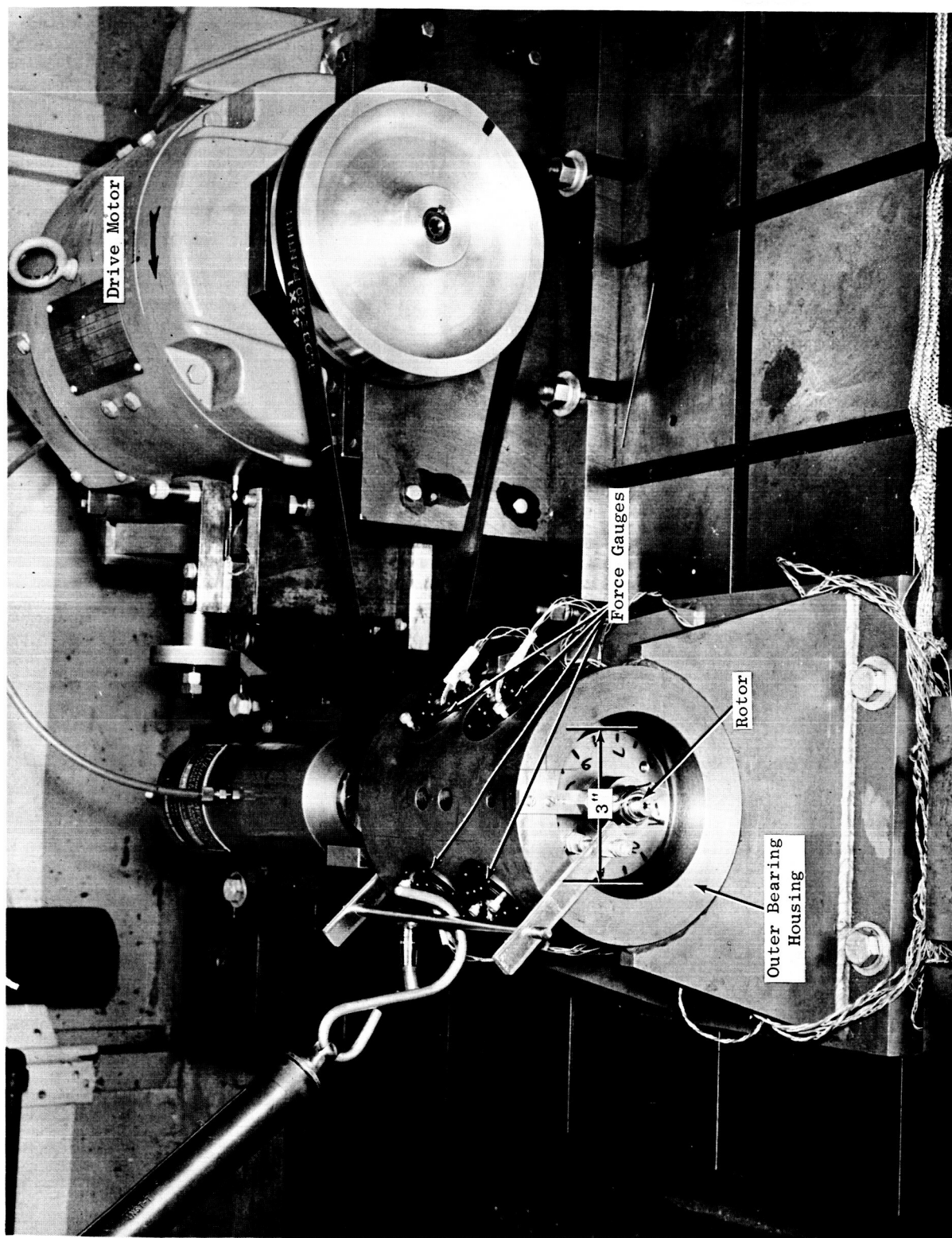


Figure 48. View of Assembled Force - Gauge Checkout Device.

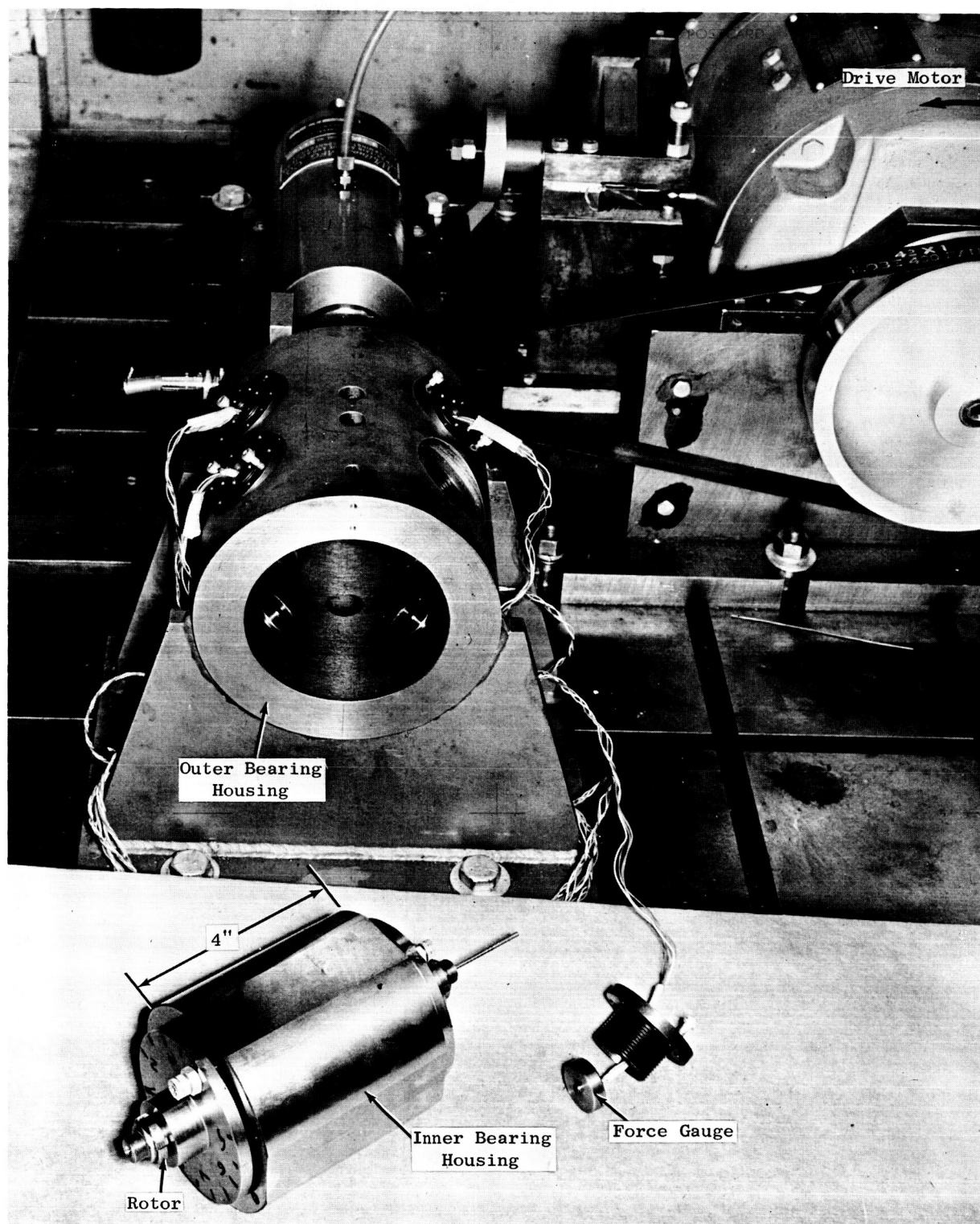


Figure 49. View of Partially Assembled Force Gauge Checkout Device.

FORCE GAUGE DYNAMIC EVALUATION

TOTAL UNBALANCE = 0.0430 LB-INCHES

SCOPE SENSITIVITY = 2 VOLTS PER CM

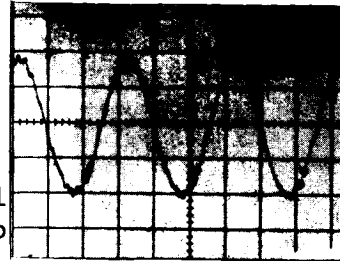
NET ASSEMBLED LOAD-CELL SENSITIVITY: 11.3 LBS/VOLT

PRELOAD 125 LBS/CELL

DATA OF 10/30/65



Z - Modulation by
One-Per-Rev. Signal
(Photo Includes Two
Sweeps of Trace)



RPM = 5000

P/R Volts = 5.4

Measured Force P/P lbs = 61

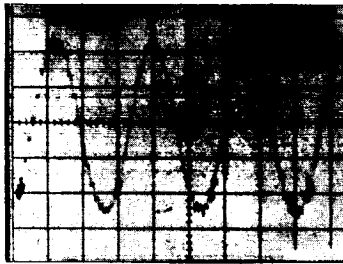
Theoretical Force = 61.2

RPM = 6000

P/P Volts = 7.6

Measured Force P/P lbs = 86

Theoretical Force P/P lbs = 88

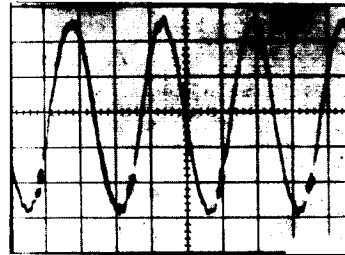


RPM = 6600

P/P Volts = 9.4

Measured Force P/P lbs = 106

Theoretical Force P/P lbs = 106.5



RPM = 7100

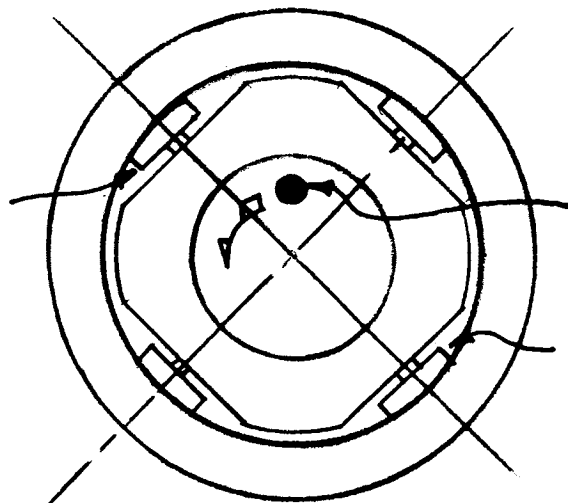
P/P Volts = 11.2

Measured Force P/P lbs = 126.5

Theoretical Force P/P lbs = 123

Figure 50. Oscilloscope Photographs - Unbalance Force vs. Time.

CELLS 7 AND 9



UNBALANCE

CELLS 3 AND 5

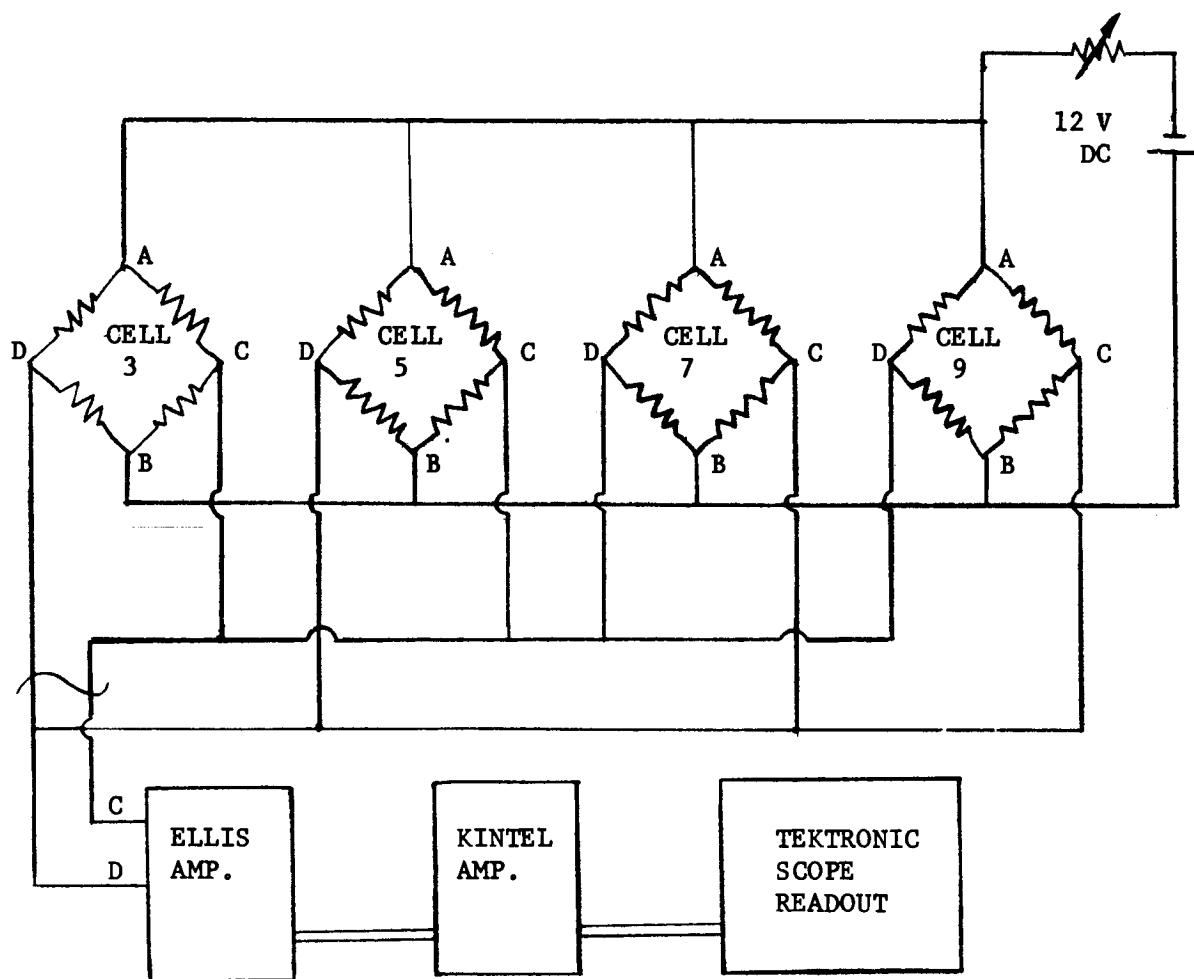
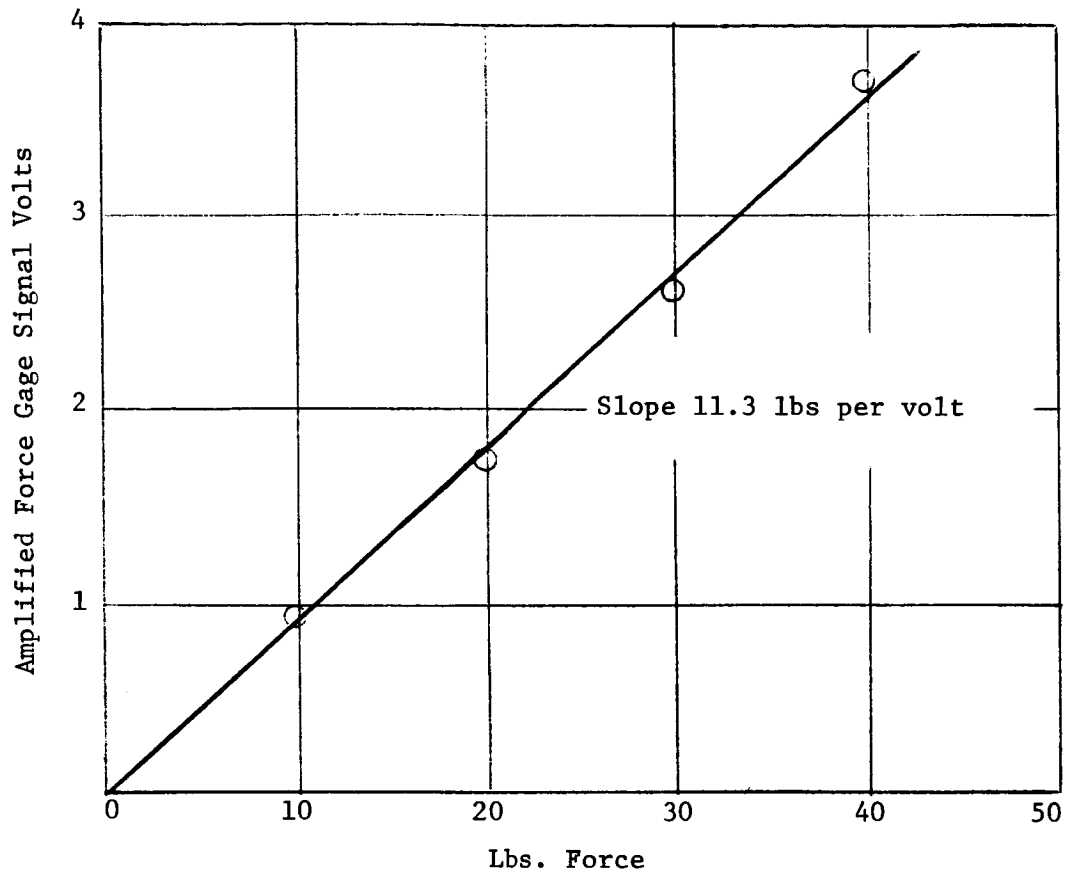


Figure 51. Schematic Diagram and Arrangement of Load Cells For Radial Force Measurement



Preload 125 lbs Per Cell (10-30-65)

Figure 52. Typical Static Calibration - Four Force Gages Assembled in Checkout Device.

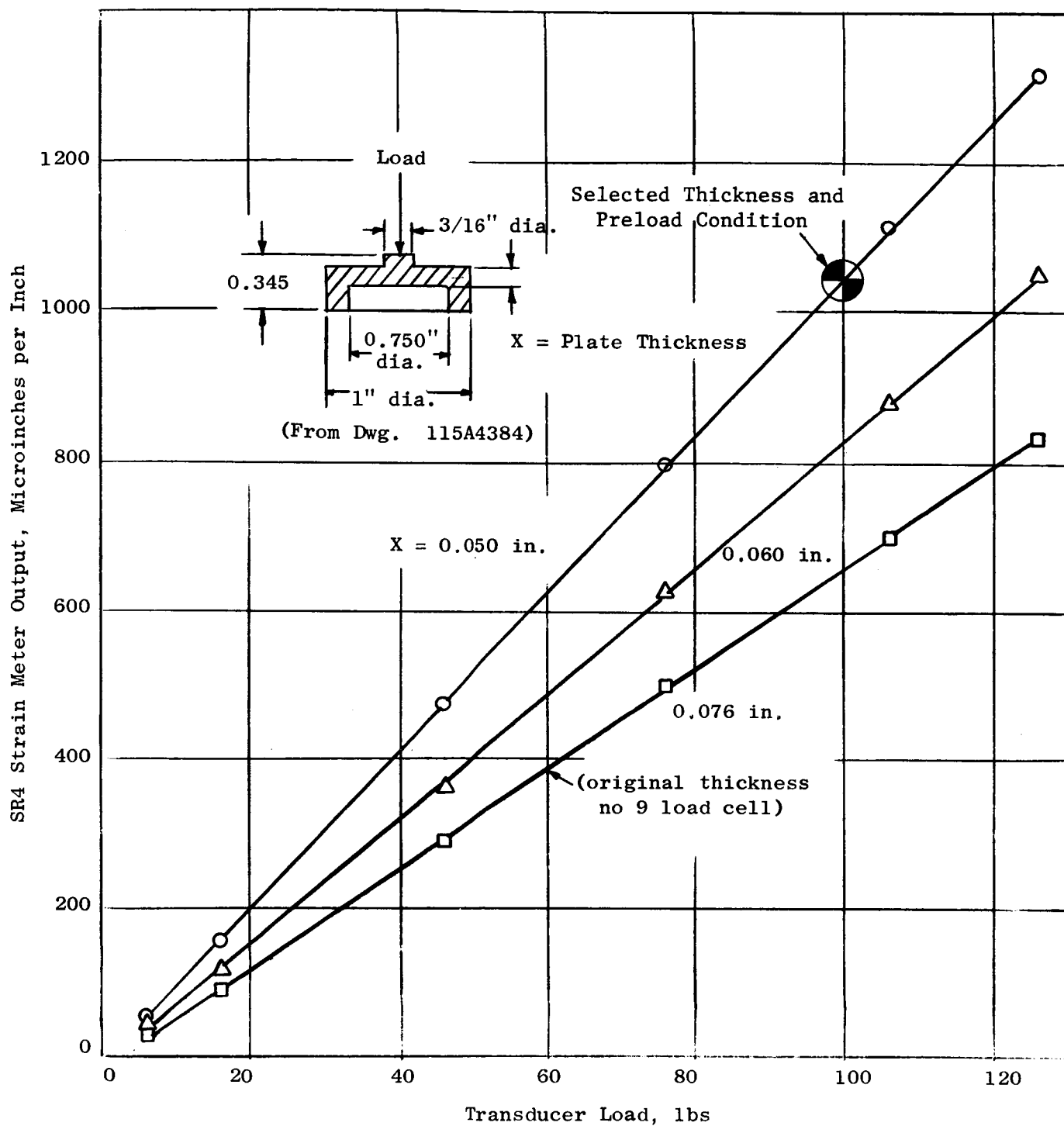


Figure 53. Load Cell Calibration Curves at Various Plate Thicknesses.

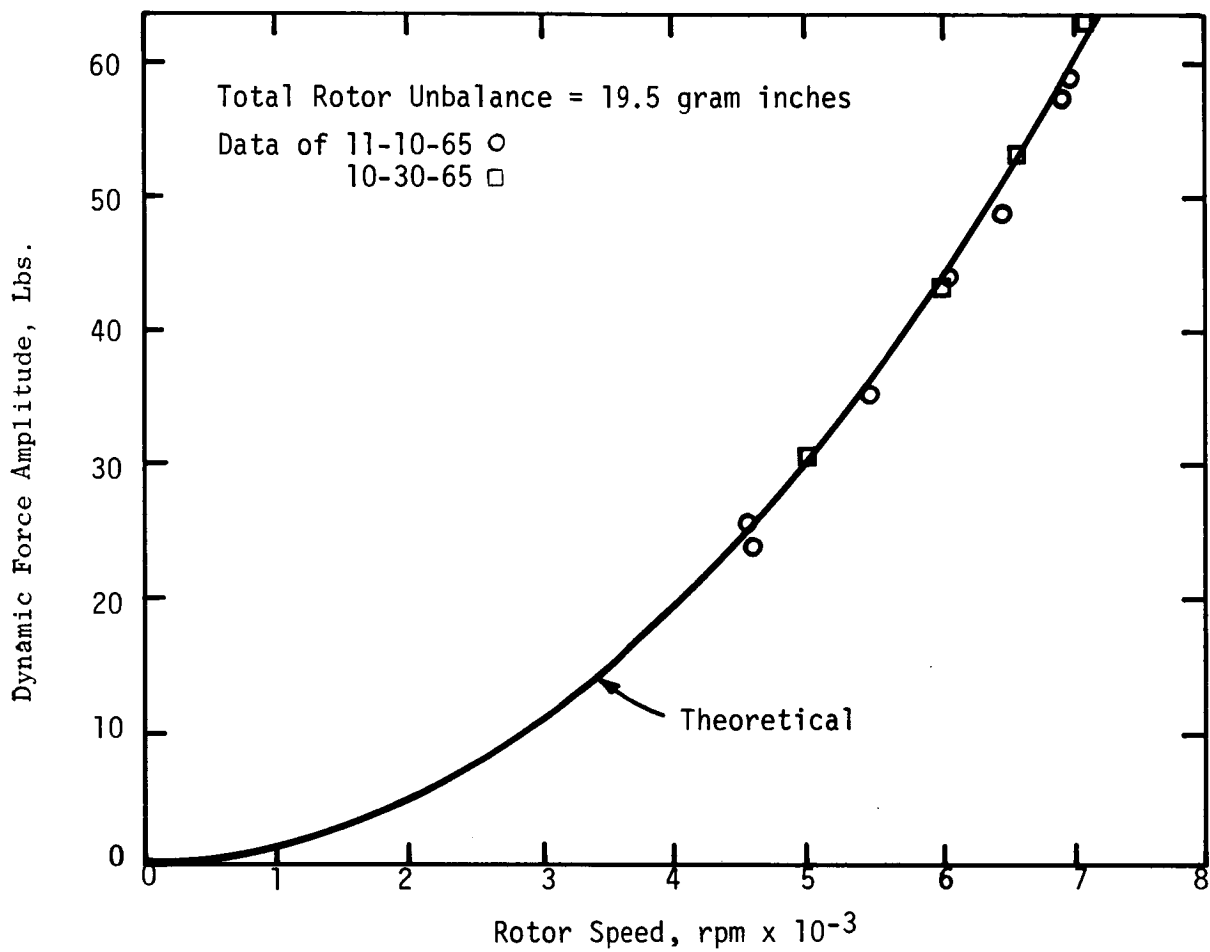


Figure 54. Force Gage Evaluation - Dynamic Load Amplitude Vs Rotor Speed.

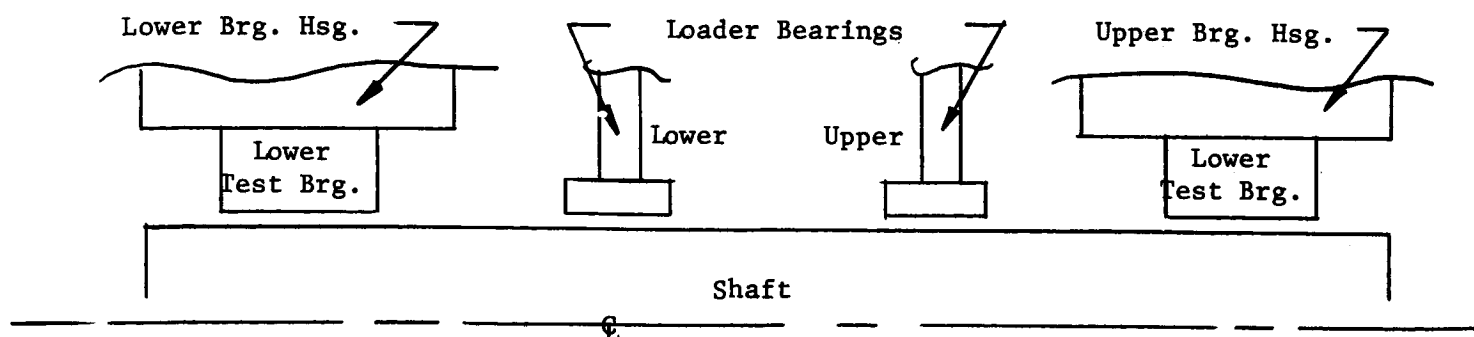


Figure 56. Analytical Model Established by Representing the Two Test Bearings and the Loader Bearings by Springs.

These springs are attached to the shaft on one end and to the supporting housings on the other end which is simulated as ground.

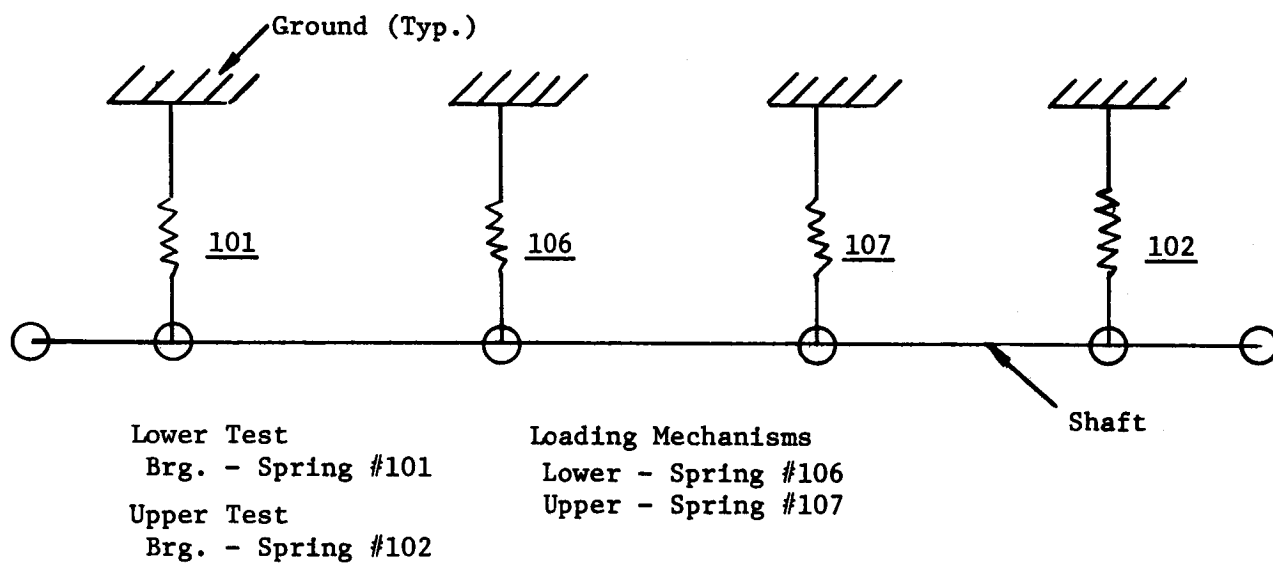
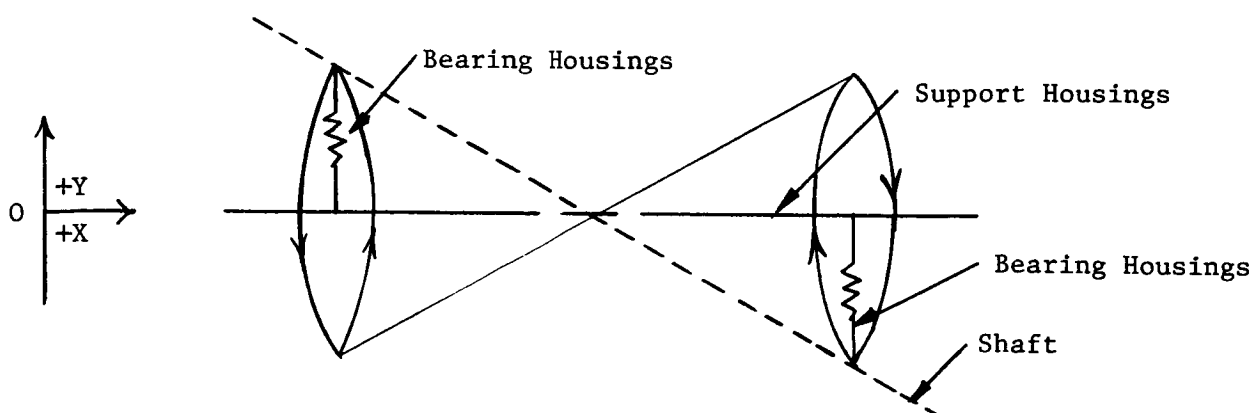
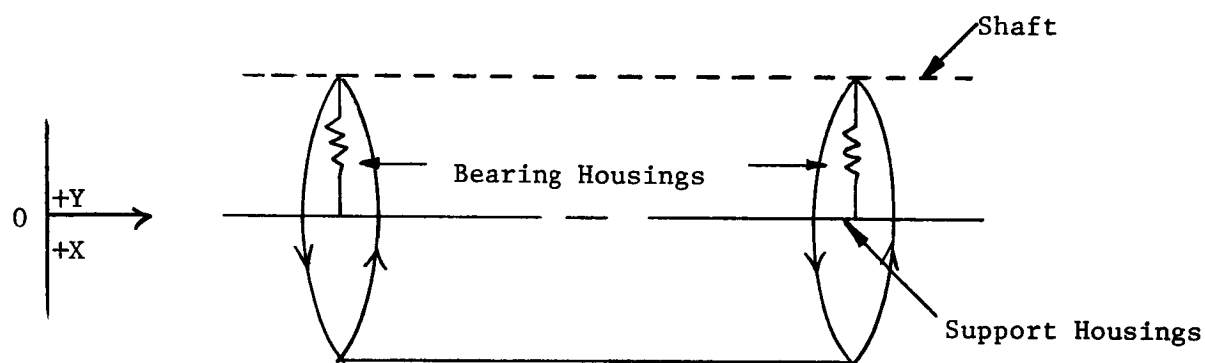


Figure 57. Analytical Model of Shaft System.

First Critical - Conical Whirl



Second Critical - Cylindrical Whirl



Third Critical - Bending Beam

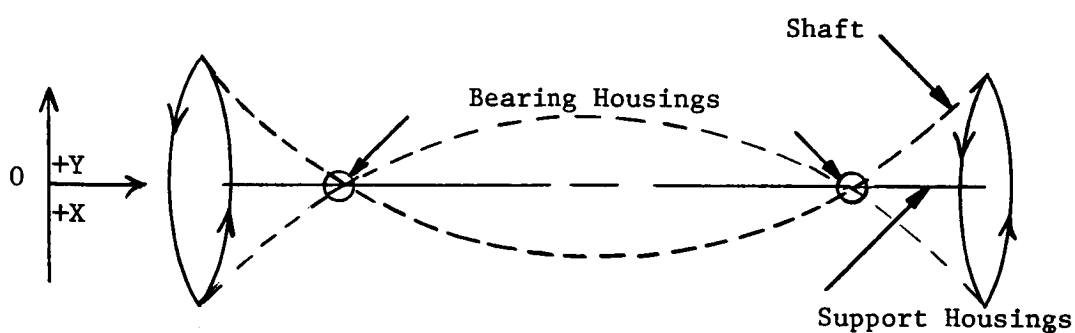


Figure 58. Plot of Mode Shapes at Critical Speeds of System Bearing Stability Test Rig.

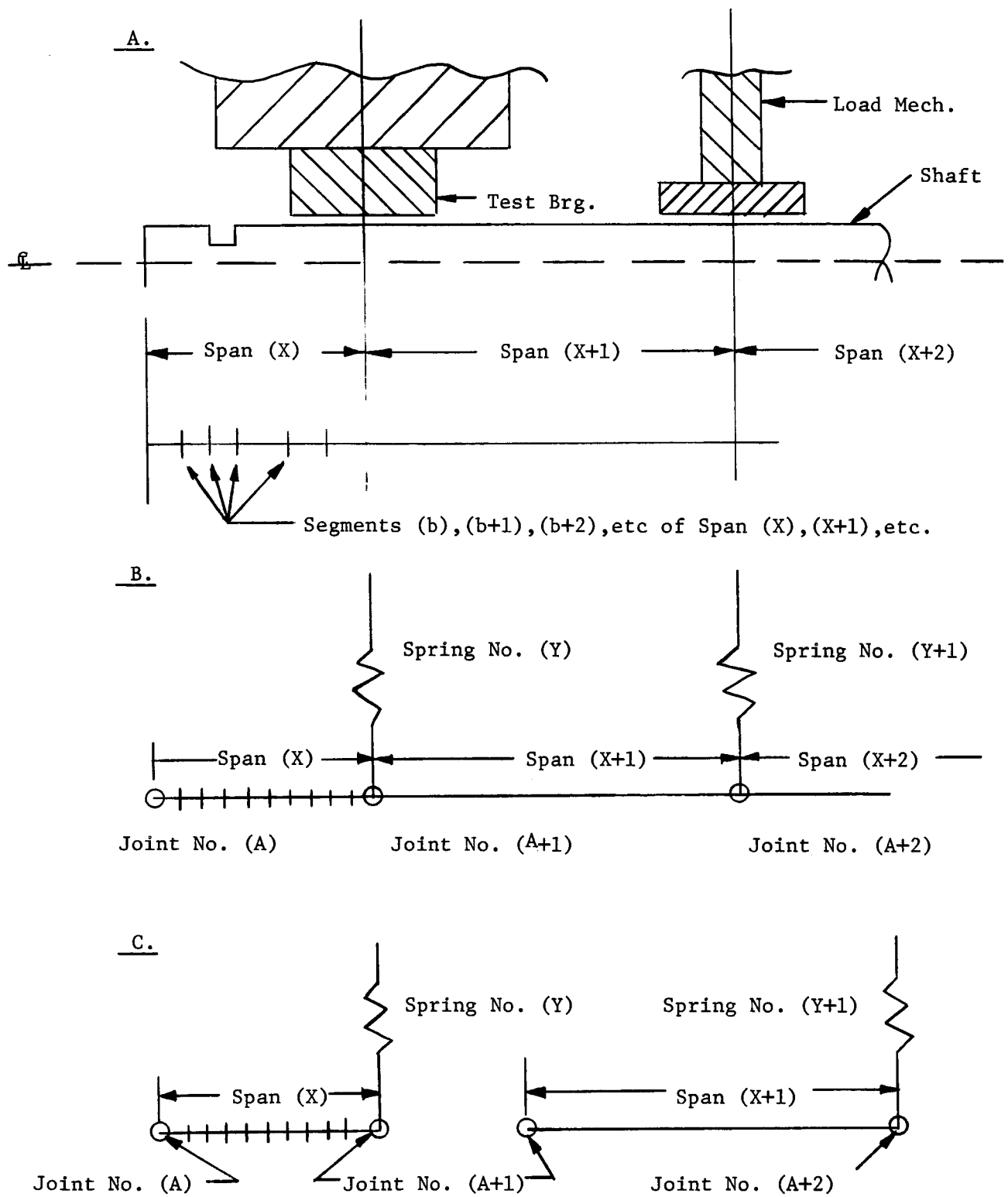


Figure 59. System Evaluation Bearing Stability Test Rig.

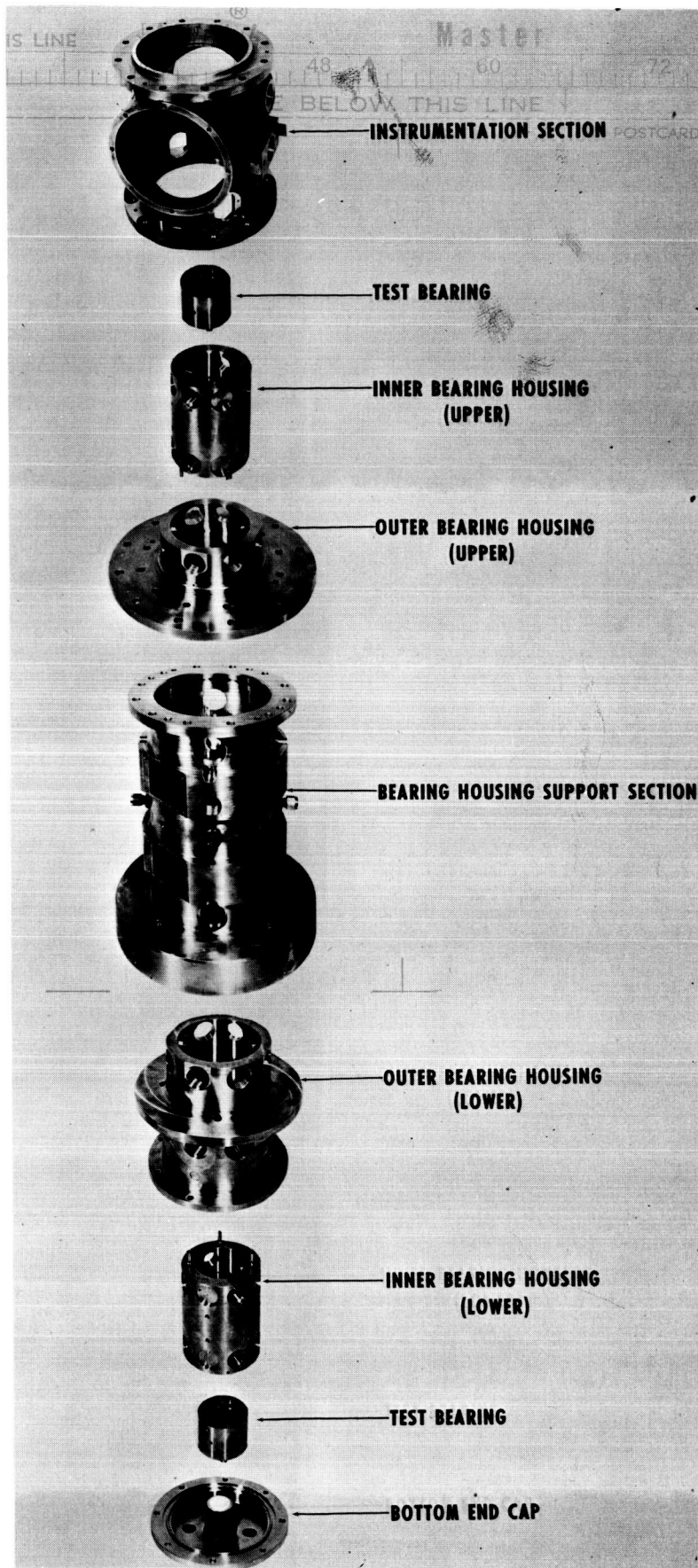


Figure 60. Exploded View of Test Housings.

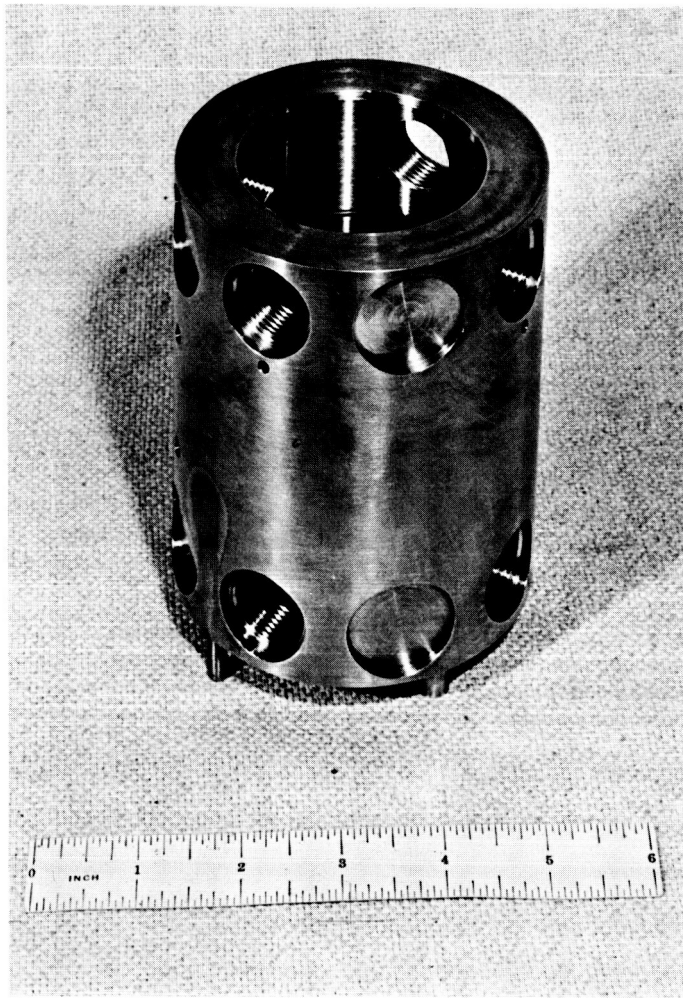


Figure 61. Inner Bearing Housing (Upper).

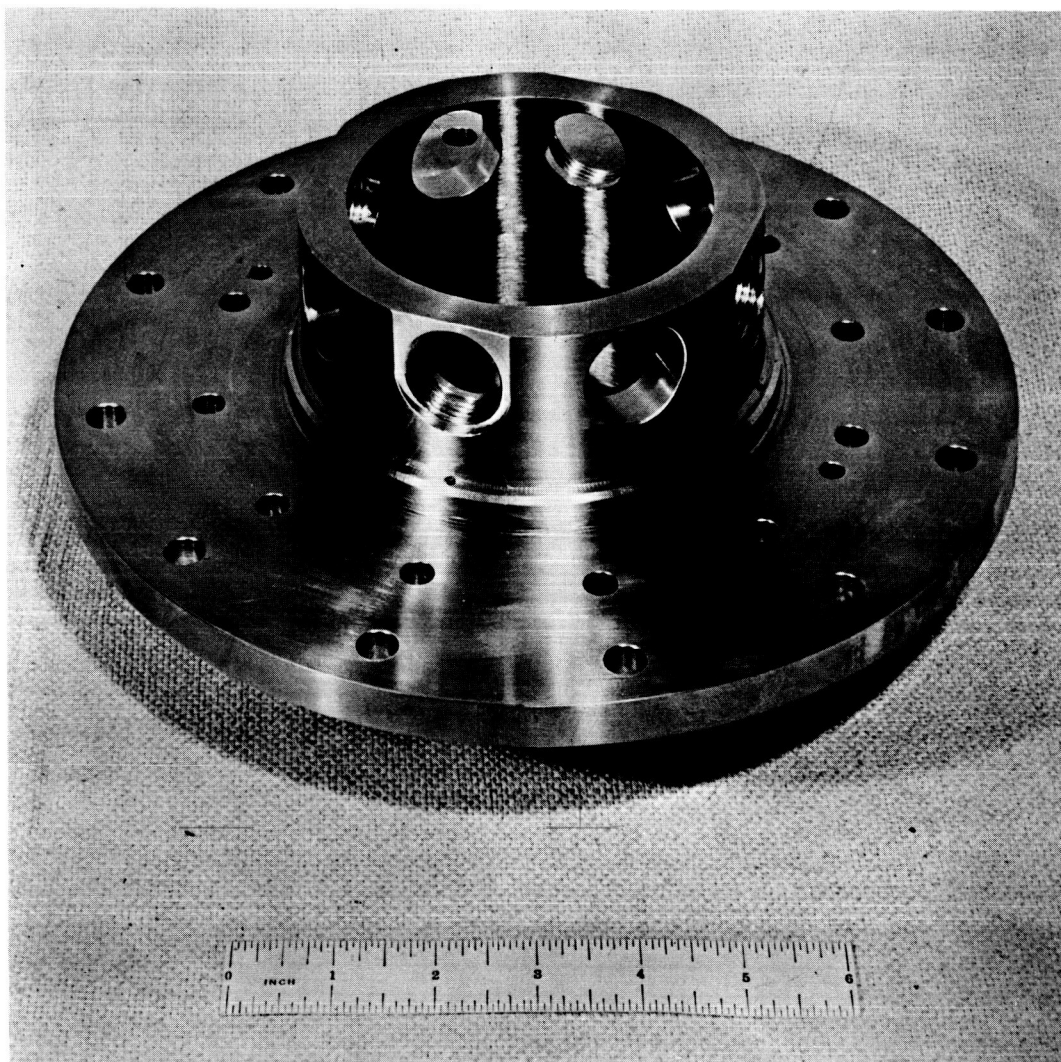


Figure 62. Outer Bearing Housing (Upper).

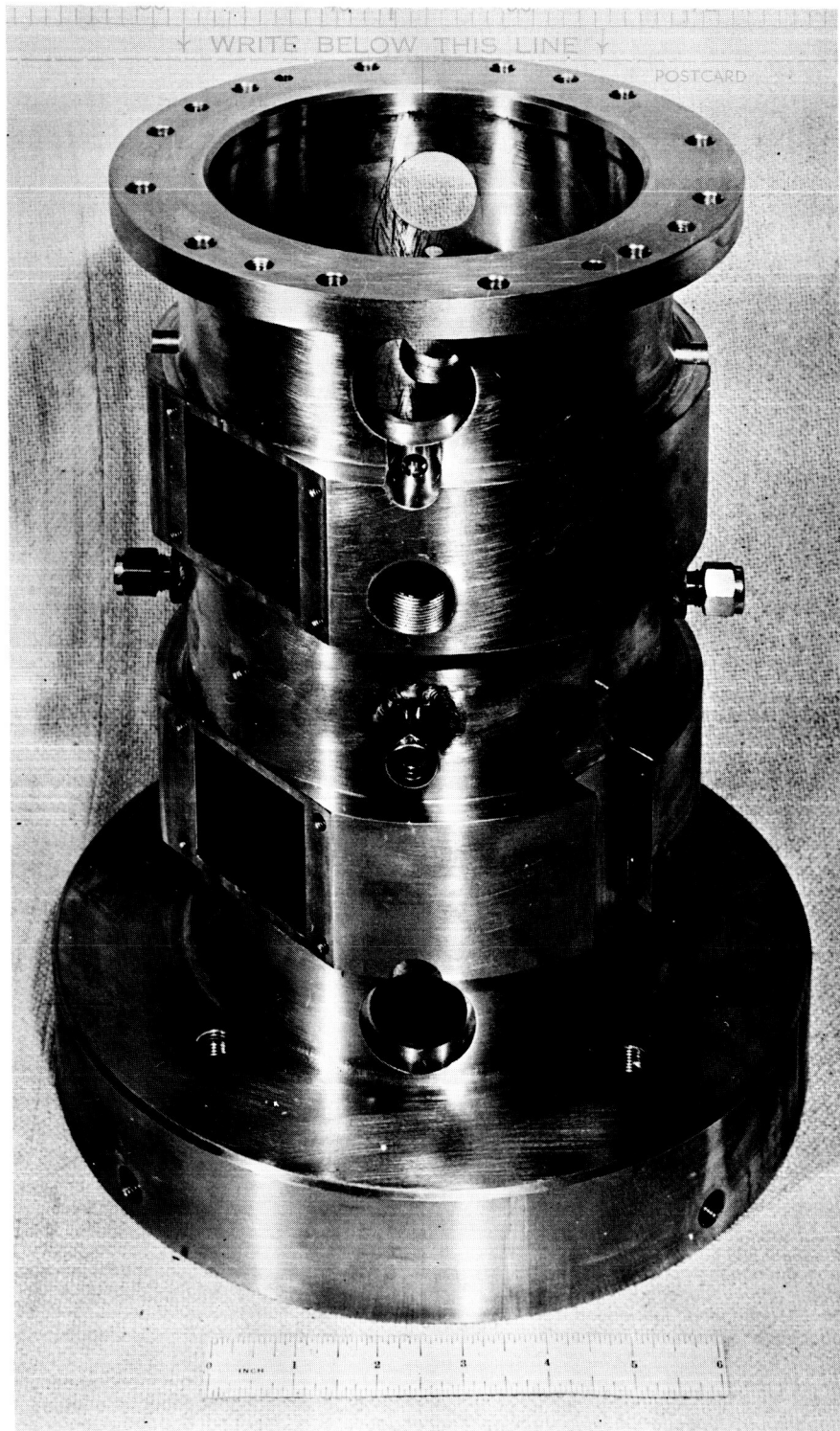


Figure 63. Bearing Housing Support Section.

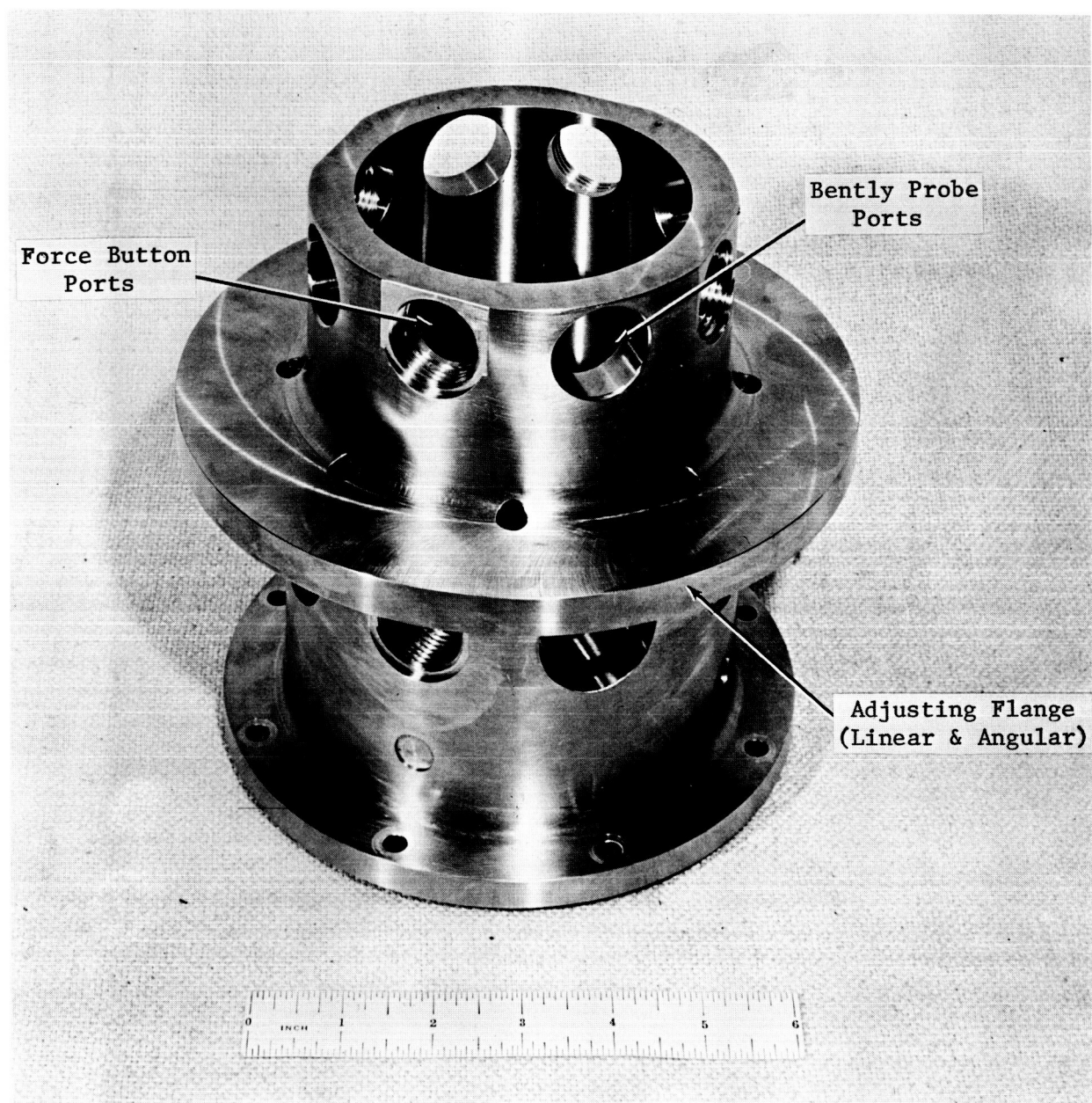


Figure 64. Outer Bearing Housing (Lower).

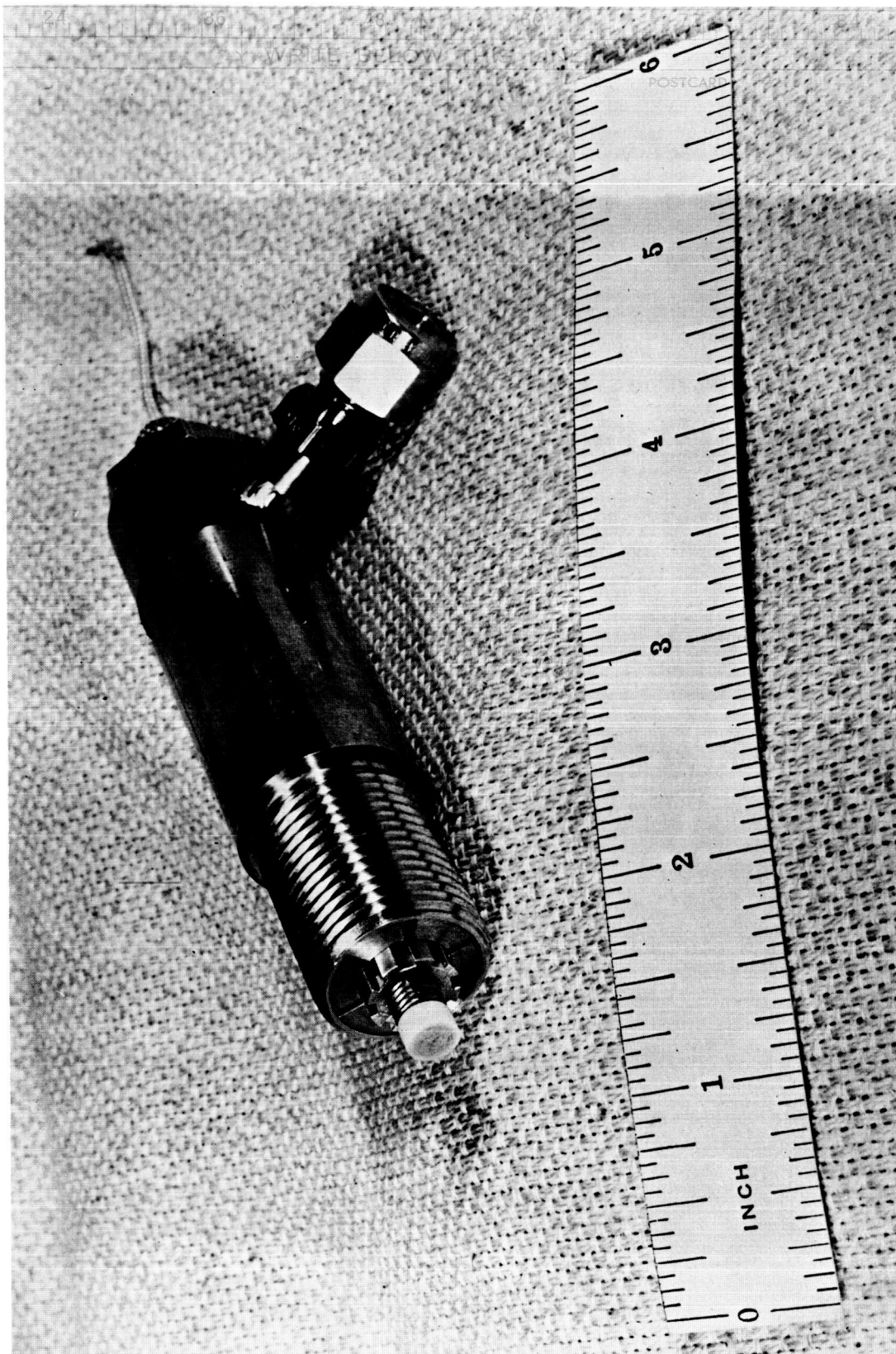


Figure 65a. Bently Probe Mounted in Gauge Holder.

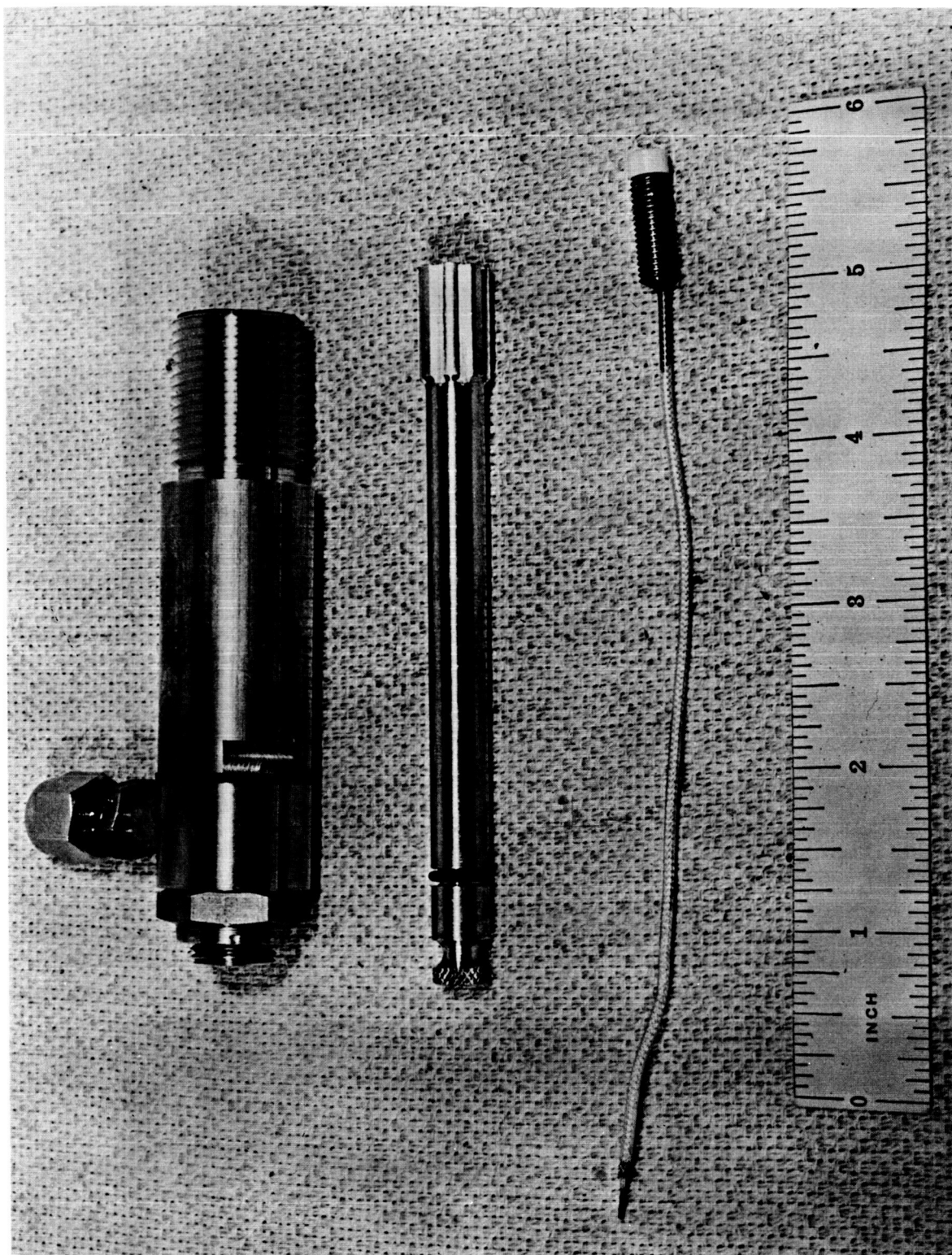


Figure 65b. Bently Probe and Gauge Holder Disassembled.

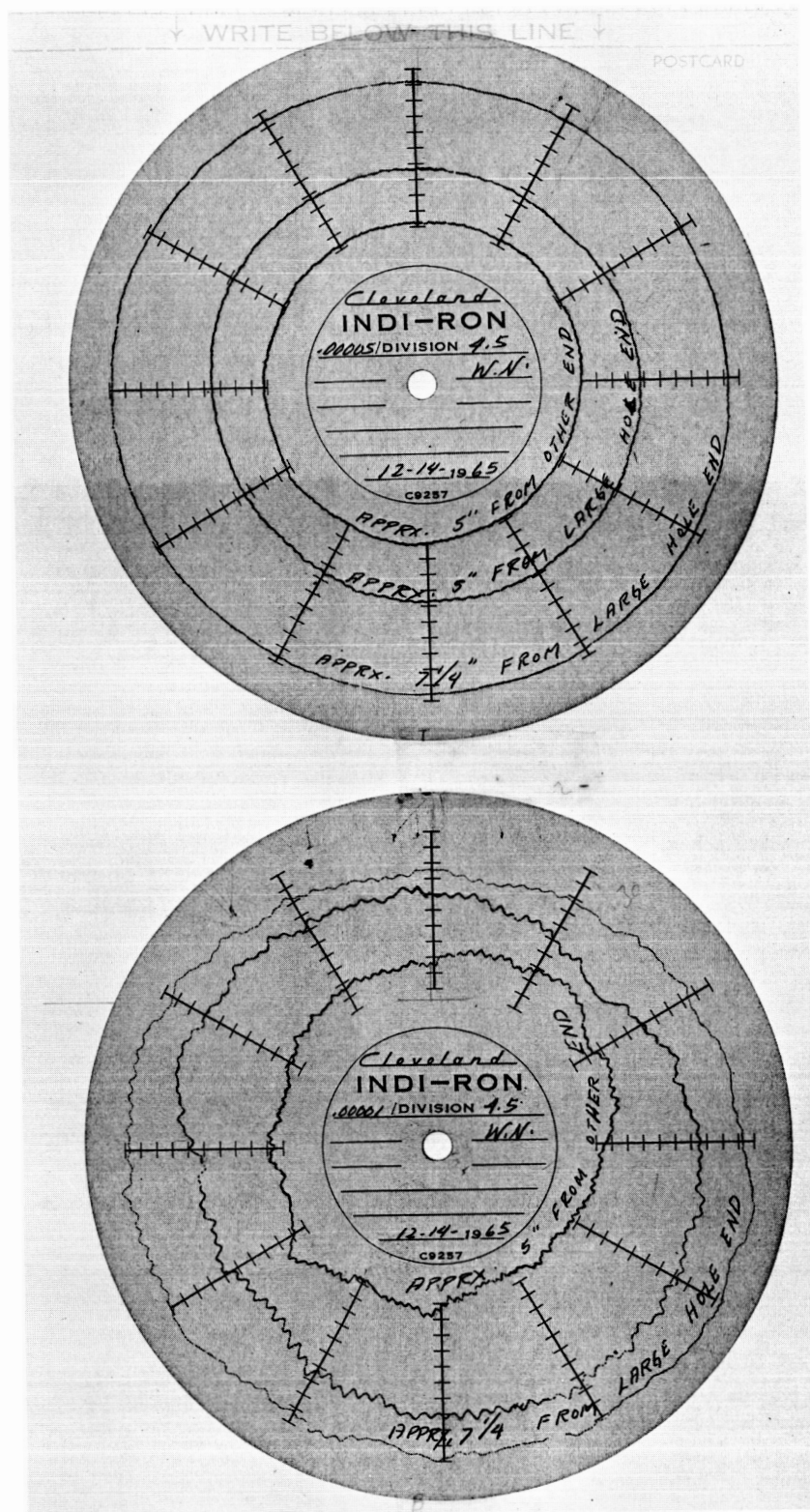


Figure 66. Test Shaft Inspection Traces.

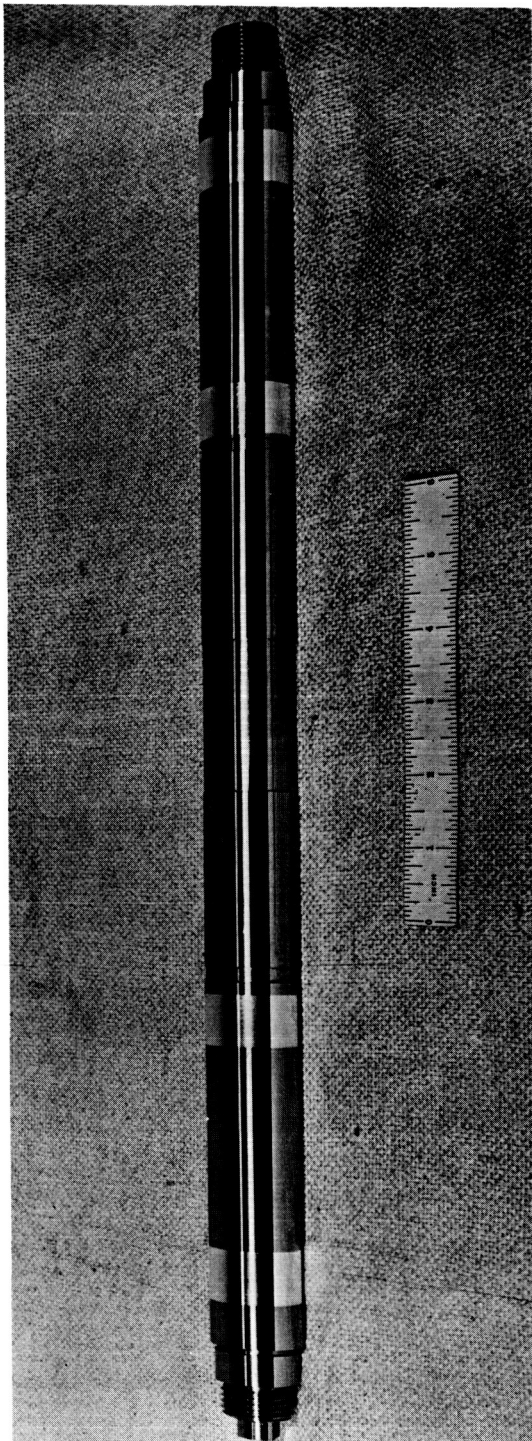


Figure 67a. Test Shaft.

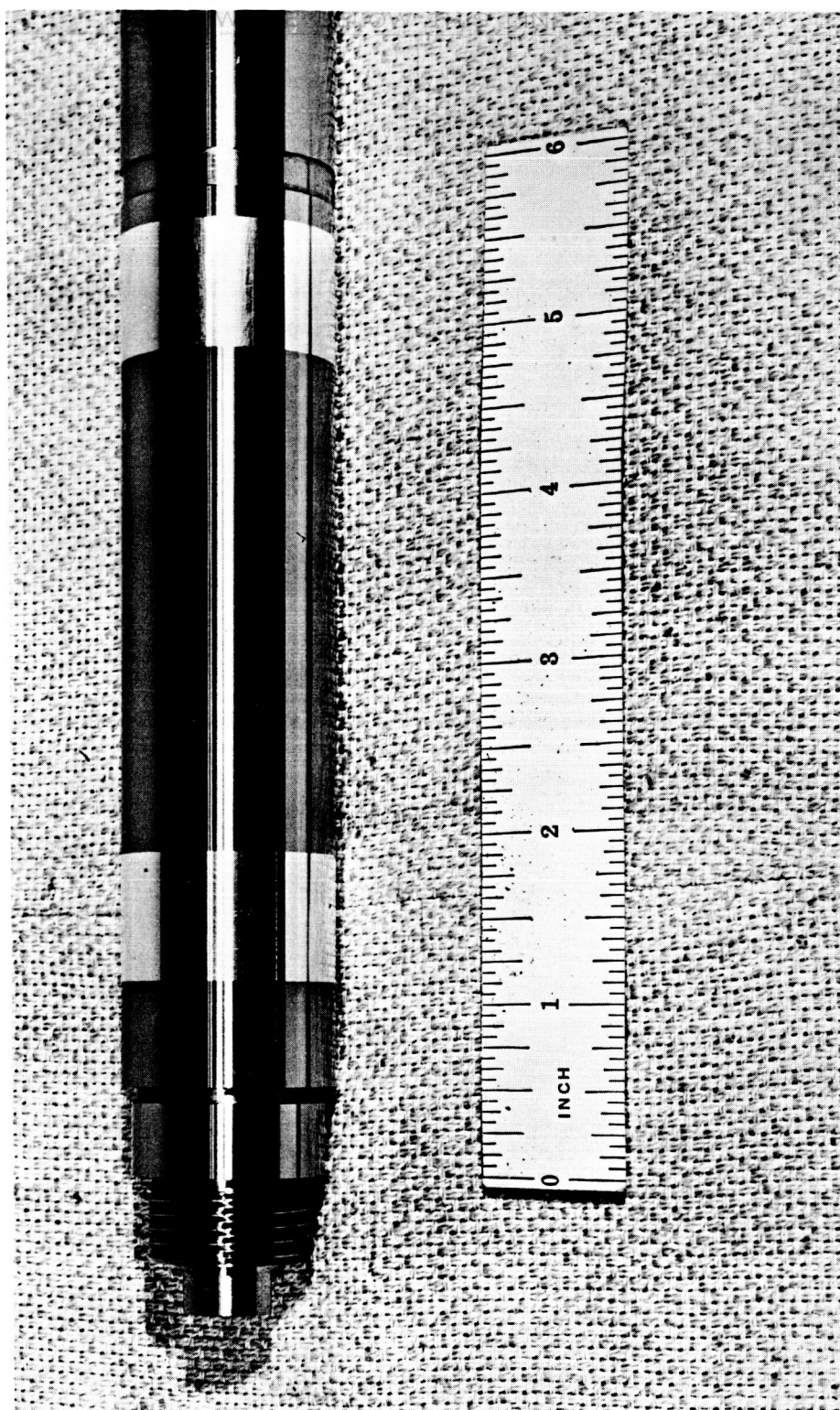


Figure 67b. Test Shaft.

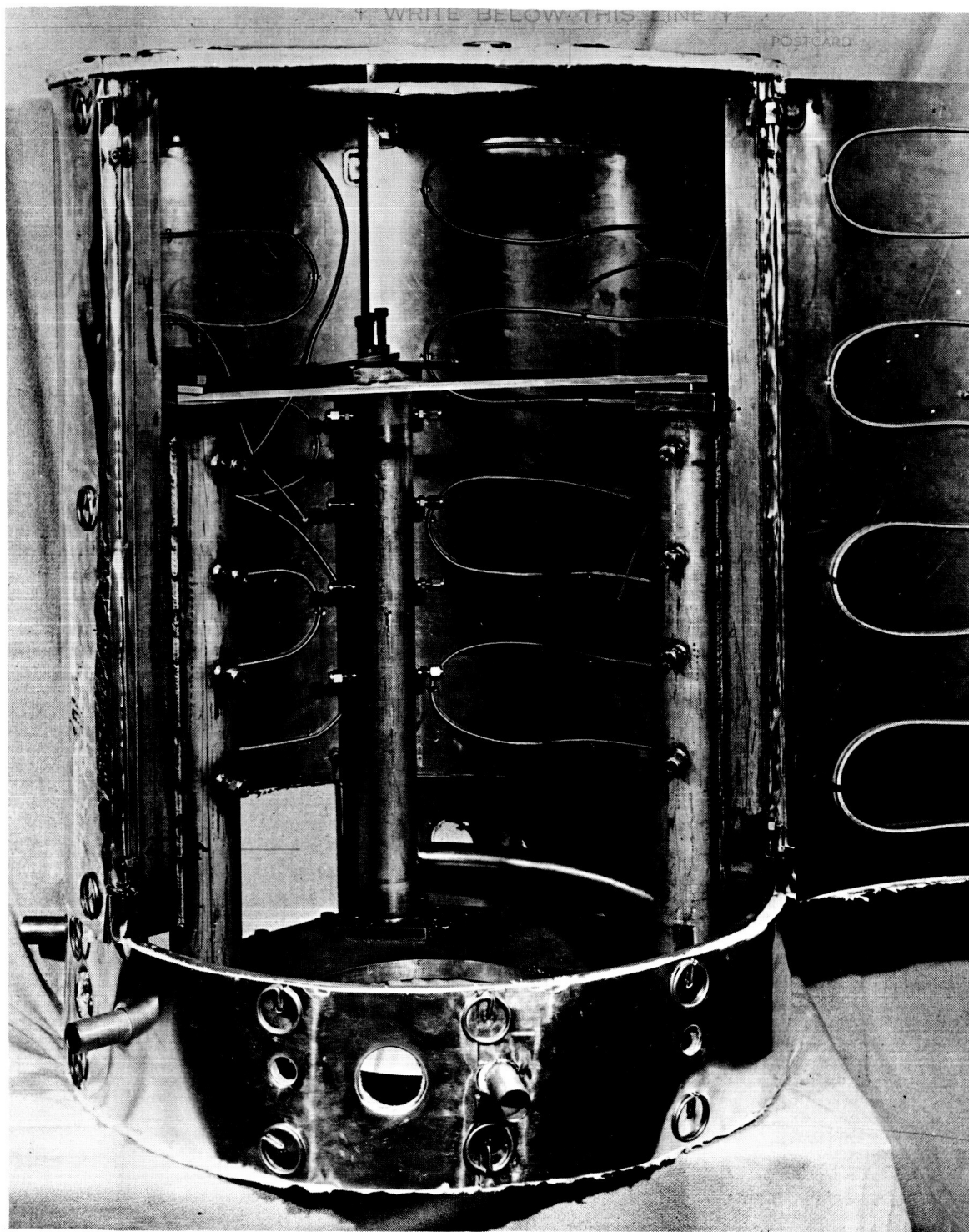


Figure 68. Support Structure.

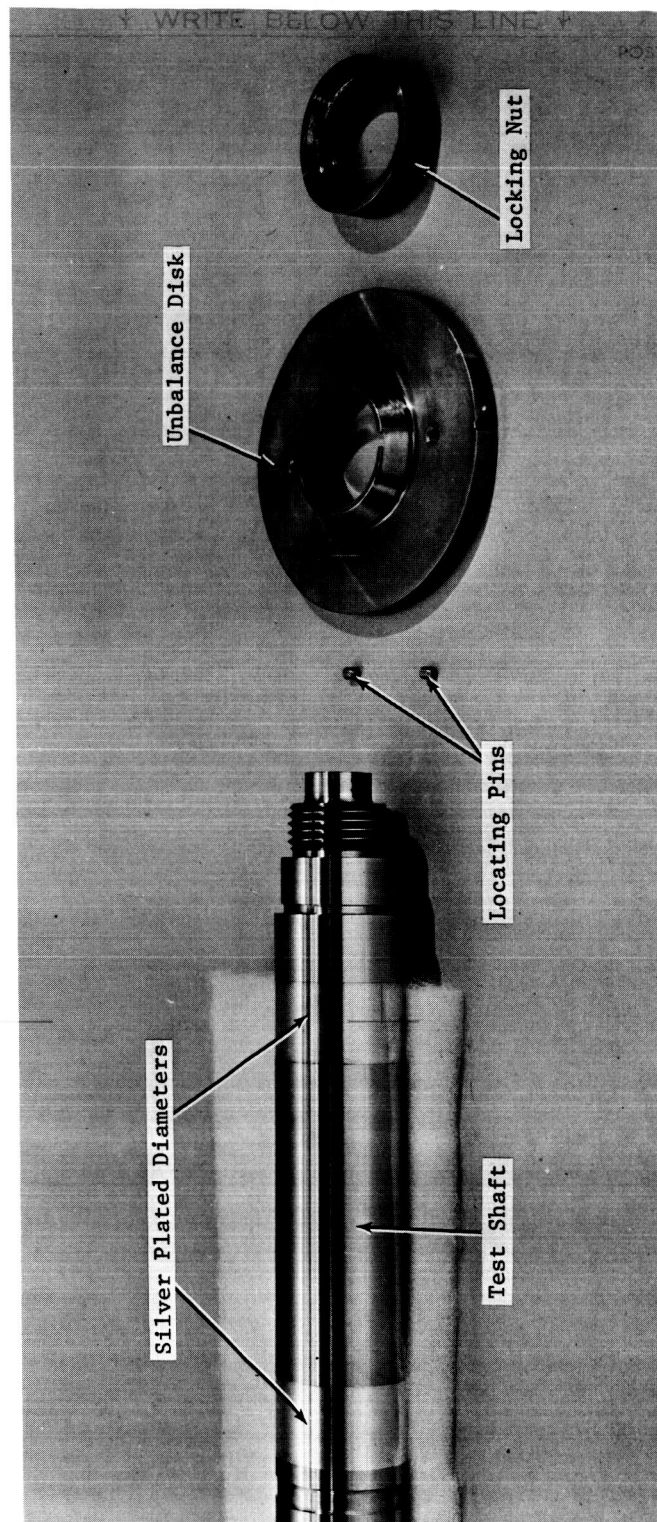


Figure 69. Exploded View of Modified Shaft and New Unbalance Disk.

	Loss in Diametral Clearance (mils)	Shaft-Bearing Slope
I.	0.404	$\frac{1}{3100}$
II.	2.376	$\frac{1}{527}$
III.	1.972	$\frac{1}{634}$
IV.	2.780	$\frac{1}{450}$

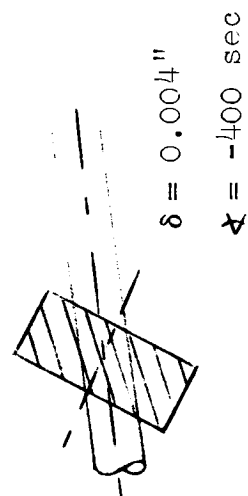
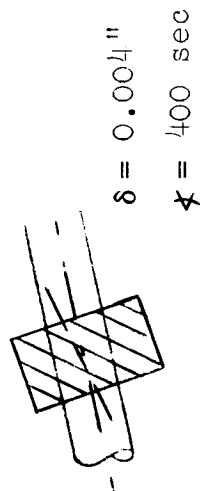
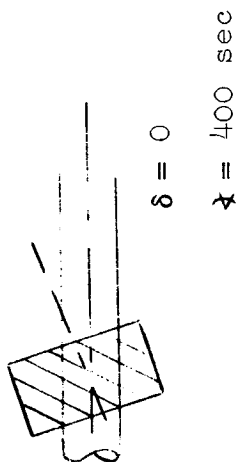
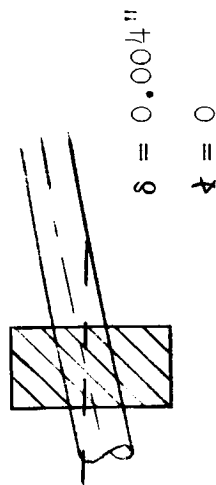
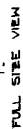


Figure 70. Loss of Bearing Clearance as Result of Misalignment.

GROUP NO.	DIAMETRAL CL. (IN.)	PRE-LOAD CONDITION	LOCKED PAD
1	.005	0	0
2	.005	0	0
3	.005	0	0
4	.005	0	0
5	.005	4	0
6	.005	4	0
7	.005	4	0
8	.005	4	0



A) ALLMETAL SCREW PRODUCTS CO. INC., CHICAGO, ILL.
B) PIC PRECISION SHAFTING, PIC DESIGN CORP., E. ROCKAWAY, N.Y.

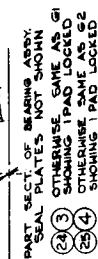
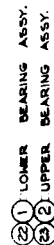


Figure 71. Self-Aligning Pivoted Pad Bearing Flooded Design.

DISTRIBUTION LIST FOR QUARTERLY REPORTS

CONTRACT NAS 3-6479

National Aeronautics and Space Administration
Washington, D.C. 20546
Attn: S. V. Manson - Code RNP

National Aeronautics and Space Administration
Washington, D.C. 20546
Attn: Dr. F. Schulman - Code RNP

National Aeronautics and Space Administration
Lewis Research Center
21000 Brookpark Road
Cleveland, Ohio 44135
Attn: Dr. B. Lubarsky - M.S. 500-201

National Aeronautics and Space Administration
Lewis Research Center
21000 Brookpark Road
Cleveland, Ohio 44135
Attn: Robert Cummings - M.S. 500-201

National Aeronautics and Space Administration
Lewis Research Center
21000 Brookpark Road
Cleveland, Ohio 44135
Attn: Ruth Weltmann - M.S. 500-309

National Aeronautics and Space Administration
Lewis Research Center
21000 Brookpark Road
Cleveland, Ohio 44135
Attn: John Weber - M.S. 3-19
Technical Utilization Office

National Aeronautics and Space Administration
Lewis Research Center
21000 Brookpark Road
Cleveland, Ohio 44135
Attn: Joseph Joyce - M.S. 500-309 (2)

National Aeronautics and Space Administration
Lewis Research Center
21000 Brookpark Road
Cleveland, Ohio 44135
Attn: James Dunn - M.S. 500-201

National Aeronautics and Space Administration
Lewis Research Center
21000 Brookpark Road
Cleveland, Ohio 44135
Attn: Report Control - M.S. 5-5

National Aeronautics and Space Administration
Lewis Research Center
21000 Brookpark Road
Cleveland, Ohio 44135
Attn: William J. Anderson - M.S. 6-1

National Aeronautics and Space Administration
Lewis Research Center
21000 Brookpark Road
Cleveland, Ohio 44135
Attn: Henry Slone - M.S. 500-201

National Aeronautics and Space Administration
Lewis Research Center
21000 Brookpark Road
Cleveland, Ohio 44135
Attn: Warner Stewart - M.S. 5-9

National Aeronautics and Space Administration
Lewis Research Center
21000 Brookpark Road
Cleveland, Ohio 44135
Attn: Edmond Bisson - M.S. 5-3

National Aeronautics and Space Administration
Lewis Research Center
21000 Brookpark Road
Cleveland, Ohio 44135
Attn: Dorothy Morris - M.S. 3-7

National Aeronautics and Space Administration
Lewis Research Center
21000 Brookpark Road
Cleveland, Ohio 44135
Attn: John Dilley - M.S. 500-309

Report Distribution List - NAS 3-6479 - Quarterly (Continued)

National Aeronautics and Space Administration
Jet Propulsion Laboratories
California Institute of Technology
4800 Oak Grove Drive
Pasadena, California 91103
Attn: John W. Stearns

National Aeronautics and Space Administration
Scientific & Technical Information Agency
P.O. Box 5700
Bethesda, Maryland 20014 (2 + Repro)

National Aeronautics and Space Administration
Western Operations Office
150 Pico Boulevard
Santa Monica, California 90406
Attn: John Keeler

Aeronautical Systems Division
Wright-Patterson Air Force Base
Dayton, Ohio 45433
Attn: George Sherman - API

Aeronautical Systems Division
Wright-Patterson Air Force Base
Dayton, Ohio 45433
Attn: Charles Armbruster - ASRMFP-1

Aeronautical Systems Division
Wright-Patterson Air Force Base
Dayton, Ohio 45433
Attn: John Morris - ASRCNL-2

U.S. Atomic Energy Commission
Germantown, Maryland 20545
Attn: Col. E. L. Douthett

U.S. Atomic Energy Commission
Germantown, Maryland 20545
Attn: Dr. Nicholas Grossman
Chief, Engineering Department

U.S. Atomic Energy Commission
Washington, D.C. 20546
Attn: Herbert D. Rothen RNP

Air University Library
Maxwell Air Force Base, Alabama
Attn: Director

U.S. Atomic Energy Commission
Technical Information Service Extension
P.O. Box 62
Oak Ridge, Tennessee

Oak Ridge National Laboratory
Post Office Box Y
Oak Ridge, Tennessee
Attn: H. W. Savage

Office of Naval Research
Washington, D.C. 20546
Attn: S. Doroff - Code 438

Armed Services Technical Information Agency
Arlington Hall Station
Arlington, Virginia 22212

Aerojet-General Corporation
Technical Library
Building 2015, Department 2410
P.O. Box 1947
Sacramento 9, California

Aerojet-General Corporation
Attn: Robert Gordon
SNAP-8 Program Director
Azusa, California 91703

Aerojet-General Corporation
Attn: John Marick
Azusa, California 91703

AiResearch Manufacturing Company
Sky Harbor Airport
402 South 35th Street
Phoenix, Arizona
Attn: Librarian

AiResearch Manufacturing Company
Sky Harbor Airport
402 South 35th Street
Phoenix, Arizona
Attn: Robert Gruntz

Report Distribution List - NAS 3-6479 - Quarterly (Continued)

AiResearch Manufacturing Company
Sky Harbor Airport
402 South 35th Street
Phoenix, Arizona
Attn: George Wheeler

Atomics International
Division of NAA
Canoga Park, California
Attn: L. M. Flower

The Barden Corporation
Research Precision Division
Danbury, Connecticut
Attn: Mrs. Bernice P. Tucos

The Barden Corporation
Research Precision Division
Danbury, Connecticut
Attn: Technical Library

Battelle Memorial Institute
505 King Avenue
Columbus, Ohio 43201
Attn: C. M. Allen

The Franklin Institute
Benjamin Franklin Parkway at 20th Street
Philadelphia, Pennsylvania 19103
Attn: William Shuggarts

General Electric Company
Missile & Space Vehicle Department
3198 Chestnut Street
Philadelphia 4, Pennsylvania
Attn: Edward Ray

Mechanical Technology, Inc.
968 Albany-Shaker Road
Latham, New York
Attn: Dr. Beno Sternlicht

Mechanical Technology, Inc.
9680 Albany-Shaker Road
Latham, New York
Attn: Eli Arwas

M.S.A. Research Foundation
Callery, Pennsylvania
Attn: G. E. Kennedy

Pratt & Whitney Aircraft Division
United Aircraft Corporation
East Hartford, Connecticut 06108
Attn: Dr. William Lueckel
Eng. Bldg. 2-H

Pratt & Whitney Aircraft Division
United Aircraft Corporation
East Hartford, Connecticut 06108
Attn: R. P. Shevchenko

Pratt & Whitney Aircraft Division
United Aircraft Corporation
East Hartford, Connecticut 06108
Attn: Karl A. Domeisen
Exp. Eng. Eng. 1-F

Rocketdyne
Division of North American Aviation, Inc.
6633 Canoga Avenue
Canoga, California 91303
Attn: Robert Spies

Sundstrand Aviation - Denver
A Division of Sundstrand Corporation
Denver, Colorado 80221
Attn: P. H. Stahlhuth

Southwest Research Institute
8500 Culebra Road
San Antonio, Texas 78206
Attn: Dr. R. A. Benton

The Franklin Institute
Benjamin Franklin Parkway
at 20th Street
Philadelphia, Pennsylvania 19103
Attn: Otto Decker

UAC Library
United Aircraft Research Laboratories
Gate 5R, Silver Lane
East Hartford, Connecticut 06108

Report Distribution List - NAS 3-6479 - Quarterly (Continued)

Westinghouse Electric Corporation
Research Laboratories
Pittsburgh, Pennsylvania 15236
Attn: Mr. J. Boyd

Westinghouse Electric Corporation
Aerospace Division
Advanced Machine Systems Group
Lima, Ohio
Attn: Allen King

North American Aviation, Inc.
Atomics International
P.O. Box 309
Canoga Park, California 91304
Attn: Director, Liquid Metals Info.Center

National Aeronautics & Space Administration
Lewis Research Center
21000 Brookpark Road
Cleveland, Ohio 44135
Attn: Jack Heller - M.S. 500-201

Aeronautical Systems Division
Wright-Patterson Air Force Base
Dayton, Ohio 45433
Attn: John Zmurk APIP-1